UNH-

Polarization of the Light from the 3^1P-2^1S Transition in Proton Beam Excited Helium

by

Martin S. Weinhous
B.S., Rensselaer Polytechnic Institute, 1966
M.S., University of New Hampshire, 1970

Department of Physics
UNIVERSITY OF NEW HAMPSHIRE
Durham

POLARIZATION OF THE LIGHT FROM THE 3^1P-2^1S TRANSITION IN PROTON BEAM EXCITED HELIUM

by

MARTIN S. WEINHOUS

B.S., Rensselaer Polytechnic Institute, 1966
M.S., University of New Hampshire, 1970

A THESIS

Submitted to the University of New Hampshire

In Partial Fulfillment of
The Requirements for the Degree of

Doctor of Philosophy

Graduate School
Department of Physics

December 1973

This Thesis has been examined and approved.

E. L. Chupp, Thesis Chairman, Professor of Physics

J. F. Dawson, Assistant Professor of Physics

H. H. Hall, Professor Emeritus of Physics

R. E. Houston, Jr., Professor of Physics

R. H. Lambert, Professor of Physics

20 December, 1973
Date

ACKNOWLEDGMENTS

The author wishes to express his sincere thanks to his advisor Dr. Edward L. Chupp for suggesting the research topic and then providing support and advice.

Thanks are also given to Dr. Robert E. Houston, and Dr. Robert H. Lambert for their critisisms, encouragements and assistance.

Bill Dotchin was very helpful in and around the Van De Graaff Accelerator.

Thanks finally go to Mrs. Mary Chupp for her faith and encouragement.

This work was supported by the National Aeronautics and Space Administration under Grant NGL 30-002-018, NGL-30-002-021, NGR-30-002-104 and NAS5-11054

DEDICATION

The author would like to express his deep appreciation and gratitude to his parents. It was their love, devotion and support which made this work possible.

TABLE OF CONTENTS

LIST OF TABLES

LIST OF FIGURES

ABSTRACT

POLARIZATION OF THE LIGHT FROM
THE 3^1P-2^1S TRANSITION IN PROTON BEAM-
EXCITED HELIUM

by

MARTIN S. WEINHOUS

Measurements of the polarization of the light from the 3^1P-2^1S (λ 5016 Å) transition in proton beam excited Helium have shown both a proton beam energy and Helium target gas pressure dependence. Results for the linear polarization fraction (at right angles to the proton beam and at .2 mtorr He target pressure) range from +2.6% at 100 keV proton energy to -5.5% at 450 keV. The zero cross-over occurs at approximately 225 keV. This is in good agreement with other experimental work in the field, but in poor agreement with theoretical predictions. The other experimental workers have used .2 mtorr as their lowest He target gas pressure, while in this work measurements have been made at He target gas pressures as low as .01 mtorr. The results have shown that the linear polarization fraction is still pressure dependent at .01 mtorr.

We also have found a pressure dependence of photons per proton per He target atom. We then conclude that experimental deteriminations of the linear polarization fraction have not yet been made under conditions which allow for strict comparison with theoretical predictions.

SECTION I

INTRODUCTION

1.1 Purpose of the Investigation

In the early 1900's it was known that spectral lines could exhibit polarization when magnetic fields were applied to the light source (the π and σ components in a Zeeman effect spectrum). However in about 1920 the yellow mercury lines, 5770 Å and 5791 Å created in a gas discharge tube, were found to be weakly polarized even in the absence of a magnetic field. The light was polarized such that the maximum electric vector was parallel to the path of current in the discharge tube. This fact led the investigators of the period, notably Skinner (1926) to test the hypothesis that the polarization was caused by the electron "beam" within the discharge tube. The hypothesis proved to be correct and so began the study of collisionally-produced polarized atomic line radiation. Many such studies have been completed since that time. Percival (1958) has published an extensive article on electron excitation of polarized atomic line radiation. Included in this article are Born approximation calculations for excitation of the various magnetic substates of the target atom. More recently,

investigators have become interested in the polarization due to proton impact. Bell (1961) has calculated theoretical excitation cross-sections for proton-excited helium. He has used both the Born and Distorted Wave Approximations for his calculations. The results of these calculations can easily be converted into an expected polarization of the light emitted after the collision. Two independent research groups have done just that. A Dutch group, Van Eck (1964) and Van Den Bos (1968) were able to compare these theoretical polarization values with experiments in the 5 to 35 keV and 1 to 150 keV proton energy ranges respectively. A second group working at the University of Giessen, Germany, has also done an experimental check of Bell's work. Scharmann (1967), (1969) has also investigated the polarization of light emitted by He after proton impact in the energy range 100 to 1000 keV. Unfortunately, there is little overlap and only mediocre agreement between these two groups.

It is the purpose of this thesis then to make a detailed study of the polarization of the light emitted by He which has been excited by proton impact; to provide a confirmation of the work of either the Dutch or German research groups; and to extend the work in the direction of lower He target gas pressures in the hope of finding the "free atom" value for the polarization. Only then can one make a valid comparison with the theoretical

models which are available.

1.2 Polarization Measurements

The polarization of linearly polarized light is usually described by a quantity called the linear polarization fraction, denoted by the symbol π. Two quantities are required to calculate π, the light intensities with the electric field vectors parallel to and perpendicular to a "preferred" direction. The observation is made along a line which meets the "preferred" direction line at right angles. See Figure 1. Then

$$\pi = \frac{I_{//} - I_{\perp}}{I_{//} + I_{\perp}} \qquad 1.2.1$$

obviously π can range from -1 to +1.

To measure the polarization one must separate and measure the intensities of $I_{//}$ and $I_{\perp}$. This can be done by a number of methods. In this work a glass laminated polaroid-type HN 32 sheet polarizer was placed on the observer's line of sight such that the light of interest passed normally through the polarizer and such that the polarizer could be rotated (about the line of sight) by 90°. If one now replaces the observer by an instrument capable of measuring intensities and then uses the polarizer to pass first $E_{//}$ light and then $E_{\perp}$ light for measurements of $I_{//}$ and $I_{\perp}$ respectively, one can then calculate π.

SPECIFICATION OF DIRECTIONS

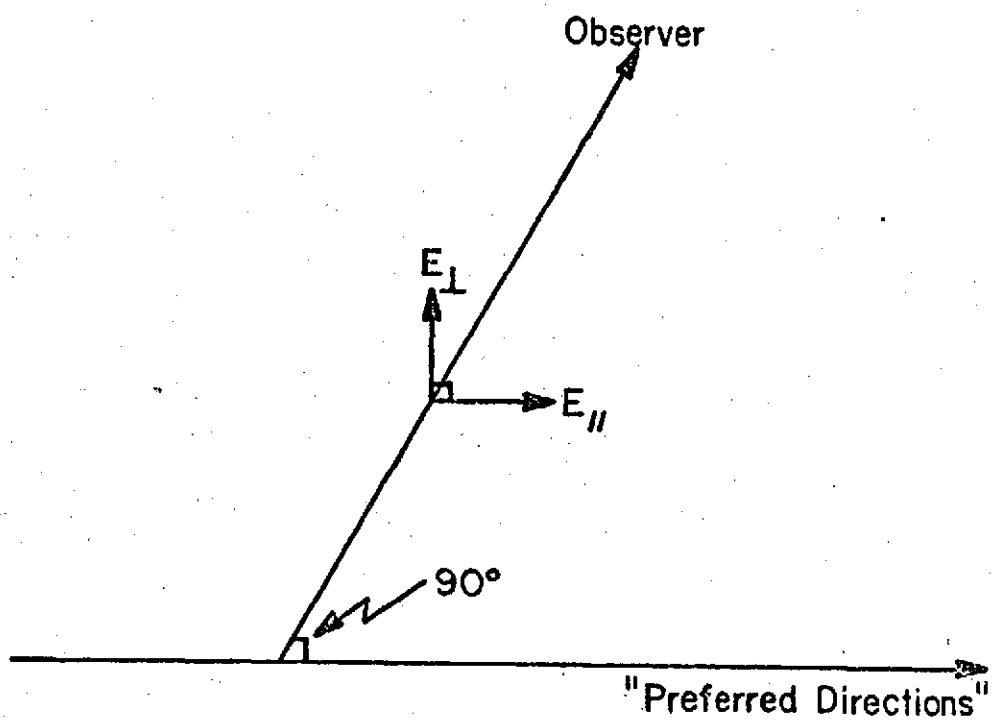

FIGURE 1

In this experiment the "preferred" direction is the proton beam direction; the light originates from a He gas filled target chamber, an interference filter selects the 5016 Å line (of He), and a photomultiplier measures the light intensity. See Figure 2.

A detailed discussion of polarized light and its measurement is found in Appendix A.

1.3 Astrophysical Interest

Astronomy has its very roots in the observation of the heavens via visible light. As the science matured more and more information was extracted from that light. Just as the intensity, wavelength, and phase of the light convey information to the observer, so does the polarization. In fact the magnetic field of some stars has been determined from measurements of the polarization of the Zeeman components of spectral lines. A similar analysis of light from the sunspots on our own sun lead to a determination of the intensities and polarities of the magnetic fields associated with those spots. The radial polarization exhibited in the light from reflection nebula can be used to calculate the average particle size in the nebula. The correlation between the interstellar reddening of starlight and the amount of polarization of that light can be used to gain information about the magnetic field of our galaxy. The light from the

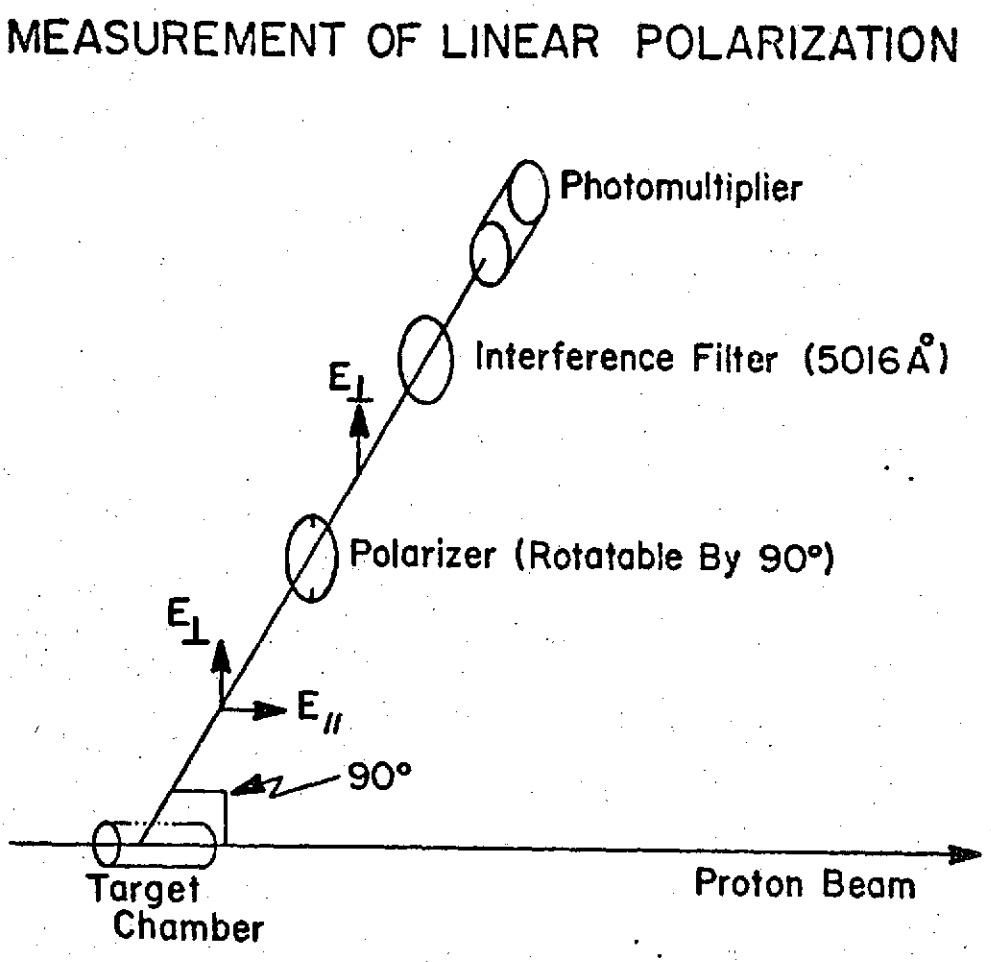
MEASUREMENT OF LINEAR POLARIZATION
Photomultiplier
Interference Filter (5016 Å)
$E_\perp$
Polarizer (Rotatable By 90°)
$E_\perp$
$E_{\parallel}$
90°
Target Chamber
Proton Beam

FIGURE 2

"jet" of material emanating from the giant galaxy M87 (in Virgo) is highly polarized and therefore is believed to be generated by synchrotron radiation. The astrophysicist thus needs to be informed as to what processes create polarized light and to what degree they create it. Only then can he successfully unfold his data. This work investigates one non-magnetic process which creates polarized light, a process which is certainly active in space, a proton collision with an atom.

1.4 Previous Experimental Work

Van Eck (1964) provides us with the first experimental determination of the polarization of the light resulting from proton impact on ground-state Helium. He used a Glann-Thompson prism as the polarization analyzer and a Leiss monochromator to isolate light from the transition being investigated. Since the intensity of reflected light from the grating in the monochromator depends upon the polarization of the light, Van Eck et al. had to take great care to separate the polarization of the light due to the atomic transition from that due to the instrumental polarization. His measurements covered a proton energy range of 5 to 35 keV (generated by a Von Ardenne ion source) and a Helium target gas pressure range of .2 to 1 m torr. A sensitive McLeod gauge was used to determine the pressure of the Helium.

Van Den Bos (1968) essentially repeated Van Eck's work (with some additions). He extended the proton energy range up to 150 keV and added magnetic shielding to the collision chamber. The agreement between Van Den Bos and Van Eck is very good (5 to 35 keV).

Scharmann (1967, 1969) used a very different detecting apparatus to find the polarization of the light from Helium which had been excited by proton impact. His detector used a sheet polarizer and interference filter rather than the Glan-Thompson prism and monochromator of the Dutch groups. He was also able to cover a very wide proton energy range of 100 to 1000 keV. The Helium target gas pressure range in his study was .2 m torr to 5 m torr.

1.5 Previous Theoretical Work

Percival's (1958) article on the "Polarization of Atomic Line Radiation Excited by Electron Impact" discusses both the Oppenheimer-Penney Theory and Born approximation methods for calculating the polarization. The Oppenheimer-Penney (O-P) theory is used to calculate the polarization of atomic line radiation when the cross-sections for exciting quantum states of the upper level are known. These upper level quantum states have a definite orbital angular momentum component M_L (the preferred direction being that of the electron beam). Percival pays particular attention to He and certain isotopes of

Hg for which the nuclear spin is zero. In fact one can extract from his table of polarization formulae for the He multiplets (SL→SL') the expression

$$\pi(S1 \rightarrow SL') = \frac{G(Q_0 - Q_1)}{h_0 Q_0 + h_1 Q_1}$$

where the parameters G, h_0 and h_1 are determined by the values of S and L', then for our case ($3^1P \rightarrow 2^1S$), L' = 0; and from Percival's table G = 1, h_0 = 1, h_1 = 1. Q_0 and Q_1 are of course the cross-sections for exciting the M_L = 0, and M_L = ±1 substates. This result is independent of the exciting particle.

Percival goes on to actually calculate via the Born approximation the Q_{M_L} for the excitation of the 3^1D states of He. His results however were in poor agreement with the experimental results available at the time. Percival questions the suitability of the approximate wave functions used rather than the validity of the Born approximation.

Bell's (1961) work uses both the Born and Distorted Wave Approximation methods to calculate the cross-sections for the process

$$H^+ + He(1s^2)\,^1S \longrightarrow H^+ + He(1s\,3p)\,^1P$$

He used product wave functions for the ground state of the target system and excited state wave functions proportional to $[\psi_1(r_1)\psi_n(r_2) + \psi_n(r_1)\psi_1(r_2)]$

The actual forms of the ψ_n contain "adjustable" parameters which are chosen so as to obtain particular oscillator strengths. The calculations of the Q_{0m}'s are carried out by numerical methods on high speed computers.

Theoretical details are given in Appendix B.

SECTION II

EXPERIMENTAL APPARATUS

2.1 Introductory Description of the Experimental Apparatus.

In order to implement the polarization measurement discussed in section 1.2, apparatus was assembled which would provide a relatively stable proton beam, a confined region of Helium target atoms, and a method for measuring the intensity of the two linear polarization components of the λ 5016 Å line of Helium. This apparatus was assembled in the physics department of the University of New Hampshire. The three main components of the experimental apparatus were a Van De Graaff positive ion accelerator and associated beam tube optics, a differentially pumped target chamber and vacuum system; and the polarization detection system. The proton beam is of course produced by the accelerator, the Helium target atoms are isolated within the differentially pumped target chamber, and the polarization detection system will isolate and measure the intensity of the linear polarization components of the He line. Each of these systems is described in detail in the following paragraphs.

2.2 The Van De Graaff Accelerator

Our accelerator is a model PN-400 manufactured by High Voltage Engineering of Burlington, Massachusetts. It is capable of producing positive ion beams within the energy range of ∿100 to ∿450 keV. In our work we confine ourselves to proton beams of ∿1 to ∿19 μ A's current. Within the accelerator, the protons are generated in a radio-frequency source bottle. Hydrogen gas is continuously leaked into the source bottle through a palladium leak (maintaining very high purity), where it is ionized by a radio-frequency discharge. This source bottle is located at the high potential end of the accelerator tube. A small canal (beryllium) connects the source bottle and accelerator tube. The protons then enter the accelerator tube at a rate dependent upon both the hydrogen gas pressure in the source bottle, and the magnitude of the positive probe voltage within the bottle. Once into the accelerator tube, the protons are confronted with a focusing electric field and then an accelerating electric field. These fields are maintained by a focus plane and a series of equipotential planes. The voltages within the Van de Graaff are due to the relocation of charges by the motor driven belt. So the potential difference seen by the protons depends upon the amount of charge carried by the belt, and is adjustable. The proton beam energy then depends only on the potential difference

through which the proton accelerates.

In fact, not only protons appear in the beam. Any positive ions created in the source bottle will be accelerated in the beam. One will therefore get at least H^+, H_2^+, and H_3^+. Any impurities found in the bottle may ionize and produce accelerated positive ions. Rough measurements have shown our H^+ yield to be approximately 10-40 per cent of total beam current. Since this beam is later magnetically analyzed, its content is not important so long as sufficient H^+ is present. Diagrams of the accelerator are shown in figures 3 and 4.

2.3 The Accelerator System

A large number of accessory systems are required by the Van de Graaff. The accelerator tube and beam tubes must be maintained at low pressures, and the ion beam must be steered and focused as well as energy stabilized. Our experiment also requires accessory systems to differentially pump the target chamber, and to accurately measure the pressure within the target chamber. The accelerator is also used for another research project as well as for teaching. Some of our equipment has therefore been designed around these other requirements.

The vacuum system and beam tube arrangement is shown in fig. 5. Both the main pump and left port pump No. 2 are NRC six inch diffusion pumps backed by Welch mechanical pumps. Typical operating pressures are; at

THE VAN DE GRAAFF ELECTROSTATIC ACCELERATOR

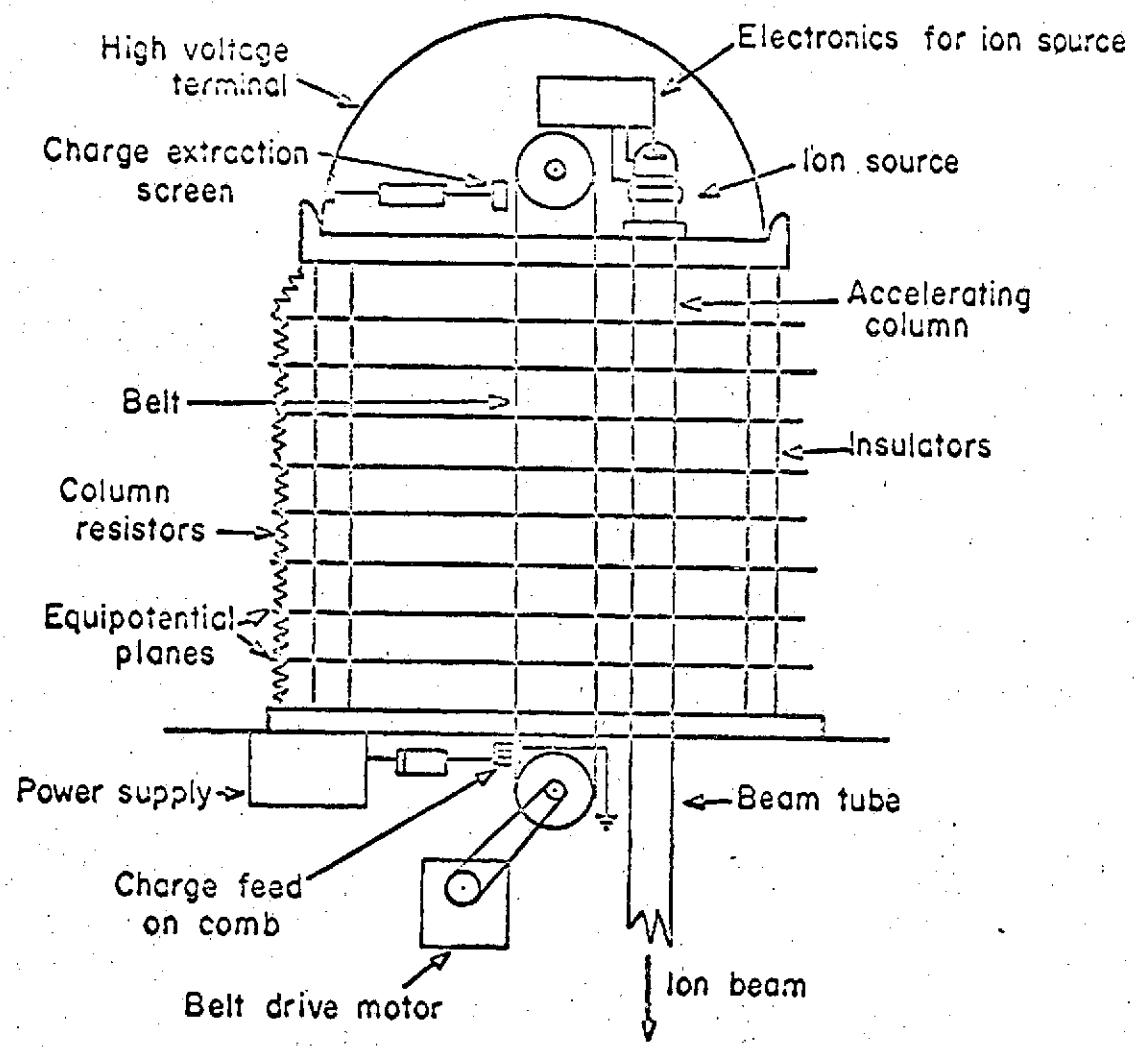

FIGURE 3

BEAM OPTICS OF THE VAN DE GRAAFF ACCELERATOR

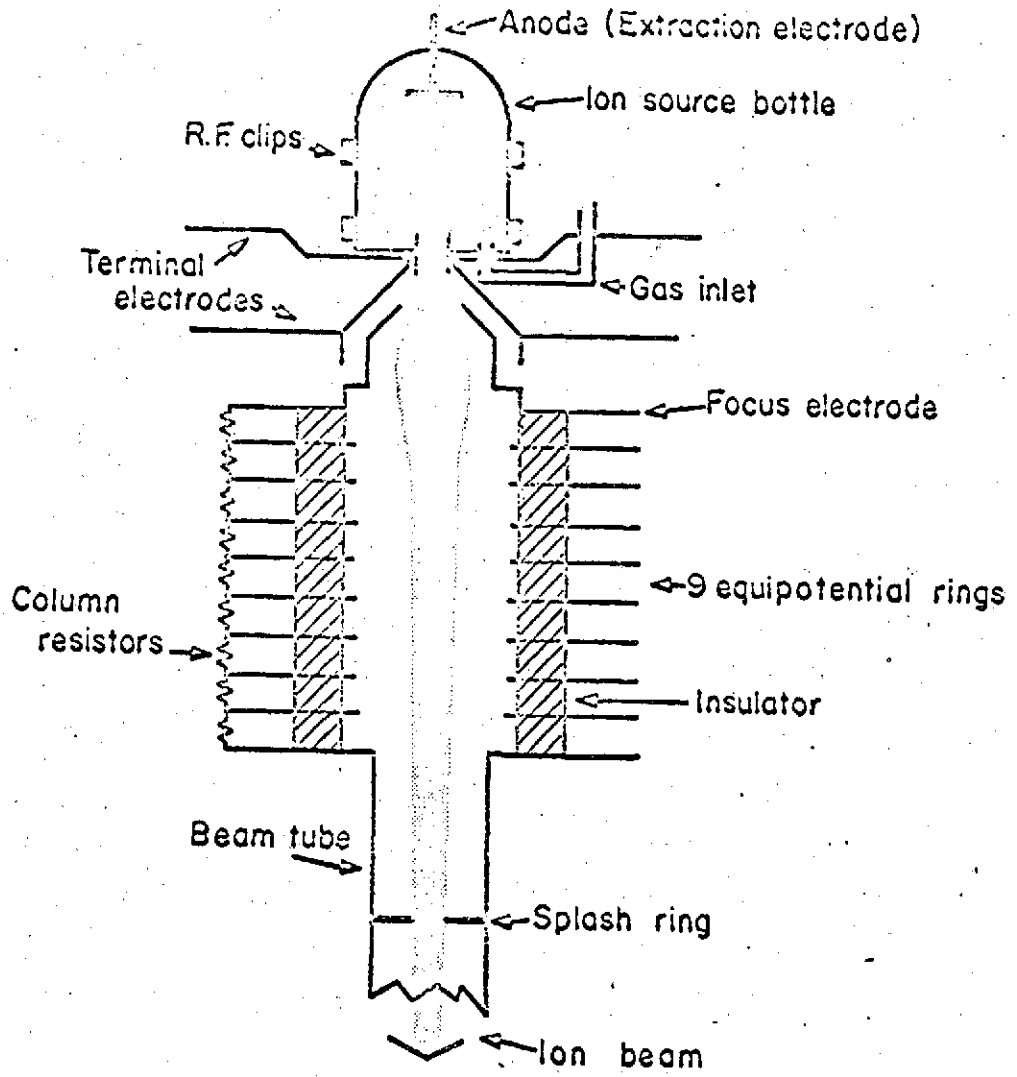

FIGURE 4

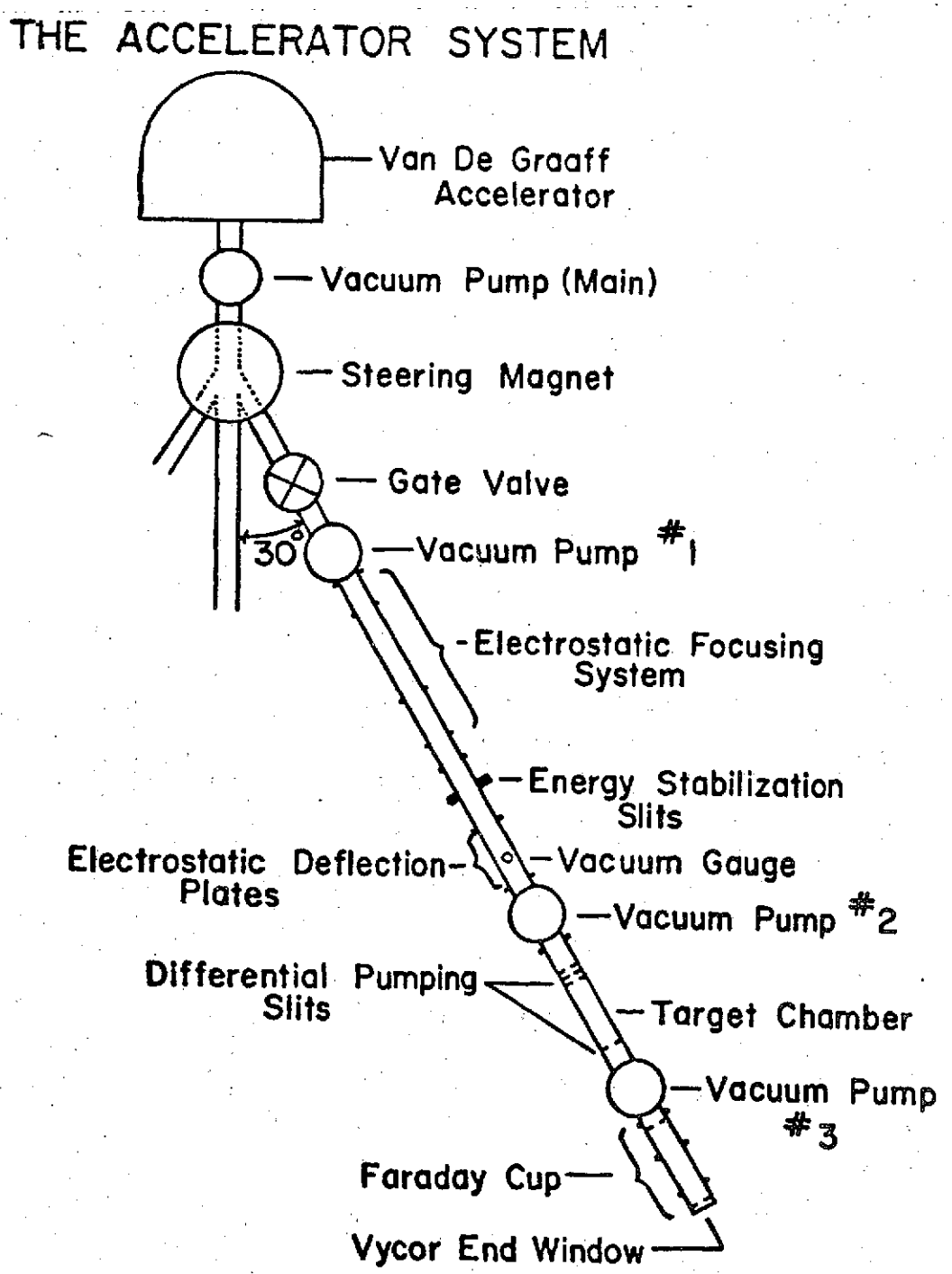
THE ACCELERATOR SYSTEM
Van De Graaff Accelerator
Vacuum Pump (Main)
Steering Magnet
Gate Valve
30°
Vacuum Pump #1
Electrostatic Focusing System
Energy Stabilization Slits
Electrostatic Deflection Plates
Vacuum Gauge
Vacuum Pump #2
Differential Pumping Slits
Target Chamber
Vacuum Pump #3
Faraday Cup
Vycor End Window

FIGURE 5

the main pump $\sim 6\text{-}8 \times 10^{-6}$ torr; and at the No. 2 pump $\sim 10 \times 10^{-6}$ torr. Left port pumps No. 1, and No. 3 are two inch diffusion pumps again backed by mechanical pumps. The center port beam tube has no pumps of its own, however, it is short enough not to need one. The only time we use the center port is during the initial tune up of the Van de Graaff. The right port beam tube (details not shown in fig. 5) is used generally for teaching experiments and not for research, and will hence be ignored.

A magnetic analyzer is used to select for a monoenergetic proton beam. It is well known that when a charged particle moves with its velocity perpendicular to a constant homogenous magnetic field, the particle will follow a circular path while it remains within the magnetic field. The Lorentz force on such a particle is

$$\vec{F} = \frac{qz}{c} \vec{v} \times \vec{B} \qquad 2.3.1$$

where in our case $z = 1$ and $q = e$. The force equation is then

$$\frac{e}{c} v \times B = \frac{m v^2}{r} \qquad 2.3.2$$

where for our nonrelativistic case

$$v = \left(\frac{2E}{m}\right)^{\frac{1}{2}} \qquad 2.3.3$$

using 2.3.3 in 2.3.2 one arrives at

$$r = \frac{c}{eB}(2Em)^{\frac{1}{2}} \qquad 2.3.4$$

This last equation shows that for a constant magnetic field B, and a constant beam energy E, the radius of curvature for any ion depends upon the square root of the ion's mass. The magnetic analyzer then can bend the different ions in the beam into different paths and thus isolate them. In practice, in our system, the accelerator will be tuned to a specific energy and beam current in the center port. The analyzing magnet will then be turned on with a current known to be insufficient to bend protons (the most easily bent positive ion) into the left port. The magnetic current will then be gently increased until our various indicators show a beam in the left port tube. The current supplied to the analyzing magnet is regulated by an Atomic Laboratories Inc. power supply and regulator (Model C). The regulator holds the current (and hence magnetic field) constant to one part in 10^5.

An Energy Stabilization System is used to prevent changes in the ion beam energy. The energy of the ion beam, as it exits from the Van de Graaff accelerator, depends upon the difference in potential between the ion source bottle and ground. This potential difference in turn is controlled by the quantity of charge located at the high voltage terminal of the accelerator. High Voltage Engineering's design of the PN-400 accelerator

includes a corona probe extending inward from the pre-sure tank wall toward the high voltage terminal. This corona probe is tipped with an array of needle-like points, which increase the probe's efficiency in draining charge from the high voltage terminal to the pressure tank and, therefore, ground. It is then clear that the beam energy is a function of the rate of charge leakage through the corona probe. The High Voltage Engineering Inc. Corona Stabilizer takes advantage of the above. The corona probe is not connected directly to tank ground, but rather to the plate of a type 4-125A vacuum tube. One can then control the charge drain from the high voltage terminal by controlling the conduction of the 4-125A, the corona stabilizer does exactly that and hence controls the beam energy.

When a beam has been magnetically analyzed, and directed down the left port, it encounters two probes (an insulated vertical slit) within the beam tube. If the beam energy drifts upward (due to drifts within the accelerator), then the beam will be bent less by the magnet and it will impact upon the center (or High energy) probe more heavily than upon the outside (or low energy) probe. This imbalance in probe currents is detected by the High Voltage Engineering Corona Stabilizer Ampli-fier, and this amplifier in turn sends a negative feed-back signal to the (grid and cathode) 4-125A. This signal changes the tube's conductance, so as to correct

the beam energy, i.e., to have equal impact on the probes (this centers the correct energy beam in the tube).

Energy calibrations of the Van de Graaff accelerator are done with a High Voltage Engineering generating voltameter. This instrument is used to measure and display (digitally) the potential of the high voltage terminal (and, therefore, the beam energy). The unit consists of a chopper (or rotor) and stator plate (both eight sectioned). The unit is located within the Van de Graaff pressure tank near the high voltage terminal. As the chopper rotates, it alternately exposes and shields the stator from the high voltage terminal. The voltage induced on the stators is then a chopped D.C. or roughly triangular A.C. which is proportional to the high voltage terminal potential and, therefore, proportional to the beam energy. The rectified output of the generating voltameter is now connected to a digital voltameter for a fast, easy, and accurate readout. We estimate an instrumental accuracy of from 1 to 2 per cent. This, however, assumes a linear response, a "good" calibration, and a focus voltage setting which remains at its calibration value.

In practice, the linearity has been verified for a two point calibration, and the focus voltages used do not vary more than $\sim$5 kV. The calibration procedure for the generating voltameter involves the use of the $F^{19}(p,\alpha\gamma)O^{16}$ nuclear resonance. The cross-section for

this reaction shows two distinct resonances, one at a (laboratory) proton energy of 340 keV, and the second at a proton energy of 484 keV. To perform the calibration experiment, a small aluminum wafer is exposed to concentrated hydroflouric acid for 15 min. This provides us with a thin target for use at the end of the beam tube. A 2 inch NaI scintillation detector is used to detect the 6 MeV γ rays emitted from the fluorine. The pulses from the detector were Amplified and sent to a single channel analyzer and then to a scalar. The scalar is generally set to repeat 10 second data acquisition periods and $\sim$5 second display periods. One then impacts a proton beam on the fluorine target, adjusting the energy of the beam to a value less than that required for a resonance. The "background" on the scalar is then noted. One then gradually increases the beam energy (by increasing the magnetic current, and belt charge) until a peak is reached, again the number of γ-ray counts is noted. The resonance occurs at that point in energy where the number of counts on the scalar is just the average of the background and peak values. The Van de Graaff's energy is adjusted so that the scalar is showing just that average value, and the digital voltameter is set to the resonance value. We will generally use the 340.5 KeV value for our calibration and the higher energy resonance for a linearity check. Using this calibration procedure, an overall energy readout accuracy of $\sim$8 KeV appears

appropriate.

An Electrostatic Focusing System was installed as an improvement for the pulsing system used by Dotchin et. al. for mean life studies. It has, however, become useful in this work due to its ability to focus the beam through the differential pumping slits (to be discussed later). The system was designed and constructed by D. L. Keator as a course project. In operation, one simply monitors the beam current (by means of a Farady cup) and adjusts the voltages supplied to the electrostatic focusing system so as to maximize that current.

The differentially pumped target chamber, shown in figure 6, is used to provide the relatively high pressures of He ($<2\times10^{-3}$torr) required for the experiment without filling the beam tube with gas and adversely influencing the operation of the accelerator. To maintain a pressure differential between the target chamber and beam tube, one continually leaks the target gas into the chamber which is then pumped through narrow slits into the beam tubes. The slit size is a compromise between maximizing beam current, and minimizing the flow of gas into the beam tube. In our case, the upstream slits (nearer the accelerator) are also a part of the pulsing system used by Dotchin et. al. There are three slits in that group, each a horizontal opening $\sim$1 x $\sim$10 mm separated by a distance of $\sim$15 mm. The downstream slit is adjustable and set such that it will not intercept any

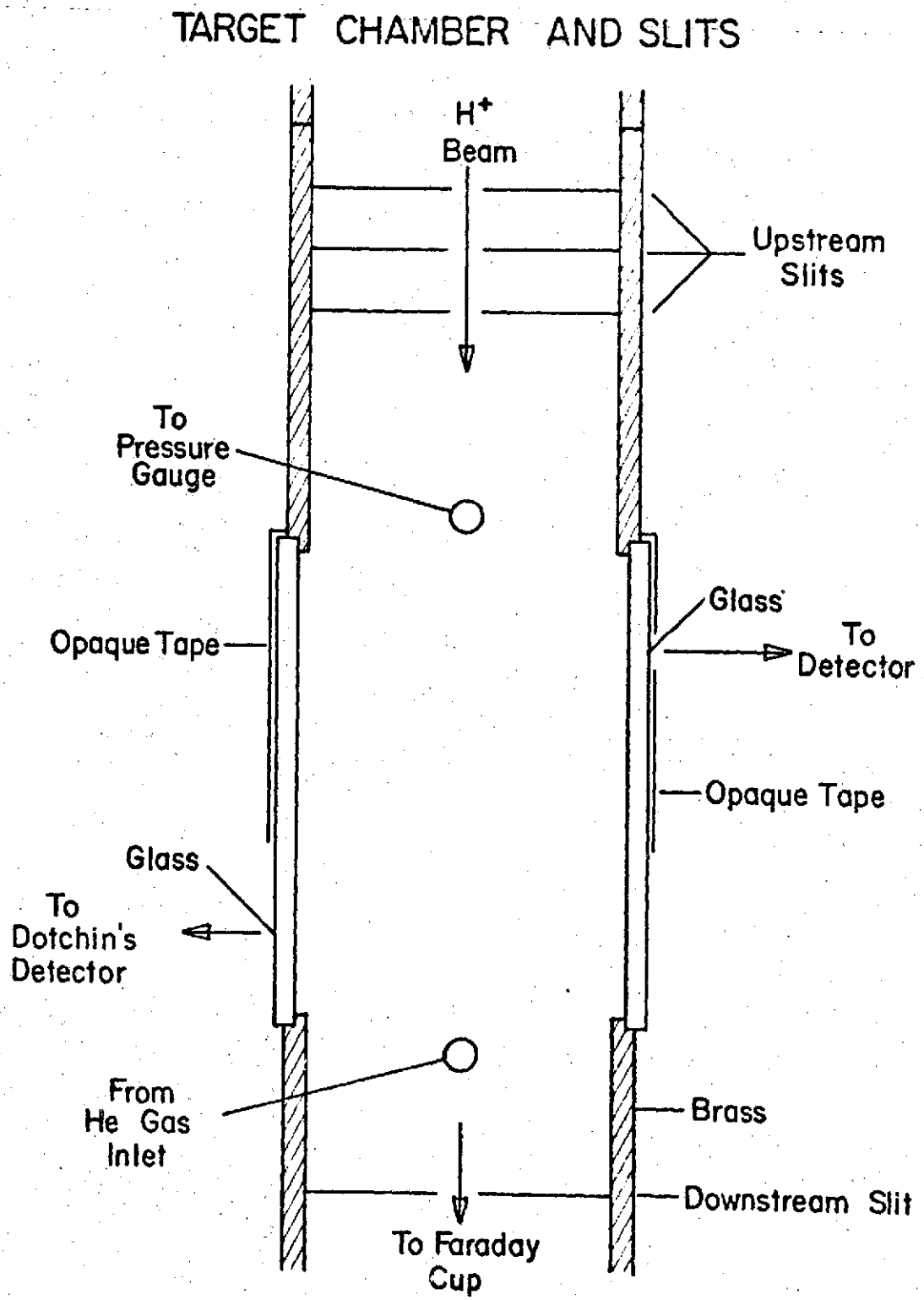
TARGET CHAMBER AND SLITS
H+
Beam
Upstream
Slits
To
Pressure
Gauge
Glass
To
Detector
Opaque Tape
Opaque Tape
Glass
To
Dotchin's
Detector
From
He Gas
Inlet
Brass
Downstream Slit
To Faraday
Cup

FIGURE 6

of the beam (typically 10 mm 45 mm). During operation, the highest pressure used in the target chamber is $\sim 1.5 \times 10^{-3}$ torr, a simultaneous pressure measurement $\sim$70 cm upstream from the triple slit will typically indicate a pressure of 6×10^{-6} torr, a ratio of 250:1. The lowest pressure used in the target chamber is $\sim 10^{-5}$ torr at which time the pressure in the beam tube is $\sim 3 \times 10^{-6}$ torr giving a ratio of $\sim$3:1. Again, differential pumping is required because the beam tube and accelerator must be kept at pressures $< 10^{-5}$ torr; and because we want to spatially localize the beam gas collisions.

The target chamber is a brass cylinder with 5 cm I.D. and 17.7 cm length. Two glass rectangular windows have been attached on opposite sides of the cylinder walls with epoxy cement. The chamber is oriented such that one may look horizontally through both windows. See again figure 6. The window sizes are both 13 cm x 2.3 cm. This target chamber is used both for the mean life studies of Dotchin et. al. and for our polarization studies, each group using one window of the chamber. There are two vacuum couplings on the top of the chamber, one connected through a series of regulators and valves to the gas supply, and the other through valves to our pressure gauge. See figure 7.

The gas supply system is quite conventional with a two stage regulator reducing the tank pressure to a value of $\sim$10 psig. The gas then flows through a

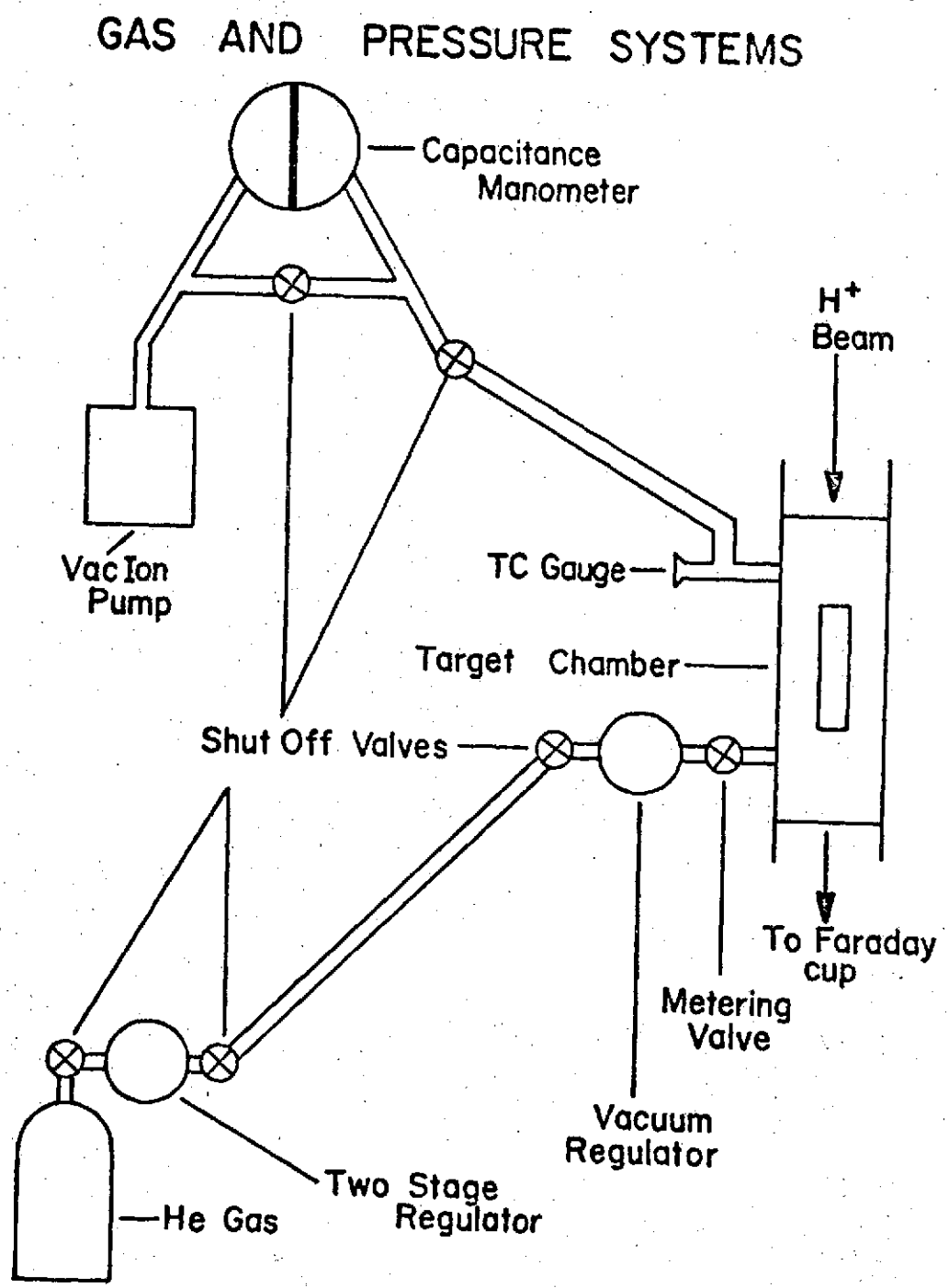
GAS AND PRESSURE SYSTEMS
Capacitance Manometer
H+ Beam
Vac Ion Pump
TC Gauge
Target Chamber
Shut Off Valves
To Faraday cup
Metering Valve
Vacuum Regulator
Two Stage Regulator
He Gas

FIGURE 7

flexible hose to another regulator. This second regulator is a Matheson Co. vacuum type, capable of regulating its output from ∿50 - 750 torr. We typically run at ∿300 torr. Next, the gas encounters a Hoke Micromite fine metering valve, which is used to control its flow into the evacuated target chamber. I would add that without the vacuum regulator, we would only be able to use the first $\frac{1}{10}$ turn of the 18 turn metering valve, whereas, with the vacuum regulator's pressure reduction, we are able to use ∿1-1/2 turns of the valve to achieve the desired pressures within the target chamber.

The pressure measuring system consists of a number of vacuum pressure gauges spread about the beam tube and target chamber, see figures 5 and 7. The gauges located at the main pump, left port pump No. 1 and left port pump No. 2 are the cold cathode type usable from $\sim 1 \times 10^{-6}$torr to 150×10^{-6}torr. The vacuum gauge on left port pump No. 3 is the ionization type usable from $\sim 10^{-9}$ to $\sim 10^{-5}$torr. The above gauges are used for general maintenance of the system and not for data acquisition. An extremely accurate and sensitive MKS Instruments Inc. Baratron capacitance manometer is connected to the target chamber for pressure data measurements. The manufacturer claims a general accuracy of .1 per cent, and repeatability of .005 per cent. The method employed by the designers is to compare the unknown pressure P_x with a smaller known reference pressure P_r. This

comparison is done in our model 77 H-1 pressure head. The head is divided by a highly stressed thin flat metallic diaphragm into two chambers, one for reference pressure, one for the unknown pressure. When the reference and unknown sides differ in pressure, the diaphragm is deformed, but the diaphragm is part of an A.C. capacitance bridge. Therefore, any imbalance in pressure will be transformed into an imbalance in the A.C. bridge. Our type 77M-XR indicator translates this bridge imbalance into a pressure reading. One great advantage of this arrangement is the ability of the indicator to null (or balance) out (digitally) the gross pressure difference and to then use the full sensitivity of the instrument on the finer levels of imbalance. One can then achieve five significant digits in the readout.

In order to achieve high accuracy, one must know the reference pressure P_r, or reduce P_r to a value low enough to cause negligible error. Recall the pressure indicated by the instrument is the difference in pressure $P_x - P_r$. We are using a Varian VacIon pump (2ℓ/sec.) to maintain a very low P_r. We estimate from the current drawn by the VacIon pump, P_r to be $<10^{-6}$torr and would therefore have <10 per cent error in our lowest pressure data.

2.4 The Polarization Detection System

This system is used to detect the intensity of

both the vertically and horizontally linearly polarized components of the 5016 Å ($3^1P - 2^1S$ transition) light from the helium target gas. The system is shown in block diagram in figure 8 and in 1:1 scale in figure 9.

The polarization analyzer consists of a type HN-32 polarizer which has been carefully mounted in a holder and aligned such that it can be rotated from one terminal position by 90 degrees to another terminal position and then back, etc. This arrangement allows the experimenter to set the analyzer (at one terminal position) to pass light whose electric field vector is vertical, and to then rotate the analyzer (blindly) to its other terminal position where it will pass only horizontally polarized light. These rotations are in fact done by the experimenter in the darkened accelerator room. Thus the need for the two (90 degrees apart) terminal positions.

Reflections from the surfaces of the polarizer are according to the manufacturer isotropic and <4 per cent; they can therefore be ignored. As previously stated, the ratio of transmissions for the desired: undesired components is $\sim 1.5 \times 10^4$. This arrangement is then quite suitable for alternate analysis of the orthogonal components of linearly polarized light.

The 5016 Å line of He is selected by an interference filter. This type of filter is a device which will transmit (by constructive interference)

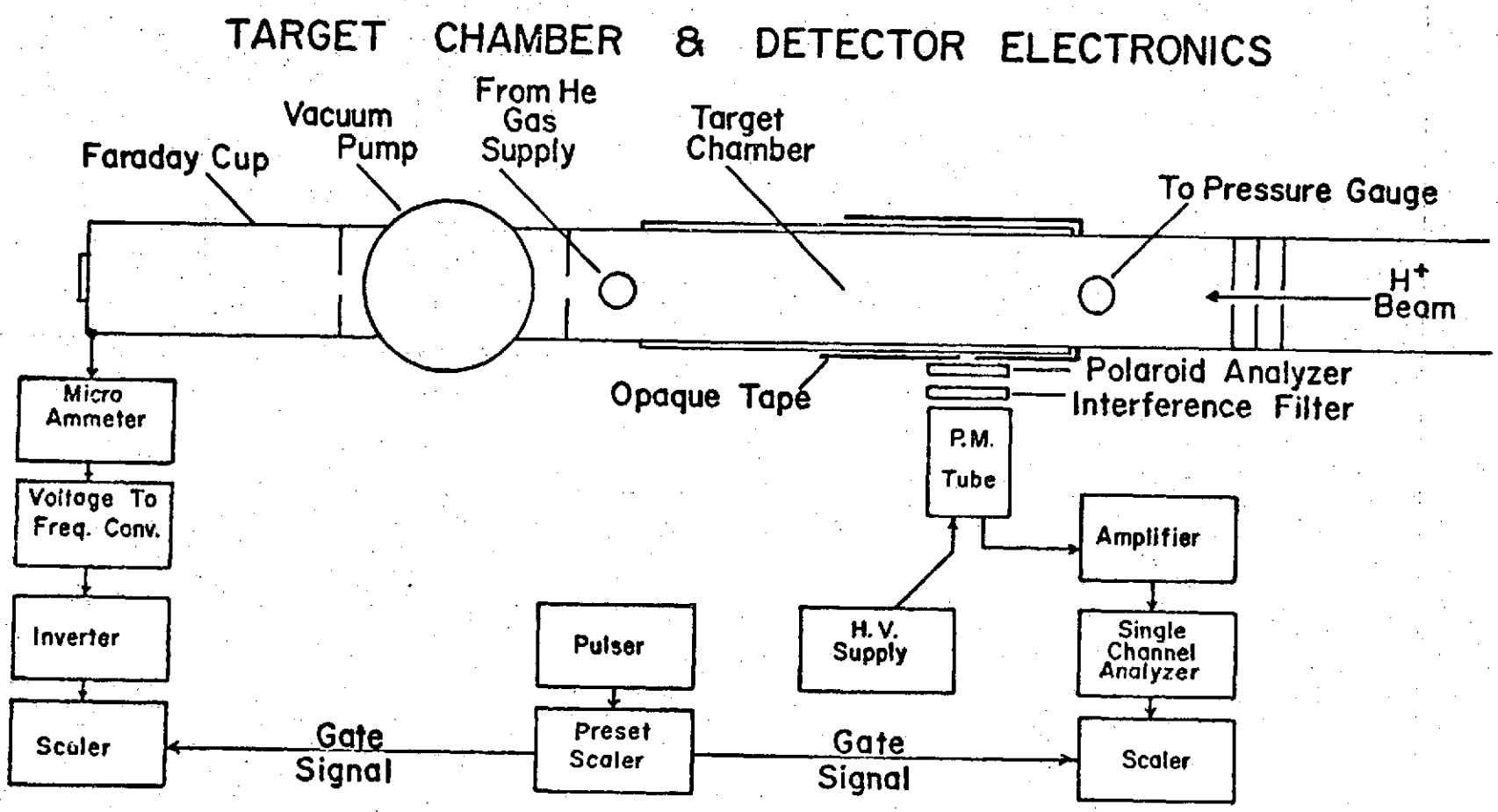
TARGET CHAMBER & DETECTOR ELECTRONICS
Faraday Cup
Vacuum Pump
From He Gas Supply
Target Chamber
To Pressure Gauge
H+ Beam
Opaque Tape
Polaroid Analyzer
Interference Filter
P.M. Tube
Micro Ammeter
Voltage To Freq. Conv.
Inverter
Scaler
Gate Signal
Pulser
Preset Scaler
H.V. Supply
Amplifier
Single Channel Analyzer
Gate Signal
Scaler

FIGURE 8

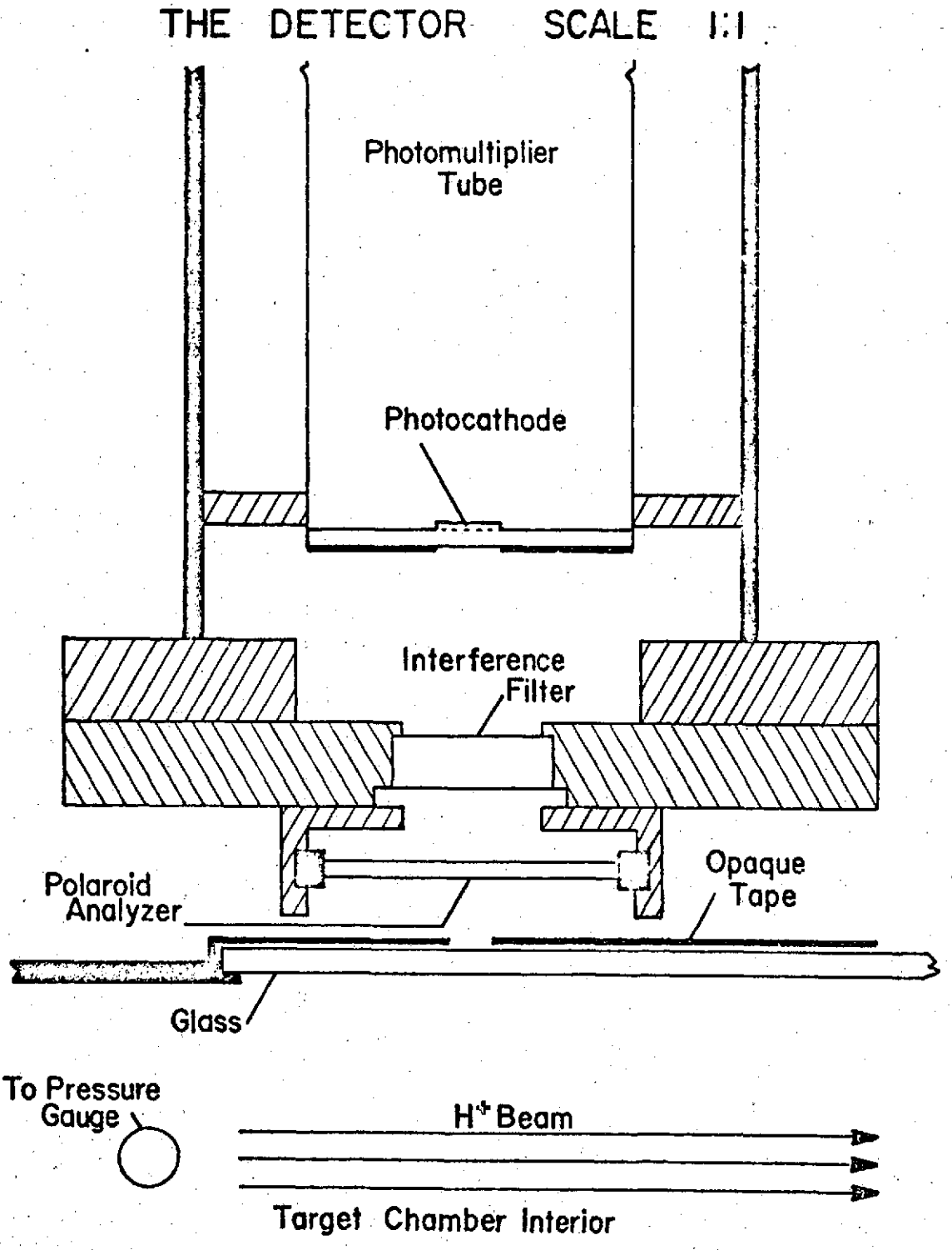

Maximum acceptance angle at photocathode is ∿7°

FIGURE 9

only certain wavelengths of light. The transmission is polarization form independent, and will therefore not effect our measurement. This polarization form independence was tested and confirmed by a rotation of the entire detector and a comparison of the polarization results for the two detector positions. This testing and confirmation process is described in section IV. The filter used for this work was manufactured by Spectra Films Inc., Winchester, Mass. It has a peak transmittance of 60 per cent at 5018 Å, and a full width at half maximum of 18.8 Å for normal incidence. The slight difference in wavelength between our line (5016 Å) and peak is not significant, it only reduces the percentage transmission for our line to 58 per cent, a 2% loss. See figure 10.

The need for such a filter becomes apparent when one examines the He spectrum. There are a large number of prominent lines in the spectrum. Table 1 lists some of those lines near our 5016 Å line. Also, a partial energy diagram for He is shown in figure 11, and figure 12 shows a spectral scan in the region around 5016 Å. The lines nearest 5018 Å are at 5047 Å and 4922 Å. It is necessary that our interference filter not transmit these or any other lines. We have no problem when the Helium light is normally incident upon the filter, the 5047 Å line is attenuated by ∿99 per cent, and the 4922 Å line is attenuated by >99 per cent. However, all the light incident upon the filter is not normally incident, and

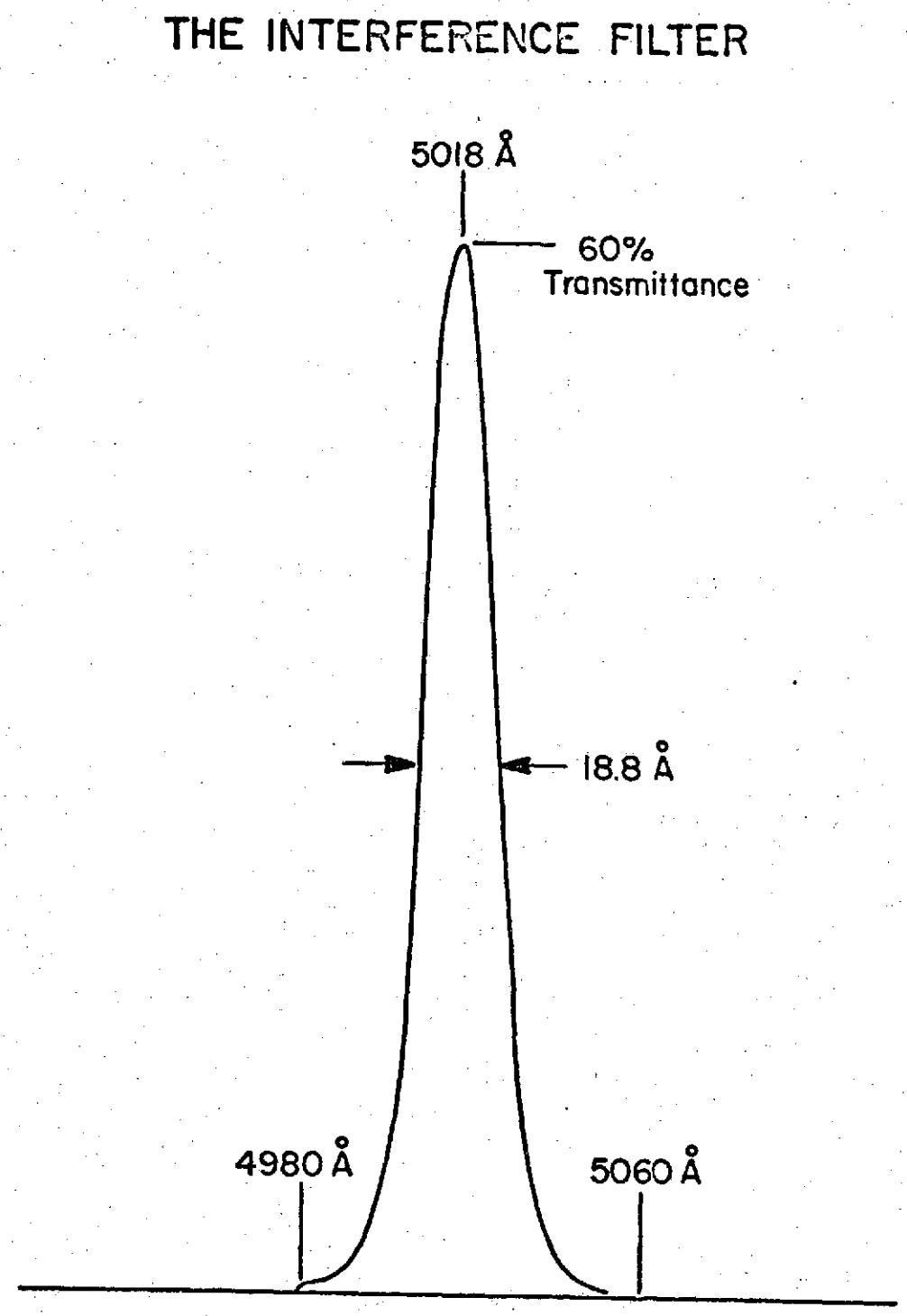
THE INTERFERENCE FILTER
5018 Å
60%
Transmittance
18.8 Å
4980 Å
5060 Å

FIGURE 10

TABLE 1

HELIUM TRANSITIONS NEAR 5016 Å

Wavelength(Å)	Transition	(5016 Å - λ)Å
4713	$4^3S \rightarrow 2^3P$	303
4859 (He II)	8→4	157
4922	$4^1D \rightarrow 2^1P$	94
5047	$4^1S \rightarrow 2^1P$	-31
5411 (He II)	7→4	-395

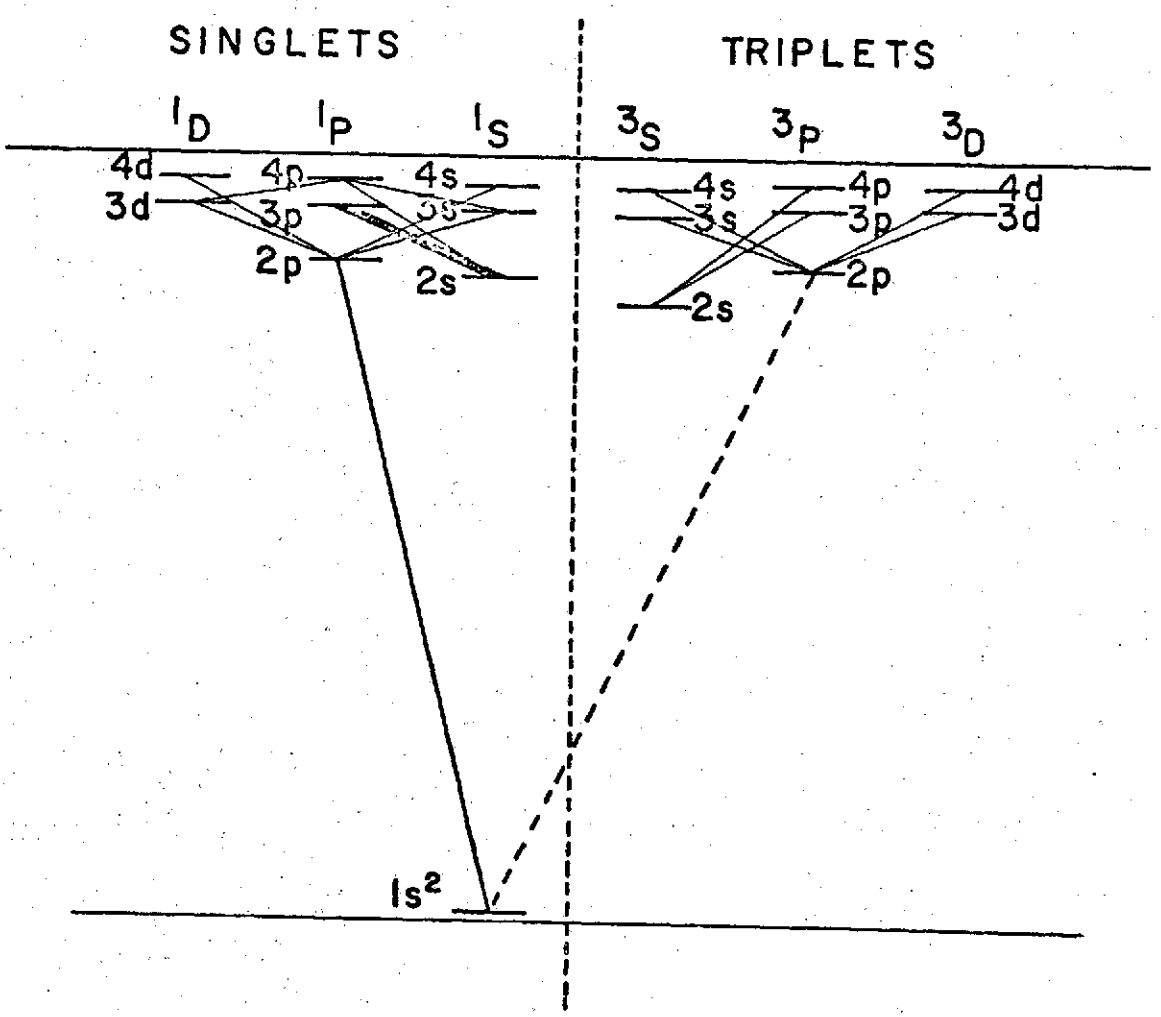

The 3^1P-2^1S transition is indicated by a heavy line

FIGURE 11

PARTIAL HELIUM SPECTRAL SCAN

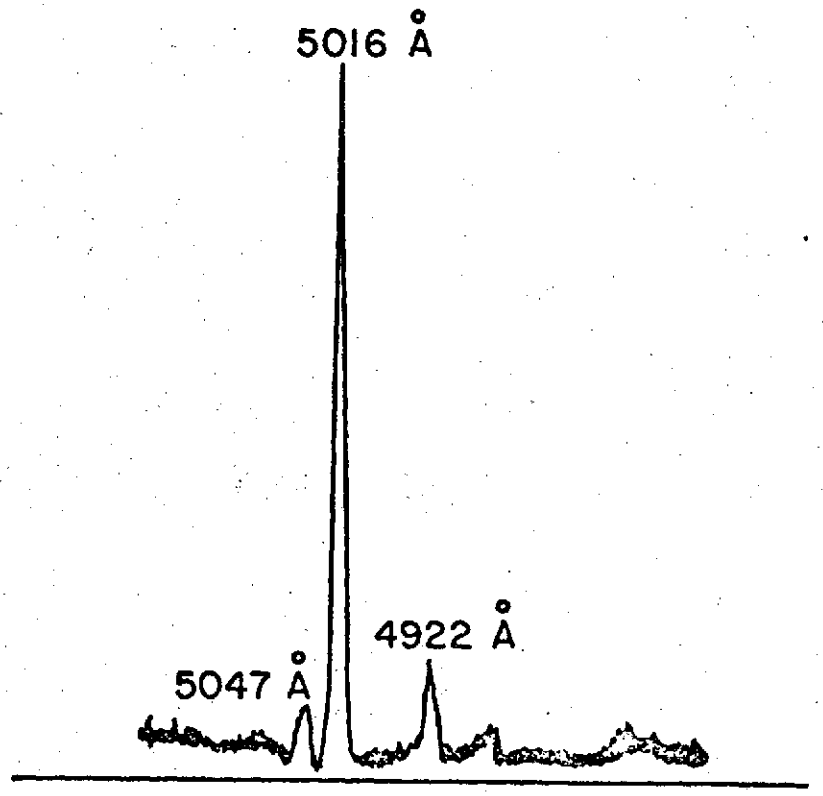

FIGURE 12

λ_{peak} is in fact, a function of the angle of incidence. According to Baird-Atomic, a manufacturer of interference filters, the wavelength of peak transmittance is lowered as the angle of incidence increases, such that

$$\lambda_\theta = \lambda_0 \left[1 - \frac{\sin^2\theta}{n^2}\right]^{\frac{1}{2}}$$

where θ is the angle of incidence, λ_θ is the wavelength of peak transmittance for the angle of incidence, λ_0 is the wavelength of peak transmittance for normal incidence and η is the effective index of refraction of the filter. A short computer program was written to compute λ_θ as a function of both θ and η. The program is listed in Appendix C.1, and the results are shown in Table 2.

In our detector (see again figure 9) the largest possible incidence angle is $\sim 7^0$. Referring to Table 2, we then see that the worst possible case (n=1) has a λ_{peak} = 4980 Å. This worst case is still quite good since ~99 per cent attenuation is achieved at only ~22 Å from λ_{peak} (see again Figure 10). Our interference filter is then quite sufficient to isolate the 5016 Å line of helium.

A photomultiplier tube and associated electronics are used to measure light intensity. We refer again to Figures 8 and 9 where the tube, its housing and the various electronics are shown. The tube is an EMI 6256S, ~2 inch diameter, S(Q), S_bC_s photocathode, and very low ($\sim 2 \times 10^{-9}$A) dark current at the operating

TABLE 2

PROPERTIES OF THE INTERFERENCE FILTER

Index of Refraction	Angle of Incidence (deg)	λ_θ (Å)
1.0	0°	5018
"	4	5005
"	8	4969
1.4	0	5018
"	4	5011
"	8	4993
1.6	0	5018
"	4	5013
"	8	4998

voltage of -1850 volts. The tube is wrapped with black tape and housed in an aluminum light-tight container with a single aperture in front of the photocathode. The tube base is wired as shown in Figure 13, and power is supplied by a Power Designs Pacific Inc., Model 2k-10 high voltage power supply. The spectral response of the photocathode is near its peak at 5000 Å (10 per cent quantum efficiency) and is well suited for measurements on the 5016 Å line. The tube was usually operated at room temperature excepting very warm days when ice water cooling was necessary to bring background count rates back down to "normal."

Signal pulses from the tube were fed into a C.I. 1416 Amplifier, these amplified pulses were next passed through a C.I. 1430 single channel analyzer which was used as a discriminator to reject pulses of less than a preset magnitude. The Scalar output of the single channel analyzer was passed to a C.I. 1470 scalar for counting. It was found that the discriminator setting had little effect upon the final signal to noise ratio, therefore, a setting was chosen to give a reasonable counting rate. This same effect was noticed by Pegg (1970), who used this same tube and similar electronics.

A second photomultiplier tube was used briefly during this research, it was mounted directly on the second window of the target chamber and monitored the helium light output for normalization purposes. The

PHOTOMULTIPLIER BASE CIRCUIT

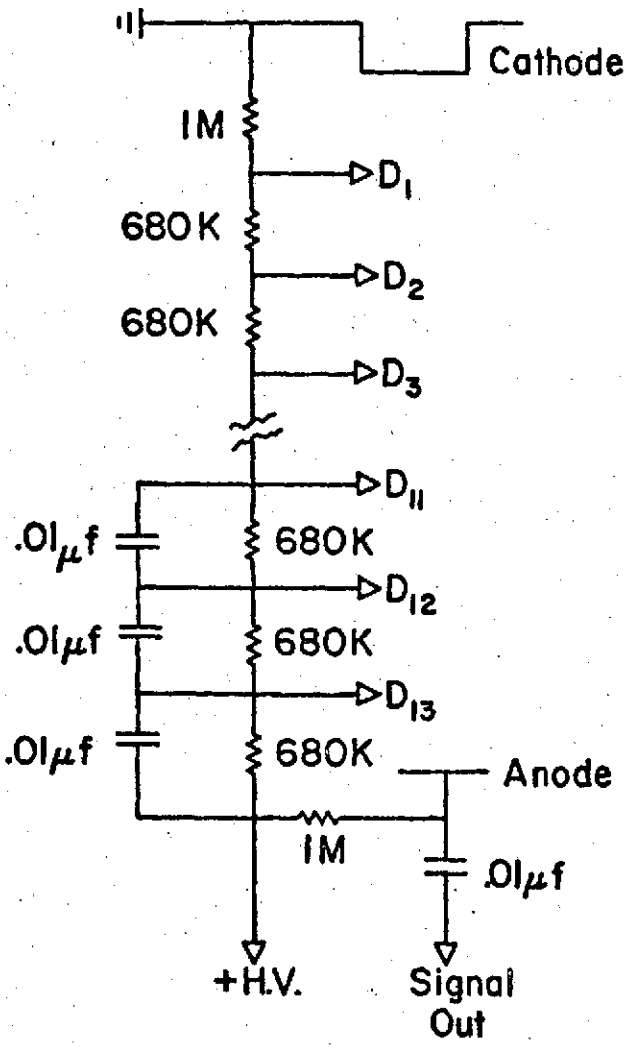

FIGURE 13

tube was an RCA 8575 run at -2500 volts, at room temperature. The arrangement is shown in figure 14. This system was used only long enough to confirm that light normalization and current normalization gave the same value for the linear polarization fraction, it was then abandoned so as to minimize the changeover time between the experiment of Dotchin et. al. and this work.

Due to the fact that the proton beam from the accelerator is not stable, we must use a Faraday cup to determine just how much beam we have had in any counting period. The cup is really just an extension of the beam tube, of length 14.5 cm, with an oval entrance aperture ($\sim$10 mm x $\sim$20 mm). The downstream end is closed by a double end window of Vycor glass. See figure 15. We depend upon the length of the cup, and the entrance aperture to contain secondary electrons. A comparison of beam current measurements was made for two lengths of the cup with and without the aperture, since the results were essentially identical, we concluded that secondary electrons were not escaping and that the cup was containing the proton beam. We therefore felt there was no need for a suppression grid. The electronics for the cup were shown in figure 8, and consist of Keithly Model 610 Microammeter, a homemade voltage to frequency convertor, a C.I. invertor, and a Mechtronics 700 scalar. In use, the microammeter is connected directly to the Faraday cup, the D.C. chart recorder output of the

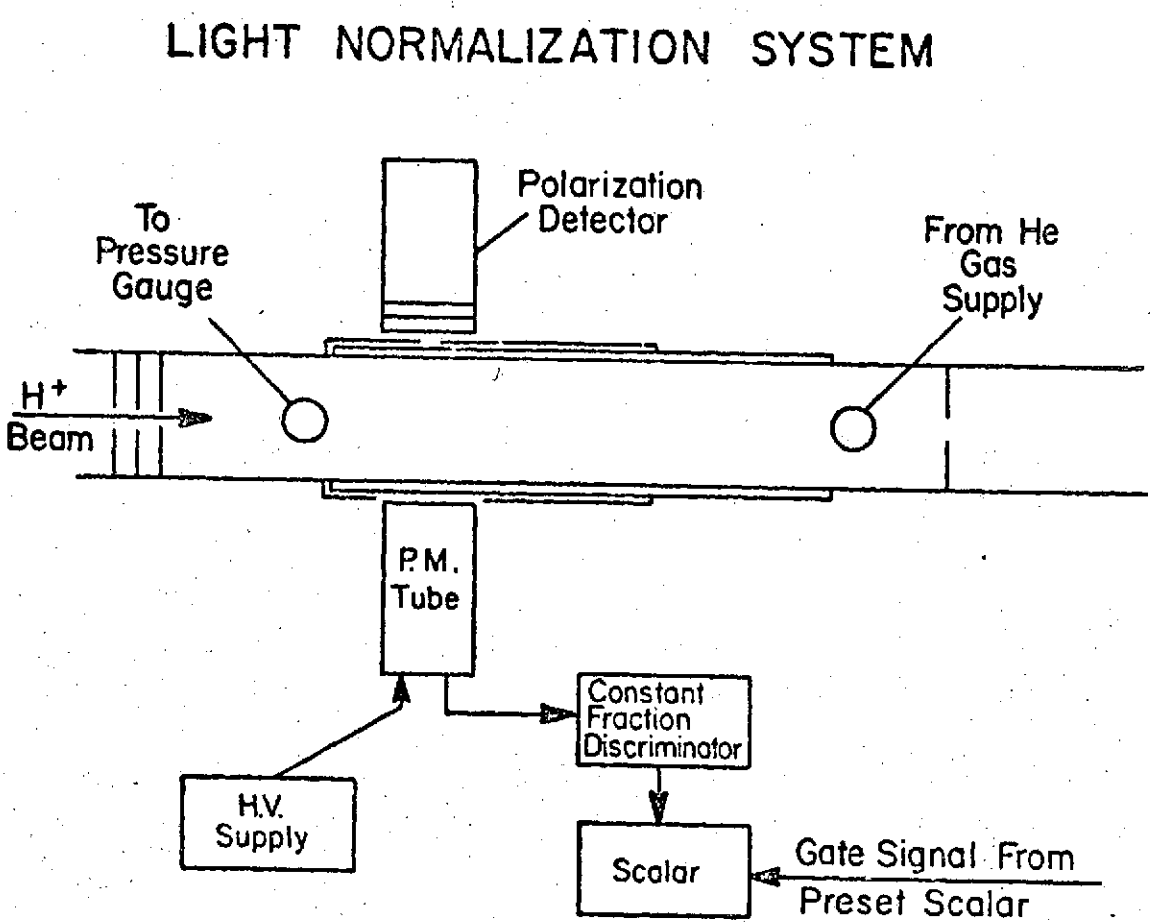
LIGHT NORMALIZATION SYSTEM
To
Pressure
Gauge
Polarization
Detector
From He
Gas
Supply
H+
Beam
P.M.
Tube
Constant
Fraction
Discriminator
H.V.
Supply
Scalar
Gate Signal From
Preset Scalar

FIGURE 14

THE FARADAY CUP

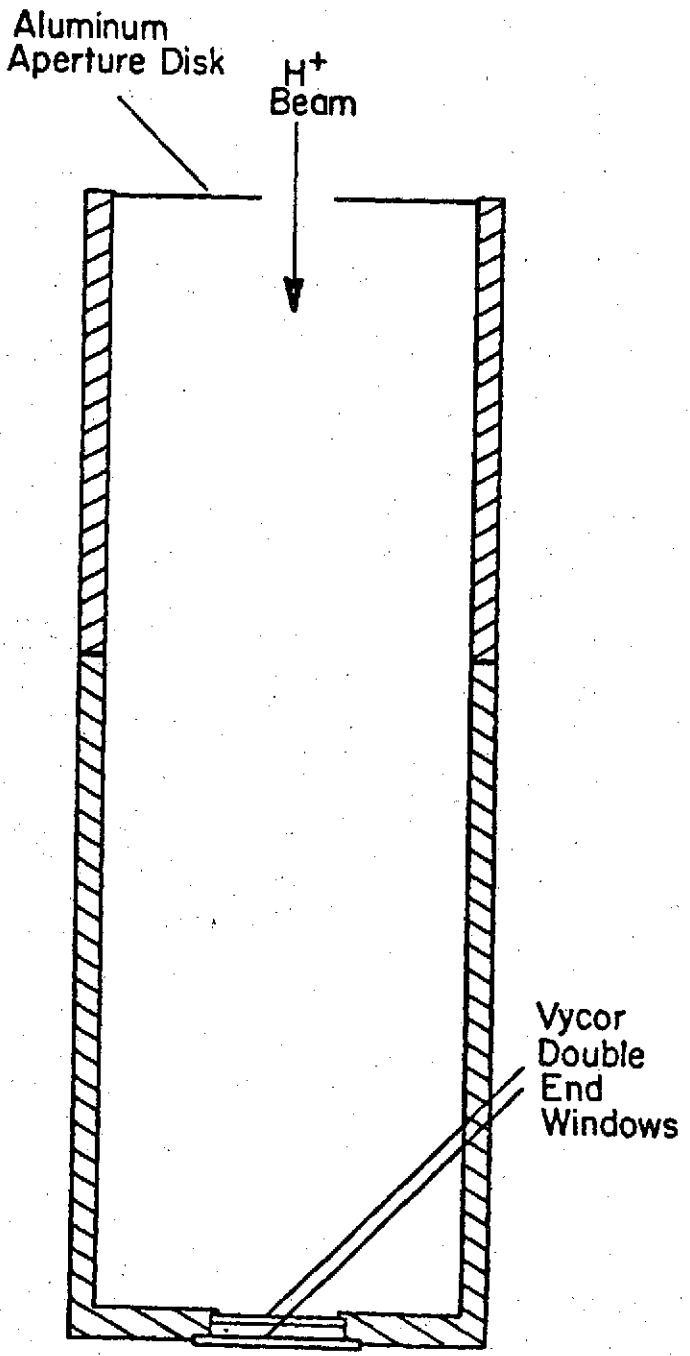

FIGURE 15

microammeter is sent to the voltage to frequency convertor (built by L. W. Dotchin from plans in the General Electric Transistor Manual, General Electric Co., Syracuse, N. Y. 1964). The pulses from the convertor are inverted to match the input requirements of the scalar where they are counted. The number of counts appearing on this scalar is directly proportional to the number of protons passing through the target chamber, and can therefore be used as a normalization base.

SECTION III

EXPERIMENTAL METHOD

3.1 Introductory Description

The methods used in this research have been evolved so as to maximize the usefulness and effectiveness of the apparatus with which we have worked. Methods were evolved to deal with the irregularities in the proton beam from the Van de Graaff accelerator. In fact two methods were developed and used simultaneously and gave the same value for the linear polarization fraction. The need for these normalization methods and their implementation will be discussed in the next paragraph.

The actual data taking process is dependent upon the type and settings of electronics used. One must remain within the useable limits of the electronics while at the same time maximizing the signal to noise ratio. Our methods for achieving this end are described in paragraph 3.3.

Finally the actual step by step data taking process is outlined in paragraph 3.4.

3.2 The Need for Normalization

The Van de Graaff accelerator, being mechanically powered, is more susceptible to irregularities than most other pieces of apparatus. The proton beam from the accelerator typically undergoes three different types of transition, irregular oscillations of beam current, long term upward or downward drift of beam current, and sudden $\sim$1/2 to 1 1/2 second complete cessations of beam.

The irregular oscillations in the beam current are probably due to a number of factors including; irregular transport of charge by the belt within the accelerator; fluctuations in the probe voltage (the probe voltage supply is powered by a generator driven by the belt); and overcorrections in the negative feedback loops of the energy stabilization system. In so far as our experiment is concerned, high frequency oscillations are of no importance, they would simply average over the >1 second observation period used in taking data. Low frequency oscillations must be accounted for in order to correctly compare intensity measurements taken at different times.

Long term upward or downward drifts of beam current must be dealt with in the same manner as the low frequency irregular oscillations, especially if these drifts are noticeable within $\sim$1 second periods. These long term drifts are most likely due to changes in the

rate of flow of H_2 through the paladium leak.

The sudden cessations of beam are usually due to sparks within the accelerator tube, sparks among the equipotential planes, or a spark from the high voltage terminal to the tank wall. Occasionally, the beam is lost for a short time when the energy stabilization system is unable to correct for an excess or lack of charge on the high voltage terminal. The beam energy will then be too high/low for the magnet to steer the beam into the left port beam tube and the beam will be lost until the charge situation corrects itself. In any case, whenever the beam is interrupted, the data taken at that time is not used, the machine is reset if necessary and new data is taken. The problem is to determine when an interruption has occurred. The problem is solved by making the experimenter a part of the apparatus. While taking data, the experimenter stands at the end of the left port beam tube and stares at the Vycor end window of the Faraday cup. In striking the Vycor, the proton beam generates a distinct blue light. With practice, the experimenter can spot beam interruptions (as an interruption of the blue light) which last for as short a time as $\sim$1/10 second. The data is then not used, the scalars are reset and new data is taken.

Again, normalization is required so that one may compare intensity measurements made at different times even though the beam current is not constant in time.

Also, the experimenter is part of the apparatus not only in the sense of making adjustments, but also as a sensor using eyes and even ears to detect irregularities in the Van de Graaff performance.

We have used two different normalization systems to monitor beam current. In the first case, we monitored the irregularities in the light output of the helium target gas. This system was based upon the assumption that the light output was directly proportional to the number of excitations which had occurred within the target chamber. The second system was a bit more direct, we used a Faraday cup to collect the beam after its passage through the target chamber (assuming very little loss) and integrated the beam current. The first system then normalizes to the number of excited helium atoms (assuming no saturation occurs), while the second system normalized to the number of protons passing through the target chamber. We formulated the hypothesis that the number of excitations should be directly proportional to the number of protons passing through the chamber, i.e. that calculations based upon data taken simultaneously with both systems should give the same result. This was in fact the case demonstrating that our two normalizing systems were equivalent. Once we were satisfied as to that equivalence, the light normalization system was deleted from the experiment. Its continued use would have created large scale problems during the

changeovers between this work and that of Dotchin et al. All the data and results presented in this work are based upon the current normalization system.

3.3 Setting the Detector System

The system is "set" by properly adjusting all discriminators, amplifier gains, and miscellaneous other parameters.

A very simple and direct method is used to time the runs, in fact, all runs have the same duration. As shown in Figure 8 , an Ortec 480 pulser drives a presetable Mectronics 702 scalar/timer. Pulses are generated by the pulser in syncronization with the A.C. line frequency, i.e. 60 pulses/second. The Mectronics scalar/timer is preset to turn off at 80 counts, (or 80/60 of a second = $1.\overline{3}$ second). When the scalar/timer shuts off, it will simultaneously (i.e. in a time which is short compared with the average time between data pulses to the other scalers) shut off, via built-in gating circuits, the other two scalars. The counting time of $1.\overline{3}$ second was in part forced upon us by the data count rates, and by the tendency of the Van de Graaff to spark quite often. We wanted a counting time of the order of 1 to 1 1/2 seconds in order to get convenient count rates and yet still be short enough so that the probability of a spark (beam interruption) would be small, $1.\overline{3}$ second

was the best available compromise.

The amplifier gains, discriminators, and photomultiplier tube high voltage have been set for single photon counting and zero dead time correction. Typical count rates are shown in table 3.

The scalars used are capable of count rates on the order of 10^4-10^5 counts/second before dead time corrections are needed.

The signal count rate for the normalization scalar is controlled by the range switch on the Keithly microammeter. The output of the Keithly is the same percentage of 10 volts as is the indicator of full scale. We limit, by choice of range, the percentage of full scale such that the input voltage to the voltage to frequency converted does not exceed 2 volts, which in turn limits the count rate.

The criteria for the polarized light intensity scalar is that the tube be operating in the single photon counting mode and that extraneous noise not be counted. The count rate is then controlled by tube voltage, amplifier gain, and the single channel analyzer's discriminator.

The sources of background counts are noise pulses (both thermal and light noise) in the case of the polarized light intensity scalar; and zero offset of the Keithly microammeter in the case of the normalization scalar. To minimize background counts in the first case,

TABLE 3

SCALAR COUNTING RATES

Scalar	Signal + Background rate	Background rate
Scalar/timer	60/sec	0
Light intensity	100 to 5000/sec	10 to 50/sec
Normalization	∿1300/sec	∿7/sec

one darkens the accelerator room, uses lead bricks to shield the tube from tank x-rays, and when necessary, cools the tube. In the case of the normalization scalar, one can "adjust" the background count rate by adjusting the zero of the microammeter. We have always chosen to carry a background rate of ∿2 to ∿8 counts/second so that we were sure that the "zero" was not negative. A negative zeroing of the microammeter would have given us a false (low) value for the integrated beam current.

Our next problem is that of maximizing the signal to noise ratio. Only in the polarized light intensity scalar is the S/N ratio low enough to merit concern. The only option, after external noise sources have been eliminated, is to try adjusting the discriminator of the single channel analyzer. We have found no appreciable changes in S/N over a wide range of discriminator settings. (The S/N ratio is a function of the pressure and ranges from ∿3 to ∿100.) We have therefore arbitrarily chosen a discriminator setting which results in a convenient count rate. Again, see Pegg (1970) for further discussion.

3.4 Taking Data

The steps followed in the actual data taking are:

1. Warm up phototube and electronics for ∿12 hours.

2. Warm up accelerator for ∿1 hour
3. Turn on beam in center port, adjust current and energy
4. Steer beam into left port, adjust current and energy
5. Go downstairs and . . .
6. Start flow of He into target chamber, adjust pressure
7. Assume data taking position at end of left port beam tube
8. Reset all scalars
9. Switch beam off by remote switch
10. Start scalars for background count
11. Record values on scalars
12. Turn beam back on
13. Rotate polarizer (by hand) for passing E vector vertical
14. Reset scalars
15. Start scalars
16. Record values
17. Rotate polarizer 90° (by hand)
18. Start scalars
19. Record values
20. Repeat 13-19 with occasional background runs (beam off)

A normal data run will consist of first a background reading for the polarization and normalization

scalars; then 7 sets of "polarization vertical" - normalization - "polarization horizontal" - normalization; then a background run; then 6 sets of data; then a background run; then 7 sets of data; and finally a last background run. Typically, a data run (20 measurements + 4 backgrounds) will take ∿3/4 hour exclusive of tune up time for the Van de Graaff (another ∿1/2 hour). Table 4 is an actual data page from the laboratory notebook.

TABLE 4

DATA FROM THE LAB NOTEBOOK

300 kev .2 μHe 11.5 ±2 μAHr

Zero Bm Vac Ion < 5 mA

.2 μHe

49	8		4	c
V	c			
899	1467		818	1502
902	1523		815	1533
863	1533		852	1539
782	1486		838	1524
792	1531		795	1546
809	1538		778	1553
809	1558	.19	780	1553
35	8	.2		
847	1430		795	1514
894	1559		784	1565
804	1569		784	1546
819	1549		802	1547
824	1550		873	1553
900	1564	.19	793	1567
52	9	.2		
885	1633		883	1638
952	1634		838	1557
906	1587		878	1600
871	1604		888	1606
892	1609		844	1607
936	1606		927	1599
661	1421		880	1484
47	10	.2		

Zero check ± .01μ for was .19μ

SECTION IV

ANALYSIS

4.1 Calculating π

The linear polarization fraction π is defined as . . .

$$\Pi = \frac{I_{//} - I_{\perp}}{I_{//} + I_{\perp}} \qquad 4.1.1$$

where $I_{//}$ and $I_{\perp}$ are the intensities of the light with electric field vectors respectively horizontal (parallel) and vertical (perpendicular). These intensities are determined from the number of counts showing on the scalars at the end of each parallel and perpendicular data acquisition period. We must of course subtract any background counts which are included in the scalar display. Furthermore we must normalize these intensities to integrated beam current (as discussed in section 3). Therefore the intensities are expressed as . . .

$$I_{//} = \frac{C_{//} - B_{I}}{N_{//} - B_{N}}$$

$$I_{\perp} = \frac{C_{\perp} - B_{I}}{N_{\perp} - B_{N}} \qquad 4.1.2$$

where in both cases the numerator represents signal counts, i.e. total counts (on the light intensity scalar) minus background counts. The denominator in both cases is proportional to the number of protons which have passed through the target chamber, represented by total counts (or the normalization scalar) minus background counts. Thus $I_{//}$ and $I_{\perp}$ are the intensities per proton, and are therefore independent of small fluctuations of the proton beam current. We then have the following definitions . . .

$C_{//}$, $C_{\perp}$ = The number of counts on the light intensity scalar for the parallel and perpendicular data acquisition periods.

B_I = The average number of background counts on the light intensity scalar.

$N_{//}$, $N_{\perp}$ = The number of counts on the normalization scalar for the parallel and perpendicular data acquisition periods.

B_N = The average number of background counts on the normalization scalar.

At first glance a non zero B_N is not expected, however we purposely set the zero adjustment of the Keithly microammeter to give a small background on the normalization scalar. This was done so that we could be assured (by checking background counts) that the microammeter zero adjustment was not set negative. Therefore we were

assured that no counts were lost.

We then do the actual calculation of the linear polarization fraction π from . . .

$$\pi = \frac{\frac{C_{//} - B_I}{N_{//} - B_N} - \frac{C_{\perp} - B_I}{N_{\perp} - B_N}}{\frac{C_{//} - B_I}{N_{//} - B_N} + \frac{C_{\perp} - B_I}{N_{\perp} - B_N}} \qquad 4.1.3$$

Note that a calculation of π requires two data acquisition periods, one for the parallel and one for the perpendicular orientation of the polarization analyzer. A typical data run then consisted of twenty measurements of $I_{//}$ and $I_{\perp}$, and then the twenty calculations of π. The average backgrounds B_I and B_N were found from four measurements taken before, during and after the data run. See again table 4.

The actual calculations are done on the University of New Hampshire's IBM Call 360 time sharing computer system.

The computer program which does this calculation (called NEWPOL and listed in Appendix C.2) will print out $C_{//}$, $N_{//}$, $C_{\perp}$, $N_{\perp}$, and π all twenty times and will then print a mean π, the standard deviation, and the standard error of the mean, the beam energy, current, the He target pressure, and the number of π's deviating by more than two standard deviations from the mean π. Table 5 shows the program output created from the data of table 4.

TABLE 5

OUTPUT OF THE PROGRAM NEWPOL

```
LINEAR POLARIZATION FRACTION
# OF RUNS TO ANALYZE IS?1
LIST ALL P?YES
```

V	C	H	C	P
899	1467	818	1502	-0.06165
902	1523	815	1533	-0.05680
863	1533	852	1539	-0.00874
782	1486	838	1524	0.02395
792	1531	795	1546	-0.00290
809	1538	778	1553	-0.02561
809	1558	780	1553	-0.01775
847	1430	795	1514	-0.06218
894	1559	784	1565	-0.07126
804	1569	784	1546	-0.00594
819	1549	802	1547	-0.01047
824	1550	873	1553	0.02955
900	1564	793	1567	-0.06777
885	1633	883	1638	-0.00273
952	1634	838	1557	-0.04292
906	1587	878	1600	-0.02064
871	1604	888	1606	0.00957
892	1609	844	1607	-0.02856
936	1606	927	1599	-0.00288
861	1421	880	1484	-0.01030

```
300 KEV,   .20 U HE,  11.5 U A H+,   20 TRIALS
ST DV = .02991     0 PTS DV > 2 SIG    S.E.= .00669
(P-SE)=-.02849     MEAN P =-0.02180    (P+SE)=-.01511
```

4.2 Polarization Measurement Error Analysis

There are of course two types of error inherent in this experiment. Random errors occur due to the normal variations (fluctuations) in counting rates; and systematic errors occur if faulty equipment and/or methodology is used. The random errors present a problem only in that they limit the precision of the calculation of π; any systematic error could reduce the accuracy of the experimental result.

We will first discuss the random errors present in this work. The linear polarization fraction π is calculated from Eq. 4.1.3. The variables which appear in this equation are simply the numbers which are displayed by the scalars at the conclusion of each of two 1 1/3 second intensity data acquisition periods, as well as the average of four 1 1/3 seconds background count acquisition periods. Every one of these scalar displayed numbers is subject to normal statistical fluctuations, thus when π is calculated, the precision of a single calculation is quite poor. We therefore repeat the measurements from which π is calculated twenty times for each "run," and take many runs for every "final" value of π. The π which we will report as a result is the average of Nx20 values, (where N is the number of runs at some particular pressure, beam current, and beam energy). Thus, the precision of this work is enhanced by repeating our

measurement a multitude of times.

In order to analyze our random errors, we must take care to distinguish between sample variables and population variables. We will follow the notation of Parratt (1971) and Wilson (1952) where the sample (run) mean, standard deviation, and standard error are symbolized by m,s, and s_m; while the population mean, standard deviation, and standard error are symbolized by μ, σ, and σ_m. We are of course most interested in μ and σ_m since we will report the linear polarization fraction in terms of our best estimate of the parent population mean, and its standard error. The procedure is outlined in the following formulae where π_{ij} is the calculated π from one set of measurements for the j^{th} run (i.e. 1/20 of a run) and n=20. All π_{ij} are equally weighed. For each run, where j is the run index

$$m_j = \sum_{i=1}^{n} \frac{1}{n} \pi_{ij} \qquad 4.2.1$$

while for the best estimate of the parent population mean . . .

$$\mu' = \sum_{j=1}^{N} \frac{1}{N} \sum_{i=1}^{n} \frac{1}{n} \pi_{ij} \qquad 4.2.2$$

where N is the number of runs at some particular He target gas pressure, beam current and energy. It now remains to calculate and estimate the dispersions in the sample and parent populations. The standard deviations s and σ are

suitable dispersion indicies. For each run we have

$$S_j = \left[\sum_{i=1}^{n} \frac{1}{n} \left(\pi_{ij} - m_j \right)^2 \right]^{\frac{1}{2}} \qquad 4.2.3$$

while for the parent population we have

$$\sigma = \left[\sum_{j=1}^{N} \frac{1}{N} \sum_{i=1}^{n} \frac{1}{n} \left(\pi_{ij} - \mu \right)^2 \right]^{\frac{1}{2}} \qquad 4.2.4$$

However, μ is never known exactly, only estimated as μ' from Eq. 4.2.2. The best estimate of σ (see the appendix of Bacon (1953) is then

$$\sigma = \left[\sum_{j=1}^{N} \sum_{i=1}^{n} \frac{1}{(nN-1)} \left(\pi_{ij} - \mu' \right)^2 \right]^{\frac{1}{2}} \qquad 4.2.5$$

Since in this work we take many runs and calculate a mean π for each, it is useful to also calculate the standard error σ_m (also called the standard deviation in the mean). The experimental standard error S_m is

$$S_m = \left[\sum_{j=1}^{N} \frac{1}{N} \left(m_j - \sum_{j=1}^{N} \frac{1}{N} m_j \right)^2 \right]^{\frac{1}{2}} \qquad 4.2.6$$

where $\sum_{j=1}^{N} \frac{1}{N} m_j$ is the grand mean, or mean of means. S_m is more easily estimated from the standard deviation s by

$$S_m = \frac{1}{\sqrt{n}} S \qquad 4.2.7$$

where in our case n=20, the number of π's in one run. We are in fact more interested in the standard error σ_m of the parent distribution.

$$\sigma_m = \lim_{N\to\infty} \left[\sum_{j=1}^{N} \frac{1}{N} (m_j - \mu)^2 \right]^{\frac{1}{2}} \qquad 4.2.8$$

and

$$\sigma_m = \frac{1}{\sqrt{nN}} \sigma \qquad 4.2.9$$

Again μ is unknowable exactly and we must estimate σ_m. Using 4.2.9 with 4.2.5, we arrive at the useful result that

$$\sigma_m = \left[\sum_{j=1}^{N} \sum_{i=1}^{n} \frac{1}{nN(nN-1)} (\pi_{ij} - \mu')^2 \right]^{\frac{1}{2}} \qquad 4.2.10$$

According to statistical theory, the mean π of any run has a probability of 68.3% of falling between the values of $\mu \pm \sigma_m$.

We calculate and report as follows . . . for every run of n=20 π's, we calculate the mean for the run m_j (Eq. 4.2.1); an estimate of the parent population standard deviation for the run σ_j (Eq. 4.2.5, with N = 1) and the estimated population standard error σ_m (Eq. 4.2.10, with N = 1).

When sufficient runs at a particular He target gas pressure, beam current and energy have been

accumulated, the Nx20 π values are combined to estimate the population mean μ' (Eq. 4.2.2), usually written simply as π; the population standard deviation σ (Eq. 4.2.5); and the population standard error σ_m (Eq. 4.2.9).

In the first case where single runs are analyzed, the computer program NEWPOL is used (Appendix C.2), for calculation of the accumulated result the computer program STAT is used (Appendix C.3).

When our results are given in the next section, we will report the estimated population mean and the standard error σ_m.

We must now discuss possible systematic errors since this type of error will reduce the accuracy of any experiment. Some typical examples of systematic error are . . .

1. Subconscious bias on the part of the observer
2. Incorrectly calibrated instrument(s)
3. Misaligned apparatus
4. Lack of correction for changing environmental conditions
5. False assumptions of independence of result from an experimental parameter
6. etc.

In this work, the greatest possibility for a

systematic error lies in whether or not our polarization detector is biased. We evolved a simple method for determining the existence of any bias. Our polarization detector housing was modified such that it was possible to rotate the entire detector, about its line of sight, by 90°. When we then compared π results arrived at for the detector normal (N) position and the results for the detector rotated (R) position, we could unfold any detector bias. We chose to do this procedure over a range of proton beam energies with constant beam current and He target gas pressure. Many runs were taken at each energy with detector (N) and (R). The means π_N and π_R were calculated at each energy along with the estimated population standard deviations σ_N and σ_R. We are then able to use the "student" t test for the significance of the difference of means as described by Spiegel (1961). The t test is derived from small sampling theory (although, under conditions of large samples, it becomes equivalent to the z statistic). Using our notation . . .

$$t = \frac{\mu'_N - \mu'_R}{\sigma' \sqrt{\frac{1}{nN_N} + \frac{1}{nN_R}}} \qquad 4.2.11$$

where n again is 20 and N_N (N_R) is the number of runs with detector N(R). Also,

$$\sigma' = \sqrt{\frac{nN_N S_N^2 + nN_R S_R^2}{nN_N + nN_R - 2}} \qquad 4.2.12$$

where $S_N(S_R)$ are the detector N(R) standard deviations calculated from

$$S = \left[\sum_{j=1}^{N} \sum_{i=1}^{N} \frac{1}{nN} \left(\pi_{ij} - \mu' \right)^2 \right]^{\frac{1}{2}} \qquad 4.2.13$$

Note that $S = \sqrt{\frac{nN-1}{nN}}\,\sigma$ where σ was defined in Eq. 4.2.5.

Having done these calculations, we are then faced with the statistical decision making process. In order to compare two means, we must do a two-tailed test on the t statistic. Let us state the hypothesis H_0: there is no significant difference in the means; and H_1: there is a significant difference in the means. It is customary to make the test at both the .05 and .01 levels of significance. The range of acceptable t values at the .01 and .05 levels is shown in table 6 for various degrees of freedom $\nu = nN_N + nN_R - 2$. If when we calculate t from Eq. 4.2.11, t lies outside the range given by table 6 (for a particular ν and level of significance), we would have to reject H_0 at that level of significance. A rejection at the .05 level means we have a 5 percent probability of having made a "false" rejection, and a rejection of H_0 at the .01 level implies a probability of 1 percent of a "false" rejection. If we have a rejection at .05, but not at .01 then H_1 is "probably" true, i.e. there may be a significant difference in the means.

A computer program TTEST (Appendix C.4) was used to calculate the t values from Eq. 4.2.11 for both N and

TABLE 6

T-TEST SIGNIFICANCE LEVELS

	SIGNIFICANCE LEVEL	
ν	.01	.05
20	$-2.84 < t < 2.84$	$-2.09 < t < 2.09$
40	$-2.70 < t < 2.70$	$-2.02 < t < 2.02$
60	$-2.66 < t < 2.66$	$-2.0 < t < 2.0$
120	$-2.62 < t < 2.62$	$-1.98 < t < 1.98$
00	$-2.58 < t < 2.58$	$-1.96 < t < 1.96$

R orientations of the detector. The results are shown in table 7. Only at 450 keV proton beam energy is there any possible significant difference in the means. The last entry in table 7 compares the mean of the (N+R) results with the mean of the N results, and shows no significant difference. We therefore conclude, that our polarization detector has no inherent polarization form bias and that said detector does not contribute any systematic error to our experiment. We will henceforth combine the results of N and R runs taken at the same pressure, energy and current.

A second possible source of systematic error in this work could be caused by any drift in our electronics which was constant in sign for the greater part of a run. In order to average out any such drifts, the order of data taking was varied during a run. The linear polarization fraction was always calculated for time adjacent $I_{//}$ and $I_{\perp}$ values. Our data taking order would be . . . $[(I_{//}N_{//})(I_{\perp}N_{\perp})][(I_{\perp}N_{\perp})(I_{//}N_{//})][(I_{//}N_{//})(I_{\perp}N_{\perp})][(I_{\perp}N_{\perp})(I_{//}N_{//})]$ . . . etc. where the rectangular brackets denote a calculated π. It is our contention that any "constant" drifts would be averaged out by this method of data taking. Any random drifts would of course average themselves out of our calculations.

Another possible source of systematic error lies in the fact that stray magnetic fields can cause precession of the atomic electrons and, therefore, depolarize

TABLE 7

TEST FOR SIGNIFICANCE OF DIFFERENCE OF MEAN π FROM NORMAL AND ROTATED DETECTOR

BEAM ENERGY	t VALUE N Vs R	# of DEGREES of FREEDOM	DIFFERENCE IN MEANS SIGNIFICANT	
			.15	.01
(keV)				
150	0.00	138	No	No
200	1.75	118	"	"
250	.25	118	"	"
300	-.48	238	"	"
350	.96	118	"	"
400	1.76	118	"	"
450	2.48	138	YES	"
	t VALUE (N+R) Vs N			
450	-1.23	218	No	No

the light from a collection of atoms. Feofilov (1961) discusses this problem and gives the results of Breit as follows . . .

$$\pi_0 = \pi\sqrt{1+\left(\frac{eH}{mc}g\tau\right)^2}$$

and

$$\tan(2\phi) = \frac{eH}{mc}g\tau \qquad 4.2.14$$

where π_0 is the zero magnetic field linear polarization fraction, π is the polarization fraction measured at magnetic field strength H, τ is the mean life of the transition, g is the Lande g factor and ϕ is the angle of rotation of the plane of polarization. Using . . .

$e = 4.8\times10^{-10}$ stat c
$m = 9.1\times10^{-28}$ gm
$c = 3\times10^{10}$ cm/sec

estimating $\tau\simeq2\times10^{-9}$ seconds (from Dotchin et al.) and calculating g for the 3^1P states from

$$g = 1 + \frac{j(j+1) + s(s+1) - \ell(\ell+1)}{2j(j+1)} \qquad 4.2.15$$

where j=1, s=0, and ℓ=1 so that g=1. We then have . . .

$$\pi_0 = \pi\sqrt{1+[(.035)H]^2} \qquad 4.2.16$$

Measurements of the magnetic field strength H in the vicinity of the target chamber were made using a HeliFlux Magnetic Aspect Sensor type RAM-3. These measurements were made with the Van De Graaff steering magnet energized. In no case were we able to find a field in excess of $\sim$3/4 gauss. Using this in Equation 4.2.16, we

get . . .

$$\pi_o = \pi (1 + .0007)$$

and conclude that the magnetic depolarization is negligible when compared with the random error present. Similarly we conclude that $\phi \approx 0$ and the plane of polarization is not rotated by the magnetic field.

We must also concern ourselves with collisional depolarization. Collisions between helium atoms in the target chamber, as well as with the chamber wall, will tend to equalize the magnetic substate populations and, therefore, reduce the polarization. Referring to a mean free path calculation done in the next section (4.3), we find the mean free path (using the geometric cross-section) of the helium atoms to be $\simeq$ 47cm. The rms velocity of the helium atoms is $v_{rms} = \sqrt{\frac{3kT}{m}}$, which for room temperature helium works out to $v_{rms} \simeq 1.4 \times 10^5$ cm/sec. Therefore the mean collision time is $\simeq 3.3 \times 10^{-4}$ sec. However, we must also account for the chamber walls where the radius is $\sim$2.5cm. Thus, we can expect a wall collision in $t \approx 1.8 \times 10^{-5}$ seconds. Since even this time is 4 orders of magnitude larger than the mean life of the 3^1P state (1.8×10^{-9} sec), we can ignore the possibility of depolarizing collisions.

Another mechanism which could cause a systematic error is that of cascading, where the 3^1P level is populated not only by direct proton excitation, but also by

downward transitions from n'S and n'D levels (n>3). In general, cascading into the 3^1P level from a number of different upper levels will tend to equalize the magnetic substate populations and, therefore, reduce the amount of polarization exhibited by the $3^1P \longrightarrow 2^1s$ transition. Heddle (1962) has shown that if the percentage of the 3^1P population due to cascading is C% then the experimentally observed polarization must be multiplied by the factor (1 + c/100) in order to correct for the cascade depolarization. C is most easily calculated following the method in appendix b of Van Eck's (1964) paper, using the transition probabilities listed in Gabriel (1960). However, in order to do this calculation, we need the values of various experimental emission and excitation cross sections. All the necessary experimental cross sections for this calculation are not yet in the literature. Since the agreement between theoretical and experimental cross sections is so poor, we have decided not to do the calculation with the theoretical values, but to instead rely upon the experimental determinations of cascade given by Van den Bos (1968) and by Thomas (1967). In both of these works, the authors use their own unpublished data to calculate the cascade percentage c, which they then report. Van den Bos reports values for c of 8% at 100 keV and 6% at 150 keV; while Thomas reports 4% over the energy range 150 - 1000 keV. We will, therefore, correct for cascade as follows:

at 100 keV use 8%, at 150 keV use 5%, and above 150 keV use 4% for the cascade correction.

We must next discuss the effect of resonance trapping on the polarization of the emitted light. Resonance trapping occurs when the beam excited 3^1P level decays to the 1^1S level and the resultant photon is trapped by a ground state He atom. The ground state atom is then of course excited to the 3^1P level and may then undergo a $3^1P \longrightarrow 2^1S$ transition. This event results in our detector seeing light from atoms which were not space quantized by the proton beam, and, therefore, results in an experimental polarization which is lower than the free atom value. In order to estimate the amount of trapping which occurs, we turn first to the work of Lees (1932) and Lees et al. (1932). These works used photographic techniques to determine the excitation cross sections for various He levels excited by electron impact. When Lees' photographs showed λ 5016 Å light emanating from He gas which was not impacted upon by the beam, he and Skinner concluded that 3^1P-1^1S radiation from the beam area was being trapped and a portion of it would then be emitted as 3^1P-2^1S light. They showed that the proportion of light absorbed = $1 - e^{-nr\tau_a}$ where n is the number density, r is the target chamber radius, and τ_a is the atomic absorbtion coefficient.

Their values for τ_a were 2.3×10^{-15} (experimental) and $\sim 92 \times 10^{-15}$ (theoretical). Once we know the

percentage trapped in the 3^1P level, the ratio of the transition probabilities $A(3^1P-2^1S)/A(3^1P-1^1S) = .023$ will give us some indication of the percentage of 3^1P-1^1S which is first trapped and then radiated at 3^1P-2^1S radiation. Of course, the reradiated 3^1P-1^1S radiation may be retrapped, etc. Table 8 shows the results of these estimations as a function of pressure. This issue is obviously not resolvable with this data.

Recently more comprehensive work on the imprisonment of Resonance Radiation in gases has been done, notably by Holstein (1951) and Phelps (1958). Holstein's mathematics are not suited to our low pressure work, and in fact are not useable. Phelps on the other hand using Holstein's concept presents a transmission probability graph from which the transmission of the 3^1P-1^1S radiation of He (in terms of target chamber radius) can be abstracted. This transmission probability is then converted into % trapped (see table 8). We note that the Phelps results fall between the two extremes of Lees' work. Using Phelps' results in the worst possible case, where 93% of the 3^1P-1^1S radiation is trapped, and applying the factor of .023 from the ratio of transition probabilities, we find a trapping correction T of 2.1%. This has assumed single trapping events. In order to account for multiple trapping we arbitrarily raise that figure by $(.023)\times(.5)\approx.012$ and estimate the trapping correction T as 3.2%. Estimated trapping corrections

TABLE 8

TRAPPING CORRECTIONS

He PRESSURE mtorr	% TRAPPED LEE'S EXPERIMENTAL τ_a	LEE'S THEORETICAL τ_a	PHELPS RESULTS	TRAPPING CORRECTION T in %
.01	.15	5.9	5	.17
.05	.75	26.	20	.69
.2	3.0	70	45	1.6
.6	8.7	97	80	2.8
1.0	14	99	90	3.1
1.5	20	99	93	3.2

are listed in table 8 for the various He pressures we have used. We can then correct for resonance trapping depolarization by multiplying our experimental π by $(1 + T/100)$. We will later discuss another type of trapping which may cause error, namely trapping at the 2^1S level of a 3^1P-2^1S photon.

Since we are already making a cascade correction of the form $(1 + C/100)$, and rather than compound the correction, we define $D = C + T$ as the unpolarized light contribution to the 3^1P-2^1S radiation. Our correction therefore takes the form $\pi = \pi_{exp}(1 + D/100)$. Table 9 shows D tabulated for various proton beam energies and Helium gas pressures. Generally this correction is smaller than the standard error of the mean of π.

We must also discuss the effect of the He gas purity on the measured polarization. Since we work at quite low pressures, 1.5 mtorr and below, the gas density is quite low and as stated earlier the mean collision time is roughly 3×10^{-4} sec. However the 3^1P state has a mean life of 1.8×10^{-9} sec (Dotchin - private communication) and decays of that state should be extremely free of effects from the very infrequent collisions with not only other He atoms, but also with the rare impurity atom. We have used two sources of He in taking data, the first was standard grade ~98% pure, and the second was research grade 99.999% pure. The results obtained were identical (within S.E.) and clearly impurities pose no

TABLE 9

ESTIMATED UNPOLARIZED LIGHT CORRECTIONS

Proton Energy (keV)	He Pressure (m torr) .01	.05	.2	.6	1.0	1.5
100			9.6			
150	5.2	5.7	6.6	7.8	8.1	8.2
200			5.6			
250			5.6			
300	4.2	4.7	5.6	6.8	7.1	7.2
350			5.6			
400			5.6			
450	4.2	4.7	5.6	6.8	7.1	7.2

problem to this study.

A simple problem which could have caused a gross systematic error was dust. Any substance which might adhere to our HN-32 polaroid analyzer and scatter light, could cause an artificial difference in the intensities $I_{//}$ and $I_{\perp}$ as the analyzer was rotated between its two positions. We therefore took great care to keep the polarization analyzer clean and dust free. To insure that an error caused by dust would be reduced, we spread our data taking over many days and many analyzer cleanings, assuming that in the long run unescapable small errors would average out.

Another possible source of error is due to the shape of our proton beam. It is roughly rectangular in cross-section, $\sim$2x10 mm. This is quite a large beam area for an experiment of this type, and we need to be concerned about those processes which might occur within the beam region. We are forced to accept this unusual geometry due to both the idiosyncrasies of our electrostatic focusing system and the experimental needs of Dotchin et al. The beam region in the target chamber is a plasma region, and a Faraday rotation of the plane of polarization of light is conceivable. Faraday rotation occurs due to birefringence in the plasma, the birefringence in turn is due to a magnetic field (e.g. the earth's field). The birefringence also means that the indices of refraction are different for right and left circularly

polarized light. Since a linearly polarized wave can be considered to be the superposition of two counterrotating circularly polarized waves, and since the indices of refraction are different for each component (hence the phase velocities are different), the plane of polarization of the linearly polarized wave is rotated. The amount of rotation depends upon the differences in the two indices of refraction, and the thickness of plasma penetrated by the wave. An outline of the Faraday effect is found in a text by Marion (1965) and a very good generalized treatment is available in the work of Larson (1967). The two indices of refraction are found from

$$n_{\pm} = \left[1 - \frac{\omega_0^2}{\omega(\omega \pm s)} \right]^{\frac{1}{2}} \qquad 4.2.17$$

where ω_0 is the plasma frequency $\omega_0 = \sqrt{\frac{4\pi N_e e^2}{m}}$, N_e is the electron density; s is the gyrofrequency of the electrons in the magnetic field $s = \frac{eB}{mc}$, B is the magnetic field component along the propagation direction; and ω is the frequency of the light from the 3^1P-2^1S transition. The rotation of the plane of polarization is given by

$$\frac{d\Omega}{dL} = \frac{\omega}{2c} \left(n_+ - n_- \right) \qquad 4.2.18$$

where $\frac{d\Omega}{dL}$ is the rotation in radians/cm of penetration. The important quantity is obviously $(n_+ - n_-)$ this in turn depends upon $\omega \pm s$. For our work we have $\omega = \frac{2\pi c}{\lambda} \simeq 3.76 \times 10^{15}$ and assuming $B \simeq .5$ gauss, $s = 8.78 \times 10^6$. Using formula 4.2.17 we find that the difference between n_+ and n_- is on the order of one part in 10^{15} or $(n_+ - n_-) \simeq 10^{-15}$ and therefore $\frac{d\Omega}{dL} \simeq 6 \times 10^{-11}$ radians/cm. We can therefore state that any Faraday rotation of the plane of polarization of the light from the He atoms is totally and completely ignorable.

Another problem which could have caused a systematic error was caused by soft x-rays from the Van de Graaff tank. These x-rays contributed to the background count rate for our phototube. However to take a background count measurement, we shut off the belt charge and therefore the beam and x-rays. Thus we had been getting false (low) background count measurements. This problem has been solved by shielding our phototube with lead bricks so that essentially no x-ray counts are detected.

We have taken pains to eliminate other sources of systematic error. The detector has always been carefully aligned at 90° to the beam direction with the use of a "square." We have checked our electronic's counting rates by feeding a simultaneous pulsed signal to all systems and observing identical numbers on all scalars.

We, therefore, conclude that systematic errors in the polarization measurement have been reduced to the extent that they are not significant in comparison to the random errors present.

4.3 Other Parameters

Since it is our aim to find the linear polarization fraction as a function of Helium target gas pressure, proton beam energy, and proton beam current, we must both measure (and estimate the error in our measurements of) these parameters.

We measure the Helium target gas pressure with an instrument which, according to the manufacturers specifications is capable of five digit accuracy. This MKS Barratron capacitance manometer will not in of itself be a source of error. We could, however, have a pressure error if there is "significant" outgassing in the piping which connects the target chamber to the pressure head. See figure 7. This piping is primarily 1/4" O.D. copper tube soft soldered to brass and/or stainless steel fittings. In our observations of the behavior of this section of the vacuum system, we are able to state that under various valve closed conditions, the pressure indicators available have not shown excessive outgassing.

Another possible source of error in the pressure measurement system is the fact that the pressure measurement port of the target chamber is located $\sim$2.5 cm

"upstream" of the observation window, see figure 6. We must then ask whether or not the He gas is undergoing Laminar flow and exhibiting a relatively large pressure gradient in the target chamber, or whether the He is streaming through the chamber with little pressure gradient. The latter case is of course the desirable situation. We can decide between cases by doing a simple mean free path calculation. We have for the mean free path ℓ, Young (1964) . . .

$$\ell = \frac{KT}{4\sqrt{2}\,\pi r^2 P} \qquad 4.3.1$$

where k is the Boltzman constant $k=1.38\times10^{-23}$ J/°k, T is the temperature, estimated 300°k; πr^2 is the geometrical cross section estimated as 3×10^{-20} square meters; and P is the pressure in N/m^2. We then have . . .

$$\ell = .094\,\frac{1}{P} \qquad 4.3.2$$

The largest pressure at which we work is 1.5×10^{-3} torr = 1.5×10^{-3}mm of H_g=.2 N/m^2. Therefore, the mean free path for our highest pressure is ℓ=.47m=47cm. We then conclude that the Helium gas is streaming through our chamber and that no significant pressure gradient exists. Therefore, the fact that our pressure measuring port is upstream of the observation window will cause no significant pressure error.

Our next concern is whether or not the proton beam energy at the target chamber is the same as at the accelerator. We have previously discussed, in section 2.2, the accuracy of the beam energy readout of the Van de Graaff accelerator system. Our estimate of the accuracy of that readout was ∿8 keV. We must also, however, ask whether or not the proton beam energy is effected by the presence of the target gas, or "background" gases in the beam tube. We can use the stopping power data compiled by Allison (1953) to calculate dE/dZ, i.e. the proton beam energy loss/cm. In the energy range of 100 to 500 keV, the greatest stopping power of Helium for protons (occurring at 100 keV) is 7.3×10^{-15} evxcm^2/atom. We can easily calculate the number of atoms/cm^3 from the ideal gas law . . .

$$PV = nKT \qquad 4.3.3$$

where P=1.5×10^{-3}mm of H_g=22 dynes/cm^2, K is the Boltzman constant 1.38×10^{-16} erg/°K; and T is estimated room temperature 300°K. Therefore, the number density of He atoms in our target chamber is $\frac{n}{V} = \frac{P}{KT} = 4.8 \times 10^{13}$ atom/cm^3 Multiplying the stopping power by the number density, we arrive at the energy loss/cm = 35×10^{-2} ev/cm. Thus the beam energy lost to the target gas is completely negligible. Since the "background" gas pressure is ∿10^2 less than the target pressure, we can estimate an Energy loss to "background" gas of .0035 ev/cm, again totally

negligible. We, therefore, conclude that the systematic error in the beam energy is not significant when compared to the ∿8 keV instrumental uncertainty.

The next important parameter is the proton beam current, which is detected within our Faraday cup (discussed in section 2.3). We have avoided the common secondary electron loss problem in the cup in two ways; the proton beam impacts on Vycor glass rather than on metal thus producing fewer secondaries; and we have lengthened our cup and provided a small entrance aperture such that secondary electrons could only escape through a very small solid angle. Considering other factors such as leakage through insulators, etc., we estimate an overall accuracy of ∿5 percent on the collection of beam current by our Faraday cup.

The readout of the proton beam current measurement is then taken two ways for two purposes. The Keithly microammeter meter readout is used to tune the Van de Graaff and to provide a number for the comparison of the linear polarization fraction with beam current. We estimate an instrumental accuracy of ∿2 percent. However, in practice, the beam current is a very unstable quantity. If for example the Van de Graaff has been tuned to give a ∿10μA H^+ beam in the left port, the microammeter will show short term fluctuations in the worst case of from ∿9 to ∿11μA. The reported beam current of ∿10μA is the observers best estimate of the time

averaged beam current, uncertainty ∿5 percent. This problem is further complicated by drifts in the Van de Graaff's output current. During the course of a run (∿45 minutes) the beam current may change, e.g. from ∿10 to ∿12μA. We will, therefore, state an overall average beam current uncertainty, for any run of ∿15 percent.

The second type of beam current readout is taken from one of our scalars and used to normalize light intensity to beam current. This scalar readout is in arbitrary units since an absolute number is not required, see Eq. 4.1.3. Our main concern here is repeatability, i.e. a given number of protons impacting on the Vycor end window of the Faraday cup should produce the same number on the normalization scalar. We have no direct way of confirming this repeatability, however, our observations of the performance of this equipment has enabled us to conclude that so long as the Keithly microammeter and other electronics have been warmed up for ∿5 hours prior to a run, the repeatability will be quite good. Once the electronics have warmed up, the random errors on the normalization scalar far outweigh any remaining systematic error.

4.4 Data Manipulation

From the time data is first collected and written in our lab notebook, until the time a "final" π is reported, much computer manipulation occurs. We must

analyze each and every run prior to joining the results of that run to previous results (to guard against major systematic system error). We must maintain a separate file for every target gas pressure, proton beam Energy, proton beam current, and detector orientation (to enable us to separately analyze π as a function of each of those parameters). Table 10 shows the number of (20 polarization measurements) runs taken at each beam energy and target gas pressure for both N and R detector orientations and for normal and low beam currents, a total of 116 runs. Due to the large amounts of data involved, we have established a system whereby all of the data and calculated π's are stored in the University of New Hampshire's computer (call 360 system).

All the data taken for one run (Table 4) will be entered into the computer memory, as a program, using the data statement. Table 11 shows the section of a data program relevant to the data of Table 4. All of our data is hand typed into the computer memory and onto punched paper tape. We have used a consistent naming system for these data programs. They are labeled as DATAXXYY, where XX is a pair of numbers representing the month, and YY is a pair of numbers representing the day of the month. Any data program will include all the runs done during one day. These data programs contain nothing but data statements and are useless unless merged with an operational program.

TABLE 10

NUMBER OF RUNS AT VARIOUS PARAMETERS

H^+ Energy (keV)	Helium Target Gas Pressure (m torr)					
	.01	.05	.2	.6	1.0	1.5
100			2N			
150	5N,3R	2N,3R	4N,3R	2R	2R	2R
200			4N,2R			
250			4N,2R			
300	4N,3R	5N,2R	1H,6L,7N,3R	2N,1R	2N,1R	1N,1R
350			4N,2R			
400			4N,2R			
450	1N,3R	1N,4R	4N,3R	1N,2R	1N,2R	2R

where N = Normal, R = Rotated, L = Low Current, H = High Current

TABLE 11

DATA PROGRAM

```
DATA0414      9:36   AUGUST 27, 1973

100 REM DATA0414
110 REM ENERGY,PRESSURE,CURRENT,4,20,BACKGROUNDS
120 DATA 300,.2,11.5,4,20,49,8,35,8,52,9,47,10
130 REM DATA...COUNTS VERT,NORM,HORIZ,NORM,VERT,NORM...ETC
140 DATA 899,1467,818,1502,932,1523,815,1533,863,1533,852,1539
150 DATA 782,1486,838,1524,792,1531,795,1546,809,1538,778,1553
160 DATA 809,1558,780,1553,847,1430,795,1514,894,1559,784,1565
170 DATA 804,1569,784,1546,819,1549,802,1547,824,1550,873,1553
180 DATA 900,1564,793,1567,885,1633,883,1638,952,1634,838,1557
190 DATA 906,1587,878,1600,871,1604,888,1606,892,1609,844,1607
200 DATA 936,1606,927,1599,861,1421,860,1484
```

The first operational program used in NEWPOL (appendix C.2). Its function is, when merged with DATAXXYY; to separately and sequentially analyze each run; to calculate all 20 π's for each run; to calculate a mean π and the standard deviation and error; and to print for each run the raw data and the calculated results. See again Table 5.

In order to combine runs, their individual results have to be cumulatively stored. We have a series of programs which will analyze the runs within DATAXXYY and, instead of printing the results, add to storage files the 20 π's from each run according to target gas pressure, beam energy, and detector normalization. These programs are labeled PUTPOL, PUTPOLR, and PUTPOLP (appendicies C.5,6 and 7). The files into which the results are placed were created from the keyboard by user commands and initialized by using PUT (appendix C.8). PUTPOL is merged with detector N data with Normal beam currents. It will only analyze and file .2 m torr runs at energies from 100 to 450 keV (by 50 keV steps). These files are labeled PXXX where XXX is the beam energy in keV. PUTPOLR resembles PUTPOL except that it is used on detector R runs and the files are labeled PXXXR. Finally PUTPOLP is used for all beam energies and target gas pressures excepting .2 m torr. This program was put into use after we had concluded that our experimental result was independent of detector orientation, therefore, the

output files were labeled only by beam energy and target gas pressure. We selectively analyze and file only normal beam current data with PUTPOLP. The output files are labeled T150PYY, T300PYY, and T450PYY; or TXXX where YY represents the Helium target gas pressure: 01=.01 mmtorr, 05=.05 mmtorr, 2=.2 mtorr, 6= .6 mtorr, 1 = 1 mtorr, and 15 = 1.5 mtorr; and XXX represents beam energy for 100, 200, 250, 350, and 400 keV where only .2 mtorr data was taken. See again, Table 10. Low beam current ($\sim$1μA H^+) data were analyzed and filed using PUTPTEST (appendix C.9). The files were labeled T300LYY, where YY is defined as above.

These files are all structured alike as a one dimensional array of the form $m,1,\pi_1,\pi_2,\pi_3,\ldots$ where m = the total number of π's (nxN). This form was chosen so that we might use IBM's statistical analysis program STATPACK. Generally, we used our own programs since our files contained too many entries for use by STATPACK.

We, therefore, have over 40 different files representing different conditions of detector orientation, beam current, beam energy, and Helium target gas pressure. In order to analyze the cumulative contents of a file, we use the program STAT (appendix C.3). This program will find a mean π for a file as well as a standard deviation, standard error of the mean, etc., see Table 12 for Typical Output.

Thus, we have the capability of individually

TABLE 12

OUTPUT OF THE PROGRAM STAT

```
STAT          9:40   AUGUST 27, 1973

FILE TO BE ANALYZED IS?T300P05
140 P'S IN CALCULATION
ST DV = .05651      8 PTS DV > 2 SIG     S.E.= .00478
(P-SE)= -0.01297     MEAN P = -0.00819     (P+SE)= -0.00342
```

analyzing runs using NEWPOL, or of cumulatively filing data by parameter for later analysis by STAT.

SECTION V

RESULTS AND CONCLUSIONS

5.1 Summary of Results

In this work we have investigated the linear polarization fraction of light (λ 5016 Å) from the 3^1P-2^1S transition in Helium as a function of proton beam energy, He target gas pressure and proton beam current. Because of the large random errors inherent in our experiment, determinations of π were made in groups of twenty, i.e. twenty measurements for each run. Each run of course was done at some particular He pressure, beam current and energy. Any number of runs would be taken on a particular day depending upon the behavior of the equipment and apparatus. The run by run results are listed in table 13 in chronological order. Table 14 lists the run by run results chronologically within each section of beam energy and target pressure. In both of these tables we have reported π in percent, rather than as a (decimal) fraction, for the sake of easy readability.

Table 15 and figure 16 show our results for π (in %) as a function of proton beam energy and for constant He pressure and reasonably constant beam current. The graph (fig. 16) uses the corrected π's. Tables 16,

TABLE 13

RESULTS FOR EACH RUN, CHRONOLOGICALLY

H+ ENERGY KEV	HE PRESSURE MTORR	H+ CURRENT MICRO-A	IN %	S.E. γ_F MEAN
		DATA1216		
100	.20	4.5	2.760	0.569
150	.20	8.0	1.921	0.443
200	.20	8.0	1.507	0.495
250	.20	8.5	-0.308	0.580
300	.20	8.5	-1.359	0.730
350	.20	9.5	-2.350	0.407
400	.20	9.5	-3.418	0.672
450	.20	9.5	-3.815	0.585
		DATA1217		
450	.20	9.5	-3.477	0.740
400	.20	9.5	-2.194	0.737
350	.20	9.5	-3.142	0.640
300	.20	8.0	-1.279	0.570
250	.20	6.5	-0.883	0.795
200	.20	7.5	0.675	0.766
150	.20	4.0	2.624	1.205
100	.20	5.0	2.538	0.900
		DATA1224		
200	.20	10.0	1.097	0.505
250	.20	10.0	-0.785	0.455
300	.20	12.0	-2.451	0.527
350	.20	10.5	-4.498	0.669
400	.20	12.0	-4.513	0.529
450	.20	11.0	-6.421	0.696
		DATA1225		
450	.20	11.0	-5.832	0.886
400	.20	10.0	-4.585	0.604
350	.20	11.0	-3.304	0.569
300	.20	11.0	-3.909	0.723
300	.20	11.0	-2.224	0.451
250	.20	10.5	-0.991	0.430
200	.20	11.0	0.539	0.374
150	.20	8.5	1.791	0.536
300	.20	19.0	-3.221	0.300
300	.20	4.5	-3.358	0.699
300	.05	10.5	-1.321	1.240
300	.20	10.5	-3.850	0.542
300	.60	11.0	-4.766	0.175
300	1.00	11.0	-4.049	0.302
300	1.50	11.0	-2.896	0.157
300	2.00	11.0	-2.196	0.107

TABLE 13 CONTINUED

H+ ENERGY KEV	HE PRESSURE MTORR	H+ CURRENT MICRO-A	IN %	S.E. OF MEAN
		DATA1226		
300	.20	10.0	-2.967	0.693
450	.20	10.0	-6.940	0.463
150	.20	7.5	2.507	0.649
		DATA1230		
150	.20	7.5	0.759	0.523
200	.20	10.5	-0.320	0.605
250	.20	11.0	-1.578	0.612
300	.20	11.0	-3.054	0.439
350	.20	11.0	-4.815	0.620
400	.20	12.0	-5.210	0.679
450	.20	10.0	-6.472	0.454
450	.05	10.0	-4.430	1.548
450	.60	10.0	-7.218	0.240
		DATA0101		
150	.60	8.0	0.286	0.228
150	.05	8.0	4.766	0.918
150	.20	8.0	2.462	0.372
200	.20	10.5	0.520	0.578
250	.20	11.0	-0.153	0.550
300	.20	11.0	-1.331	0.564
350	.20	10.5	-2.836	0.557
400	.20	10.5	-4.142	0.587
450	.20	11.0	-5.237	0.763
		DATA0120		
300	1.00	11.5	-3.619	0.278
300	.60	11.5	-2.705	0.486
300	.05	10.0	1.493	1.086
300	.01	10.5	0.614	1.692
150	.01	6.0	-0.606	1.959
150	.05	6.0	5.387	1.934
150	1.00	5.5	-0.084	0.148
150	1.50	5.5	-0.519	0.137
150	.01	5.5	-2.988	2.534
		DATA0122		
150	1.50	6.5	-0.838	0.246
150	1.00	6.0	0.800	0.130
150	.60	6.0	0.937	0.275
150	.05	6.0	1.952	0.846
150	.01	6.0	0.857	1.568
300	.01	11.5	1.058	1.692
300	.05	11.5	-1.439	0.911

TABLE 13 CONTINUED

H+ ENERGY KEV	HE PRESSURE MTORR	H+ CURRENT MICRO-A	IN %	S.E. OF MEAN
300	1.50	11.5	-1.687	0.175
300	.01	11.5	-2.373	1.340
		DATA0124		
450	.01	12.0	-0.722	1.819
450	.05	10.0	-0.083	0.770
450	.60	11.0	-0.274	0.333
450	1.00	11.0	-1.061	0.310
450	1.50	11.0	-2.401	0.229
450	.01	11.0	-2.336	1.484
450	.05	10.0	-1.158	1.049
450	1.00	10.0	-3.168	0.431
450	1.50	10.0	-4.224	0.152
450	.01	12.0	-2.661	1.153
450	.05	11.0	-3.547	0.603
		DATA0220		
300	.01	12.5	3.270	3.740
300	.05	13.0	0.158	1.582
300	.60	14.0	-3.103	0.227
300	.01	14.0	2.700	3.462
300	.05	13.0	-1.673	1.081
		DATA0414		
300	.20	11.5	-2.180	0.669
300	.05	11.0	-2.381	1.455
300	.01	12.0	2.213	2.585
300	.01	10.5	-1.818	2.283
300	.05	11.0	-0.571	1.345
150	.05	6.5	0.643	1.841
150	.05	6.5	-0.085	2.194
150	.20	6.5	1.308	0.862
150	.01	6.5	4.906	3.769
150	.01	6.5	-0.239	3.161
		DATA0415		
450	1.00	11.5	-6.377	0.172
450	.60	11.0	-7.363	0.285
450	.05	11.0	-2.289	2.189
450	.01	12.0	-2.676	2.646
		DATA0513		
300	1.00	11.0	-1.112	0.228
		DATA0519		
150	.01	4.5	-6.200	3.520

TABLE 13 CONTINUED

H+ ENERGY KEV	HE PRESSURE MTORR	H+ CURRENT MICRO-A	IN %	S.E. OV MEAN
150	.01	4.5	0.667	2.725
150	.01	4.5	-3.759	2.625
300	.20	1.0	-3.706	2.075
300	.20	1.0	-4.333	2.009
300	.20	1.0	-5.940	1.712
		DATA0821		
300	.20	1.0	-0.994	2.696
300	.20	1.0	-5.336	2.346
300	.20	1.0	-2.316	2.074

16 DATA PROGRAMS 117 DATA RUNS

TABLE 14

RESULTS FOR EACH RUN, BY PARAMETER

FROM DATA PROG	H+ CURRENT MICRO-A	IN %	S.E. OF MEAN
	100 KEV BEAM	.20 MTORR HE	
DATA1216	4.5	2.760	0.569
DATA1217	5.0	2.538	0.900
	150 KEV BEAM	.01 MTORR HE	
DATA0120	6.0	-0.606	1.959
DATA0120	5.5	-2.988	2.534
DATA0122	6.0	0.857	1.568
DATA0414	6.5	4.906	3.769
DATA0414	6.5	-0.239	3.161
DATA0519	4.5	-6.200	3.520
DATA0519	4.5	0.667	2.725
DATA0519	4.5	-3.759	2.625
	150 KEV BEAM	.05 MTORR HE	
DATA0101	8.0	4.766	0.918
DATA0120	6.0	5.387	1.934
DATA0122	6.0	1.952	0.846
DATA0414	6.5	0.643	1.841
DATA0414	6.5	-0.085	2.194
	150 KEV BEAM	.20 MTORR HE	
DATA1216	8.0	1.921	0.443
DATA1217	4.0	2.624	1.205
DATA1225	8.5	1.791	0.536
DATA1226	7.5	2.507	0.649
DATA1230	7.5	0.759	0.523
DATA0101	8.0	2.462	0.372
DATA0414	6.5	1.308	0.862
	150 KEV BEAM	.60 MTORR HE	
DATA0101	8.0	0.286	0.228
DATA0122	6.0	0.937	0.275
	150 KEV BEAM	1.00 MTORR HE	
DATA0120	5.5	-0.084	0.148
DATA0122	6.0	0.800	0.130
	150 KEV BEAM	1.50 MTORR HE	
DATA0120	5.5	-0.519	0.137
DATA0122	6.5	-0.838	0.246
	200 KEV BEAM	.20 MTORR HE	
DATA1216	8.0	1.507	0.495
DATA1217	7.5	0.675	0.766
DATA1224	10.0	1.097	0.505

TABLE 14 CONTINUED

FROM DATA PROG	H+ CURRENT MICRO-A	IN %	S.E. OF MEAN
DATA1225	11.0	0.539	0.374
DATA1230	10.5	-0.320	0.605
DATA0101	10.5	0.520	0.578
	250 KEV BEAM	.20 MTORR HE	
DATA1216	8.5	-0.308	0.580
DATA1217	6.5	-0.883	0.795
DATA1224	10.0	-0.785	0.455
DATA1225	10.5	-0.991	0.430
DATA1230	11.0	-1.578	0.612
DATA0101	11.0	-0.153	0.550
	300 KEV BEAM	.01 MTORR HE	
DATA0120	10.5	0.614	1.692
DATA0122	11.5	1.058	1.692
DATA0122	11.5	-2.373	1.340
DATA0220	12.5	3.270	3.740
DATA0220	14.0	2.700	3.462
DATA0414	12.0	2.213	2.585
DATA0414	10.5	-1.818	2.283
	300 KEV BEAM	.05 MTORR HE	
DATA1225	10.5	-1.321	1.240
DATA0120	10.0	1.493	1.086
DATA0122	11.5	-1.439	0.911
DATA0220	13.0	0.158	1.582
DATA0220	13.0	-1.673	1.081
DATA0414	11.0	-2.381	1.455
DATA0414	11.0	-0.571	1.345
	300 KEV BEAM	.20 MTORR HE	
DATA1216	8.5	-1.359	0.730
DATA1217	8.0	-1.279	0.570
DATA1224	12.0	-2.451	0.527
DATA1225	11.0	-3.909	0.723
DATA1225	11.0	-2.224	0.451
DATA1225	19.0	-3.221	0.300
DATA1225	4.5	-3.358	0.699
DATA1225	10.5	-3.850	0.542
DATA1226	10.0	-2.967	0.693
DATA1230	11.0	-3.054	0.439
DATA0101	11.0	-1.331	0.564
DATA0414	11.5	-2.180	0.669
DATA0519	1.0	-3.706	2.075
DATA0519	1.0	-4.333	2.009
DATA0519	1.0	-5.940	1.712

TABLE 14 CONTINUED

FROM DATA PROG	H+ CURRENT MICRO-A	IN %	S.E. OF MEAN
DATA0821	1.0	-0.994	2.696
DATA0821	1.0	-5.336	2.346
DATA0821	1.0	-2.316	2.074
	300 KEV BEAM	.60 MTORR HE	
DATA1225	11.0	-4.766	0.175
DATA0120	11.5	-2.705	0.486
DATA0220	14.0	-3.103	0.227
	300 KEV BEAM	1.00 MT?RR HE	
DATA1225	11.0	-4.049	0.302
DATA0120	11.5	-3.619	0.278
DATA0513	11.0	-1.112	0.228
	300 KEV BEAM	1.50 MTORR HE	
DATA1225	11.0	-2.896	0.157
DATA0122	11.5	-1.687	0.175
	350 KEV BEAM	.20 MTORR HE	
DATA1216	9.5	-2.350	0.407
DATA1217	9.5	-3.142	0.640
DATA1224	10.5	-4.498	0.669
DATA1225	11.0	-3.304	0.569
DATA1230	11.0	-4.815	0.620
DATA0101	10.5	-2.836	0.557
	400 KEV BEAM	.20 MTORR HE	
DATA1216	9.5	-3.418	0.672
DATA1217	9.5	-2.194	0.737
DATA1224	12.0	-4.513	0.529
DATA1225	10.0	-4.585	0.604
DATA1230	12.0	-5.210	0.679
DATA0101	10.5	-4.142	0.587
	450 KEV BEAM	.01 MTORR HE	
DATA0124	12.0	-0.722	1.819
DATA0124	11.0	-2.336	1.484
DATA0124	12.0	-2.661	1.153
DATA0415	12.0	-2.676	2.646
	450 KEV BEAM	.05 MTORR HE	
DATA1230	10.0	-4.430	1.548
DATA0124	10.0	-0.083	0.770
DATA0124	10.0	-1.158	1.049
DATA0124	11.0	-3.547	0.603
DATA0415	11.0	-2.289	2.189

TABLE 14 CONTINUED

FROM DATA PROG	H+ CURRENT MICRO-A	IN %	S.E. OF MEAN
	450 KEV BEAM	.20 MTORR HE	
DATA1216	9.5	-3.815	0.585
DATA1217	9.5	-3.477	0.740
DATA1224	11.0	-6.421	0.696
DATA1225	11.0	-5.832	0.886
DATA1226	10.0	-6.940	0.463
DATA1230	10.0	-6.472	0.454
DATA0101	11.0	-5.237	0.763
	450 KEV BEAM	.60 MTORR HE	
DATA1230	10.0	-7.218	0.240
DATA0124	11.0	-0.274	0.333
DATA0415	11.0	-7.363	0.285
	450 KEV BEAM	1.00 MTORR HE	
DATA0124	11.0	-1.061	0.310
DATA0124	10.0	-3.168	0.431
DATA0415	11.5	-6.377	0.172
	450 KEV BEAM	1.50 MTORR HE	
DATA0124	11.0	-2.401	0.229
DATA0124	10.0	-4.224	0.152

TABLE 15

π Vs BEAM ENERGY

BEAM ENERGY (keV)	AV. BEAM CURRENT μA	# OF RUNS	# OF MEASUREMENTS OF π	π IN %	S.E. OF MEAN OF π	π FOR % CORRECTED FOR CASCADE AND TRAPPING
100	4.8	2	40	2.65	.53	2.90
150	7.1	7	140	1.91	.27	2.04
200	9.6	6	120	.67	.23	.71
250	9.6	6	120	- .78	.24	- .83
300	10.5	10	200	-2.46	.2	-2.60
350	10.3	6	120	-3.49	.25	-3.69
400	10.6	6	120	-4.01	.27	-4.23
450	10.3	7	140	-5.46	.27	-5.76

Helium target gas pressure = .2 mtorr

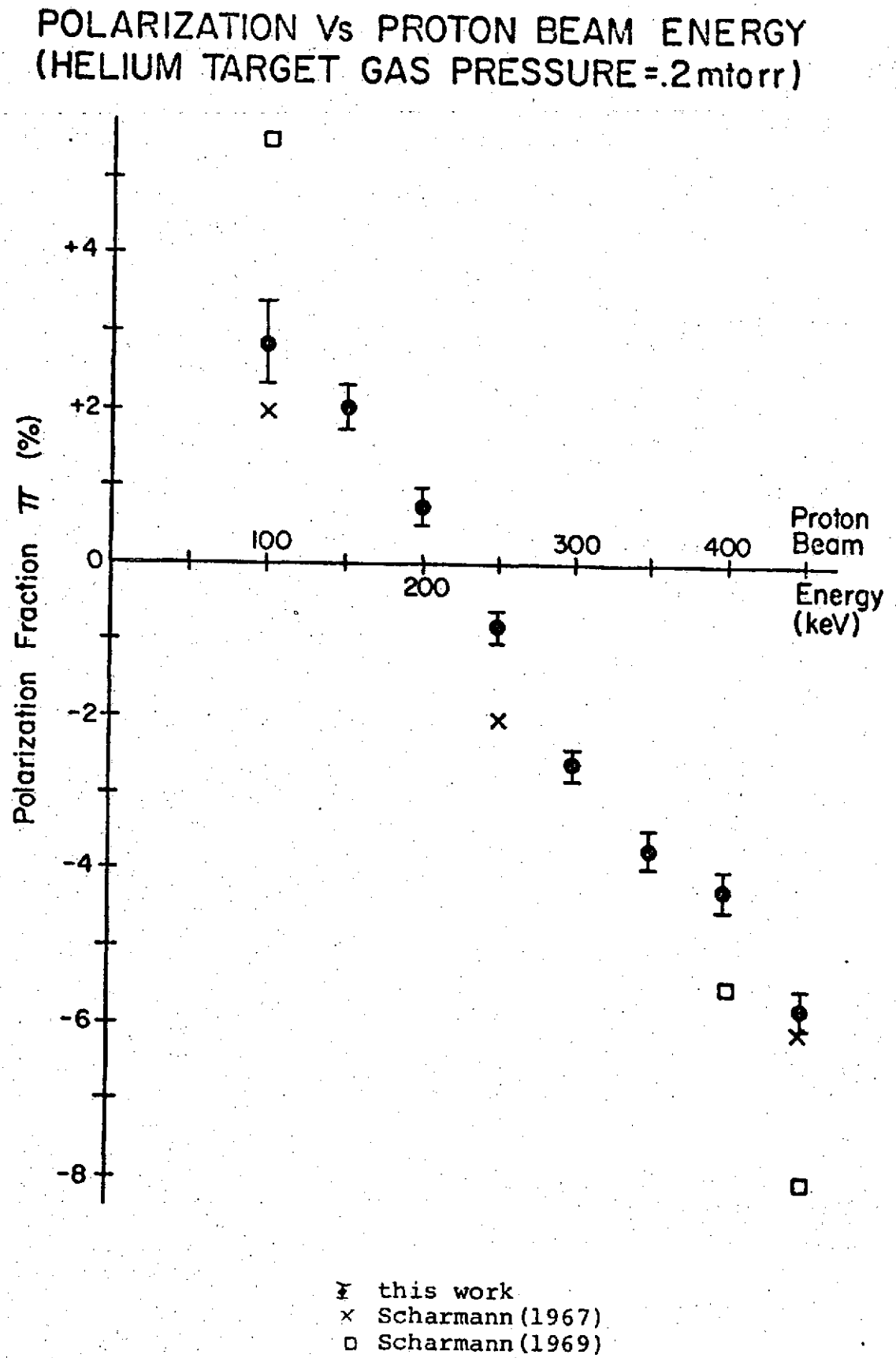
POLARIZATION Vs PROTON BEAM ENERGY
(HELIUM TARGET GAS PRESSURE=.2mtorr)
Polarization Fraction π (%)
+4
+2
0
-2
-4
-6
-8
100
200
300
400
Proton Beam Energy (keV)
this work
Scharmann (1967)
Scharmann (1969)

FIGURE 16

17, 18 and figure 17 show our results for π (in %) as a function of He gas pressure at constant beam currents and at beam energies of 150, 300, and 450 keV respectively. The graph (fig. 17) uses the corrected π's. Table 19 shows our results for π (in %) as a function of beam current at 300 keV and .2 mtorr He pressure.

5.2 Discussion of Results

Let us first note from table 19 that a t-test of the significance of the difference of the mean π's for the normal and low beam current runs shows no significant difference. In other words the polarization is not a function of beam current. As can be seen from the table, this comparison was made at 300 keV beam energy and .2 mtorr He pressure. We chose to do the comparison at these values in order to obtain good statistics. The beam current was lowered by a factor of ten in order to make the comparison. The Van de Graaff accelerator is not capable of sustained runs at higher currents, nor is the Faraday cup capable of absorbing higher current runs, therefore we were not able to compare our normal current run with other than just the one 19.5μA run of December 25, 1972. A t-test between the normal and high current runs also implies no significant difference in means. However we must realize that there was only one 19μA H^+ run and we should be leery of this single result.

TABLE 16

π Vs HELIUM PRESSURE

He PRESSURE mtorr	AV. BEAM CURRENT μA	# OF RUNS	# OF MEASUREMENTS OF π	π IN %	S.E. OF MEAN OF π	π FOR % CORRECTED FOR CASCADE AND TRAPPING
.01	5.5	8	160	- .92	1.	- .97
.05	6.6	5	100	2.53	.75	2.67
.2	7.1	7	140	1.91	.27	2.04
.6	7.	2	40	.61	.8	.66
1.0	5.8	2	40	.36	.12	.39
1.5	6.	2	40	- .68	.14	- .74

Proton beam energy = 150 keV

TABLE 17

π Vs HELIUM PRESSURE

He PRESSURE mtorr	AV. BEAM CURRENT μA	# OF RUNS	# OF MEASUREMENTS OF π	π IN %	S.E. OF MEAN OF π	π FOR % CORRECTED FOR CASCADE AND TRAPPING
.01	11.8	7	140	.81	.96	.84
.05	11.4	7	140	- .82	.48	- .86
.2	10.5	10	200	-2.46	.2	-2.6
.6	12.2	3	60	-3.53	.22	-3.76
1.0	11.2	3	60	-2.93	.23	-3.13
1.5	11.3	2	40	-2.29	.15	-2.46

Proton beam energy = 300 keV

TABLE 18

π Vs HELIUM PRESSURE

He PRESSURE mtorr	AV. BEAM CURRENT μA	# OF RUNS	# OF MEASUREMENTS OF π	π IN %	S.E.	π IN % CORRECTED FOR CASCADE AND TRAPPING
.01	11.8	4	80	-2.1	.92	-2.19
.05	10.4	5	100	-2.3	.62	-2.41
.2	10.3	7	140	-5.46	.27	-5.76
.6	10.7	3	60	-4.95	.46	-5.29
1.0	10.8	3	60	-3.54	.34	-3.79
1.5	10.5	2	40	-3.31	.2	-3.55

Proton beam energy = 450 keV

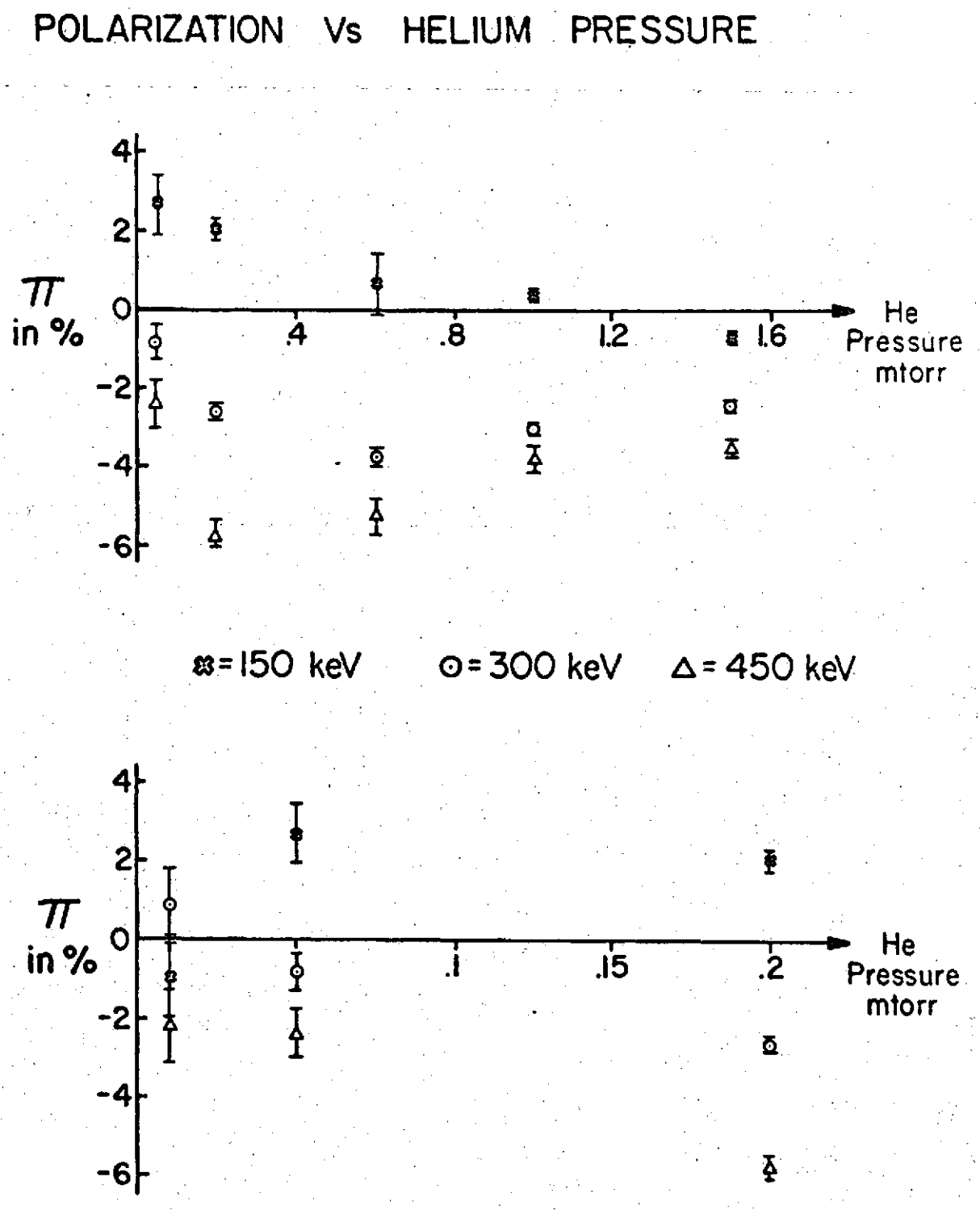

Horizontal axis expanded for lower graph

FIGURE 17

TABLE 19

π Vs BEAM CURRENT

AV. BEAM CURRENT μA	# OF RUNS	# OF MEASUREMENTS OF π	π IN %	S.E.	π IN % CORRECTED FOR CASCADE AND TRAPPING
19.0	1	20	-3.22	.3	-3.4
10.5	10	200	-2.46	.2	-2.6
1.0	6	120	-3.77	.88	-3.98

t-test Comparisons

Low Vs. Normal $t = 1.80$ $\nu = 318$

High Vs. Normal $t = 1.53$ $\nu = 218$

In any case we have shown that the polarization of the light from the 3^1P-2^1S transition in proton beam excited He is independent of beam current (over the range ∿1 to ∿20μA H^+). We are now able to compare measurements of π made at different beam energies and unavoidable different beam currents. The accelerator is most efficient at 300 keV, and less efficient at 150 and 450 keV. We were therefore unable to run at the optimum of ∿10μA for all beam energies. The accelerator maximum currents are shown in table 20. Ten micro amperes was chosen as an optimum for several reasons; signal to noise ratios were better with this high current; and the Faraday cup could tolerate this current for sustained periods of time. When possible we ran at ∿10μA H^+, otherwise (at 100, and 150 keV) we ran with as much current as we could get.

We may now compare polarization measurements made at different beam currents having shown that the data taken at these different beam currents are compatible. The energy dependent results have been shown in table 15 and in figure 16 (Corrected π Vs Beam Energy). The large error on the 100 keV point is due to the fact that we were only able to get two runs at that energy and pressure. The Van de Graaff accelerator, upon the installation of a new (and slightly larger) exit canal at the source bottle, ceased to operate at 100 keV. It was deemed impractical to attempt modification of the accelerator in order to refine measurements of that one

TABLE 20

APPROXIMATE BEAM CURRENT MAXIMUMS

BEAM ENERGY keV	BEAM CURRENT μ-A
100	5
150	8.5
200	12
250	13
300	20
350	15
400	13
450	12

point. The points in figure 16 generally form a smooth gently curving line with the exception of the 400 keV point. Theoretical predictions (Appendix B, Table B2) from the work of Bell (1961) are, except for the distortion approximation at 178 keV, in very poor agreement with our results. Previous experimental work however is in good agreement with ours. We have abstracted the results of Scharmann (1967), and Scharmann (1969), from their graphical presentations (neither of these works either tabularized their results or included error bars) and reported the estimates in table 21 along with the tabularized results of Van den Bos (1968). In the small region of overlap (100-150 keV) we find ourselves in much better agreement with Scharmann (especially considering the curve shapes which we have not shown). Van den Bos' polarization measurements were done using a monochrometer to select the λ 5016 Å line and he may not have completely corrected for the polarizing influence of the monochrometer. He also may have not taken care with regard to He pressure. He implies that he used .2 mtorr but does not explicitly say so.

All other previous experimental work on the polarization of the λ 5016 Å line has been done at pressures $\geq$ .2 mtorr. This work is the first to extend that measurement to lower pressures, see summary in table 22. It has been difficult to do so since the signal to noise ratios fall off rapidly as one lowers the He target gas

TABLE 21

COMPARISON WITH OTHER EXPERIMENTS

BEAM ENERGY (keV)	THIS WORK .2 mtorr	VAN DEN BOS NO PRESSURE STATED	SCHARMANN (1967) .2 mtorr	SCHARMANN (1969) .2 mtorr	THEORY-BELL DISTORTION
100	2.9 %	-1. %	2.5 %	5.5 %	14 %
150	2.04 %	4. %			
200	.71 %				(178 keV) 2.6%
250	- .83 %		-2 %		
300	-2.6 %				(316 keV) 13%
350	-3.69 %				
400	-4.23 %			-5.5 %	
450	-5.76 %		-6 %	-8. %	-22 %

TABLE 22

CORRECTED π Vs PRESSURE

PRESSURE mtorr	150 keV BEAM	300 keV BEAM	450 keV BEAM
.01	- .97±1.	.84±.96	-2.19±.92
.05	2.67± .75	- .86±.48	-2.41±.62
.2	2.04± .27	-2.6 ±.2	-5.76±.27
.6	.66± .8	-3.76±.22	-5.29±.46
1.0	.39± .12	-3.13±.23	-3.79±.34
1.5	- .74± .14	-2.46±.15	-3.55±.2

pressure. We consider our .05 mtorr measurements as successful, but have less faith in our .01 mtorr results. There is simply very little light reaching our detector from the target chamber when the pressure is .01 mtorr. We are therefore not surprised to find the .01 mtorr points in figure 17 to be of questionable value. The .05 mtorr and higher pressure points do lie on relatively smooth sensible curves and in fact a similar curve shape was reported by Scharmann (1969). He graphically displayed results for π as a function of pressure over the range .2 mtorr to $\sim$8. mtorr (for beam energies of 100, 450, 600, and 835 keV). Each of his curves shows a minimum (a most negative π), and as energy increases, the minimum occurs at a lower pressure. We have observed the same phenomena for our 300 and 450 keV curves. Our 150 keV curve does not show a minimum, however from Scharmann's curves, we would expect the 150 keV minimum to occur at $\sim$2 mtorr, a pressure which we do not reach. Scharmann's results also showed the polarization (at 100 keV beam energy) changing sign as the pressure changed. (Also for the 4^1P-2^1S line at 100 keV.) Our results show a change in the sign of π (for 150 keV beam) at $\sim$1.2 mtorr, and imply (at 300 keV) a change in sign at $\sim$.015 mtorr. Scharmann does take notice of this change in sign of π, however he offers no explanation and in fact states that he has no explanation for this phenomena. We discuss this problem in Appendix D.

This work is limited in a number of ways. The lowest pressure we are able to accurately measure is .01 mtorr, we would have liked to have used lower pressures. However we could just barely get data at .01 mtorr as so little light was received by our detector. We are also limited by the heat dissipation capability of our Faraday cup, our Signal/Noise ratio could have been improved by using higher beam currents. (At some energies the beam current is limited by the Van de Graaff accelerator rather than the Faraday cup.)

Improvements in this work could be made by . . .

1. Obtain a new pressure measuring system capable of accurately measuring pressures to 10^{-3} or 10^{-4} mtorr.
2. Rebuild the Van de Graaff beam tube vacuum system so that one could have a differentially pumped target chamber at 10^{-3} or 10^{-4} mtorr while the beam tube was held at 10^{-5} mtorr. (Now the beam tube is generally held at 10^{-3} mtorr.)
3. Rebuild the target chamber electrostatic focusing system and entrance slits such that we get a beam of small cross section through the axis of the chamber, and such that the detector can be brought much closer to the beam region of the chamber.
4. Modify the accelerator as so to be able to

obtain much higher beam currents especially at low energies.

5. Devise a way to cool the Faraday cup while still keeping if electrically insulated.
6. Use the PDP-8 or equivalent to automaet the data taking.
7. Shield the target chamber with mu metal so as to determine whether π is in fact effected by stray magnetic fields. Note π should not be so effected.

5.3 Conclusions

It is clear from this work that the polarization of the light from the 3^1P-2^1S transition in proton beam excited Helium is still pressure dependent even at pressures as low as .05 or .01 mtorr. The results of Scharmann, as far as they go, bear this out. We are faced with a phenomena which exhibits poor agreement between theory and experiment, however we conclude that even we have not yet reached low enough pressures to find the natural value of the polarization. It remains for the next worker in the field to extend the measurement to yet lower pressures in search of a pressure independent value for the linear polarization fraction.

REFERENCES

Allison, S. K., and Warshaw, S. D., Rev. Mod. Phys. 25, 779 (1953).

Bacon, R. H., Am. J. Phys. 21, 428 (1953).

Bell, R. J., Proc. Phys. Soc. 78, 903 (1961).

Bethe, H. A., and Jackiw, R., Intermediate Quantum Mechanics, Benjamin, New York (1968).

Condon, E. U., and Shortley, G. H., The Theory of Atomic Spectra, Cambridge University Press, Cambridge (1935).

Feofilov, P. P., The Physical Basis of Polarized Emission, Consultants Bureau, New York (1961).

Gabriel, A. H., and Heddle, D. W. O., Proc. Roy. Soc. A258, 124 (1960).

Hasted, J. B., Physics of Atomic Collisions, American Elsevier, New York (1972).

Heddle, D. W. O., and Lucas, C. B., Proc. Roy. Soc. A271, 129 (1962).

Holstein, T., Phys. Rev. 83, 1159 (1951).

Jenkins, F. A., and White, H. E., Fundamentals of Optics, McGraw-Hill, New York (1950).

Land, E. H., J. Opt. Soc. Am. 41, 957 (1951).

Larson, L., Ph.D. Thesis University of New Hampshire, Durham, New Hampshire (1967).

Lees, J. H., Proc. Roy Soc. A137, 173 (1932).

Lees, J. H., and Skinner, H. W. B., Proc. Roy Soc. A137, 186 (1932).

Marion, J. B., Classical Electromagnetic Radiation, Academic Press, New York (1965).

Merzbacher, E., Quantum Mechanics, John Wiley & Sons, Inc., New York (1961).

Mitchell, A. C. G., and Zemansky, M. W., Resonance Radiation and Excited Atoms, Cambridge University Press, Cambridge (1961).

Mott, N. F., and Massey, H. S. W., The Theory of Atomic Collisions, Oxford, London (1965).

Parratt, L. G., Probability and Experimental Errors in Science, Dover, New York (1971).

Pegg, D. J., Ph.D. Thesis University of New Hampshire, Durham, New Hampshire (1970).

Percival, I. C., and Seaton, M. J., Phil. Trans. Roy. Soc. A251, 113 (1958).

Phelps, A. V., Phys. Rev. 110, 1362 (1958).

Scharmann, A., and Schartner, K. H., Phys. Let. 26A, 51 (1967).

Scharmann, A., and Schartner, K. H., Z. Physik 219, 55 (1969).

Skinner, H. W. B., Proc. Roy. Soc., A112, 642 (1926).

Shurcliff, W. A., Polarized Light, Harvard University Press, Cambridge, Mass. (1966).

Spiegel, M. R., Theory and Problems of Statistics, Schaum, New York (1961).

Thomas, E. W., and Brent, G. W., Phys. Rev. 164, 143 (1967).

Van den Bos, J., Winter, G. J., and DeHeer, F. J., Physica 40, 357 (1968).

Van den Bos, J., Physica 42, 245 (1969).

Van Eck, J., DeHeer, F. J., and Kistemaker, J., Physica 30, 1171 (1964).

Wilson, E. B., Jr., An Introduction to Scientific Research, McGraw-Hill, New York (1952).

Young, H. D., Mechanics and Heat, McGraw-Hill, New York (1964).

APPENDIX A

DESCRIPTION AND MEASUREMENT OF POLARIZED LIGHT

A.1 Polarized Radiation

It is well known that electromagnetic radiation behaves as a transverse wave. This means that the directions of both the electronic and magnetic field vectors of the wave are at all times perpendicular to the direction of propagation of the wave, as well as perpendicular to each other. Therefore, in order to completely specify the nature of a wave, one must among the many parameters, include those which describe the direction of either the electric or magnetic field vector as a function of time and position. Conventionally, one specifies the direction of electric field vector. We will from this point on use the term "light" in place of "electromagnetic radiation." Of course it is understood that light (including infrared, visable, and ultraviolet) is the name applied to a very small section of the electromagnetic spectrum. Furthermore comments made about polarized light do usually apply to other electromagnetic radiations.

Light can be described as either unpolarized or polarized. Unpolarized light has no preferred direction

for its electric field vector, nor any preferred rotation of its electric field vector about the propagation direction. Conversely, polarized light does have preferred direction and/or rotation for its electric field vector. As a matter of convenience, one can discuss three types of polarized light: 1. linearly polarized, 2. circularly polarized, and 3. elliptically polarized.

1. Linearly polarized light. When the electric field vector of a light beam maintains a fixed direction in space, then the beam is called linearly polarized. See Fig. A.1. This is by far the simplest case of polarization and in fact is a type of polarization often produced in nature.

2. Circularly polarized light. Light is said to be circularly polarized when the magnitude of the electric field vector appears constant while the vector itself rotates about the propagation direction. There are of course 2 types of circularly polarized radiation. The conventional distinction is that if the locus of the "tip" of the electric field vector describes a right-handed helix (such as the thread of a typical machine screw), then one has a wave of positive helicity (in optics called a left circularly polarized wave). Conversely, right circularly polarized light has the "tip" of its electric field vector describing a left-handed helix, and possesses negative helicity.

3. Elliptically polarized light. This is the

LINEARLY POLARIZED ELECTROMAGNETIC WAVE

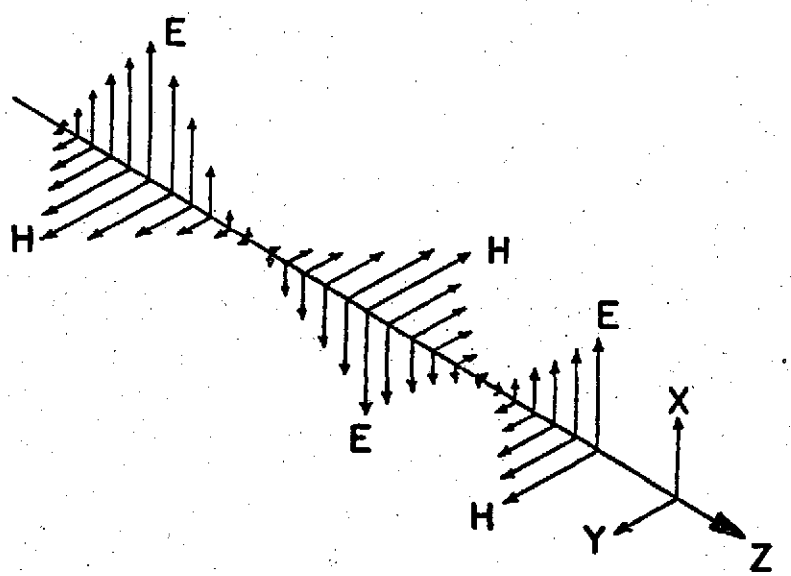

FIGURE A1

more complicated of the three cases due to the fact that both linear and circular components are present. To describe elliptically polarized radiation one must specify the handedness and magnitude of the circularly polarized component as well as the direction and magnitude of the linearly polarized component. Note that the major axis of the ellipse lies in the same direction as that of the linearly polarized component. An alternate equivalent description of elliptically polarized light is that it is made up to two linearly polarized components with differing amplitudes and non-0°, 90°, 180° phase angle differences. One must then specify each amplitude as well as the phase angle difference.

For purposes of description one can draw sectional patterns for a beam of light. These drawings represent the electric field vector as seen by an observer located on the z axis (assuming that the beam is traveling in the +z direction) and looking toward the source of the radiation. See fig. A.2. We might add at this point that a monochromatic beam has been assumed for the sake of simplicity.

A.2 Mathematical Descriptions of Polarized radiation

There are numerous equivalent mathematical descriptions of monochromatic waves, e.g.

SECTIONAL PATTERNS

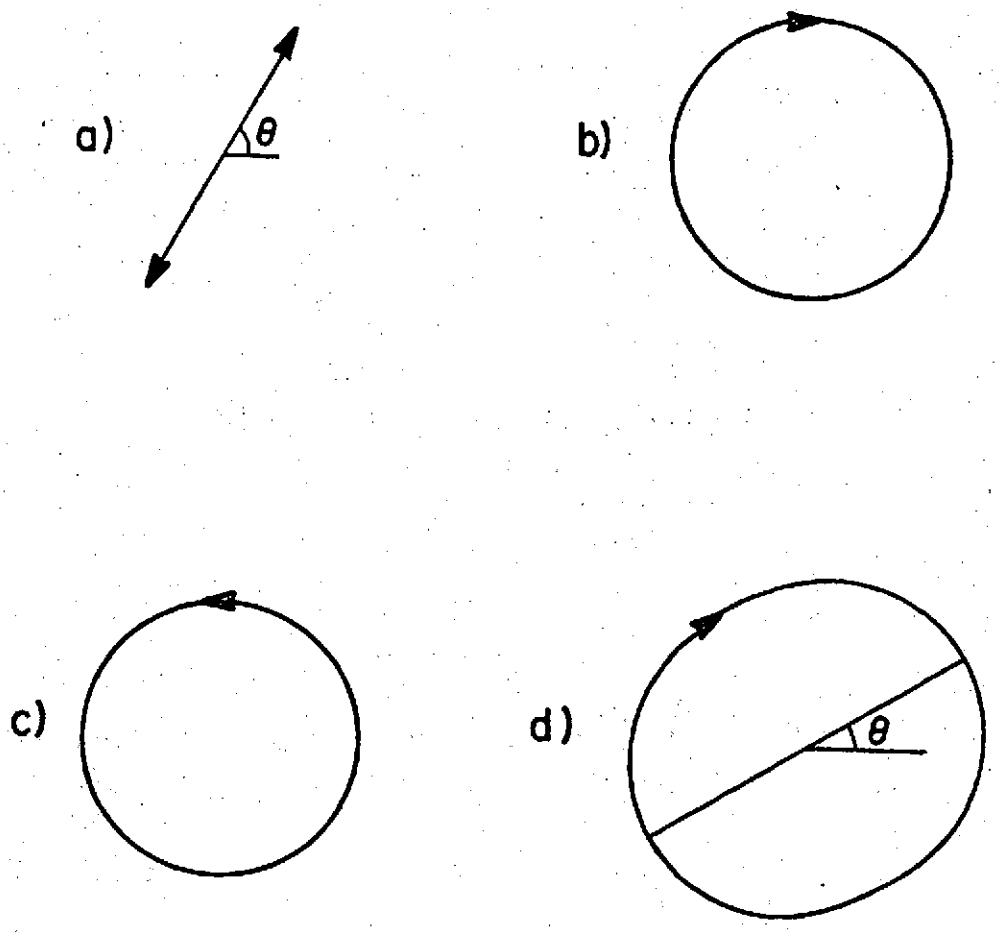

FIGURE A2

$$|E| = (E_{max}) \sin(\omega t - 2\pi z/\lambda)$$

or in complex notation

$$|E| = Re\left[E_{max}\, e^{i(\omega t - 2\pi z/\lambda)}\right]$$

or

$$|E| = Re\left[E_{max}\, e^{i\phi}\right]$$

where $|E|$ is the magnitude of the electric field vector, w is the 2π times the frequency of the wave, z is the position along the axis of propagation, λ is the wavelength, and t is the time. The last equation is just an abbreviated form of the second where

$$\phi = \omega t - \frac{2\pi z}{\lambda}$$

Let us also state that $Ee^{i\phi}$ is called the complex amplitude, ϕ is called the phase angle (at t and z) and that the intensity of the wave is proportional to $(E_{max})^2$. The direction of the electric vector has not yet been specified. Therefore the polarization of the wave has not yet been specified.

At first glance one may easily arrange a system to describe a linearly polarized beam by simply choosing the x axis along the direction of the beam's electric field vector. Then using the unit vector $\hat{\imath}$

$$\vec{E} = \left[E_{max} \sin(\omega t - 2\pi z/\lambda)\right]\hat{\imath}$$

or $$\vec{E} = Re\left[E_{max}\, e^{i\phi}\right]\hat{\imath}$$

One can then in turn describe circularly polarized light as the addition of two components of linearly polarized light of equal E_{max}, directed along the x and y axis respectively, with a phase angle difference of $\pm 90°$. By convention if the difference in phase angles, called γ ($\gamma = \phi_y - \phi_x$), is +90° the light is left-circularly polarized. Conversely, if $\gamma = -90°$ the light is right-circularly polarized.

When the x and y linearly polarized components have different amplitudes, and when $-180° < \gamma < 180°$ ($\gamma \neq 0$), the beam exhibits elliptical polarization. If $-180° < \gamma < 0°$ then the handedness is right, conversely the wave is left-elliptically polarized if $0° < \gamma < 180°$.

If one considers elliptical polarization to be the general case, then linear polarization results when $\gamma = 0°$, and circular polarization results when $|\gamma| = 90°$ and $(E_{max})_x = (E_{max})_y$.

Strangely, it is very difficult to properly describe a beam of unpolarized light. One can demand that no long term preference exist for handedness or linearity. (This precludes a "pure" coherent monochromatic wave.) Perhaps it is best to describe unpolarized light in terms of what it will and will not do (i.e., and operational definition). When a beam of unpolarized light is divided into two completely polarized components (by an ideal analyzer) the components will deliver equal power.

In the real worldlight is seldom either completely

polarized or unpolarized. One must in such a case specify the degree of polarization. This is usually accomplished by dividing the beam of light into orthogonal polarization components (e.g. right and left circular; horizontal and vertical linear, etc.), measuring the intensity of each of these components, and then calculating the degree of polarization V from

$$V = \frac{I_a - I_b}{I_a + I_b}$$

where I_a and I_b are the maximum and minimum intensities of the orthogonally polarized components respectively. Note that if one is discussing linearly polarized light, V reduces to π the linear polarization fraction.

A number of different mathematical models are in use for the treatment of beams of polarized light. These methods range from the geometrical methods of the Poincare sphere to the matrix calculus of the Stokes vector and Jones vector.

The Poincare Sphere model uses a mapping technique to describe the polarization form of a completely polarized beam. It is most useful for predicting the change in polarization form as the beam passes through various active polarizing devices (analyzers, retarders, etc.). In this model, every point on the surface of a unit sphere represents a different and specific polarization form. By definition the "north" pole represents left-circularly polarized light, and the "south" pole right. All points

on the equator represent linearly polarized light with various inclination angles (to the equator). One location on the equator (the prime meridian) is given the designation H for linearly polarized light parallel to the equator. Half way around the sphere (on the equator) the light is linearly polarized perpendicular to the equator, and given the designation V. At any location away from the poles and equator, one has elliptically polarized light. See Fig. A.3. To specify the form of a completely polarized beam, one need only specify the angles λ and ω (where 2λ = longitude and 2ω = latitude). This is easily done since λ is the azimuthal angle of the polarization ellipse and $\tan|\omega|$ is the ellipticity (b/a). See Fig. A.4. Furthermore the handedness is defined as left for the northern hemisphere ($\omega<0$) and right for the southern hemisphere ($\omega>0$).

When dealing with completely polarized beams and various retarders one can use this Poincare sphere to predict the change in the polarization form of the beam. This model is limited however in that one must be dealing with completely polarized beams.

The Stokes Vector model of polarized light is perhaps the most versitle and useful. The Stokes vector is a four parameter column vector

$$\begin{bmatrix} I \\ M \\ C \\ S \end{bmatrix}$$

THE POINCARÉ SPHERE

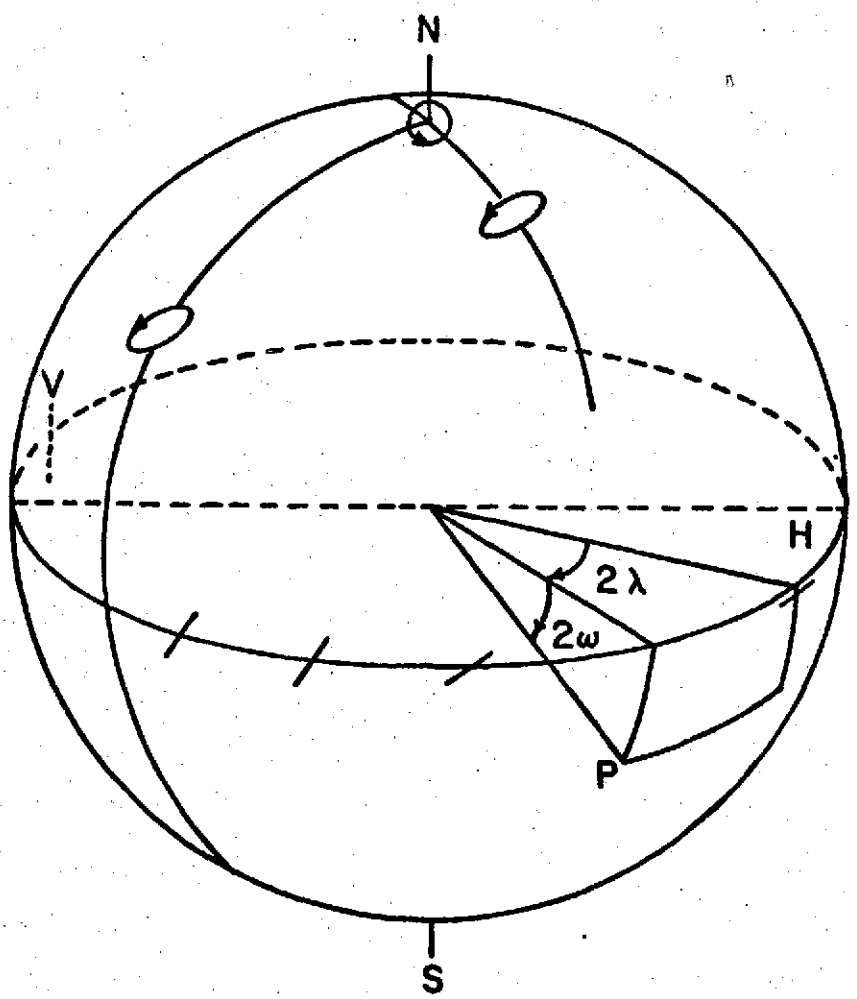

FIGURE A3

ELLIPTICALLY POLARIZED LIGHT

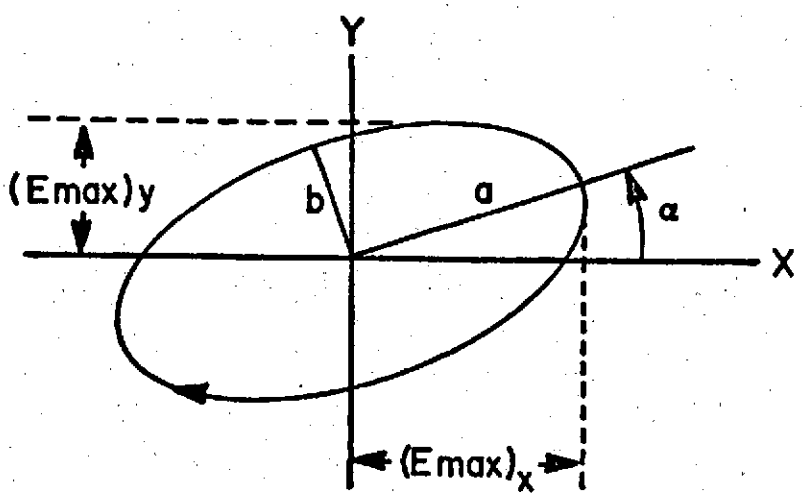

FIGURE A4

where all four entries have the units of intensity. Each of these parameters is defined in terms of a measurement made with a set of ideal polarizing filters. This set of four ideal filters have the following properties. All filters have a transmittance of .5 for unpolarized light. Then ... F_1, is a neutral isotropic filter; F_2 is a linearly (horizontally) polarizing filter; F_3 is a linearly (+45°) polarizing filter; and F_4 is a right-circularly polarizing filter. A polarization form independent detector is placed behind each of the filters in succession and four measurements are taken. The result of each measurement is multiplied by 1/.5 and the four values V_1, V_2, V_3, and V_4 are reported. The Stokes column vector is then calculated as follows

$$I = V_1$$
$$M = V_2 - V_1$$
$$C = V_3 - V_1$$
$$S = V_4 - V_1$$

An alternate and equivalent approach is to use the parameters from the wave description of light. One may then write (note time average $\langle \quad \rangle$) ...

$$I = \langle (E_{max})_x^2 + (E_{max})_y^2 \rangle$$
$$M = \langle (E_{max})_x^2 - (E_{max})_y^2 \rangle$$
$$C = \langle 2 (E_{max})_x (E_{max})_y \cos\gamma \rangle$$
$$S = \langle 2 (E_{max})_x (E_{max})_y \sin\gamma \rangle$$

It is also conventional to normalize the Stokes vectors.

This is accomplished by dividing all four entries by I (which is the largest). The Stokes vectors are very useful in that they can be applied to partially polarized beams, monochromatic as well as polychromatic beams, and incoherent beams. Furthermore, the Stokes vector can be manipulated (by Mueller calculus to be discussed later) so as to predict the behavior of a beam when passing through retarders and polarizers.

The Jones Vector model is applicable to situations in which the coherence and phase of the beam is important. For a specific location along the propagation direction (the z axis) the Jones vector is written as a two-element column vector

$$\begin{bmatrix} E_x \\ E_y \end{bmatrix}$$

or

$$\begin{bmatrix} (E_{max})_x \, e^{i(\varepsilon_x + \omega t)} \\ (E_{max})_y \, e^{i(\varepsilon_y + \omega t)} \end{bmatrix} = \begin{bmatrix} m \\ n \end{bmatrix}$$

where ε_x and ε_y are the phases of the x and y components at $t = 0$. There is a normalized form of the Jones vector where $m^2 + n^2 = 1$. Conversion of this vector to a recognizable form is a bit cumbersome and in general use of the Jones vector is confined to problems in which phase is important.

Table A.1 shows various polarization forms and the corresponding Stokes and Jones vectors.

The Mueller Calculus methodology provides a

TABLE A.1

EXAMPLES OF THE STOKES AND JONES VECTORS

Polarization Form	Normalized Stokes Vector	Normalized Jones Vector
Linear	$\begin{bmatrix} 1 \\ \cos 2\alpha \\ \sin 2\alpha \\ 0 \end{bmatrix}$	$\begin{bmatrix} \cos R \\ \pm \sin R \end{bmatrix}$
Left Circular	$\begin{bmatrix} 1 \\ 0 \\ 0 \\ -1 \end{bmatrix}$	$\frac{\sqrt{2}}{2}\begin{bmatrix} i \\ 1 \end{bmatrix}$
Right Circular	$\begin{bmatrix} 1 \\ 0 \\ 0 \\ 1 \end{bmatrix}$	$\frac{\sqrt{2}}{2}\begin{bmatrix} -i \\ 1 \end{bmatrix}$
Elliptical	$\begin{bmatrix} 1 \\ \cos 2\omega \cos 2\lambda \\ \cos 2\omega \sin 2\lambda \\ \sin 2\omega \end{bmatrix}$	$\begin{bmatrix} \cos R\, e^{-i\frac{\delta}{2}} \\ \sin R\, e^{i\frac{\delta}{2}} \end{bmatrix}$
Unpolarized	$\begin{bmatrix} 1 \\ 0 \\ 0 \\ 0 \end{bmatrix}$	none

means for manipulating the Stokes vectors so as to predict the behavior of a beam of light as it passes through any series of retarders, and or polarizers. The method itself is of a matrix-algebraic nature. For this work it is sufficient to say that every retarder and or polarizer at whatever orientation can be represented by a 4 x 4 Mueller matrix. To determine the polarization form and intensity of a beam exiting from an "active" filter one multiplies the Stokes Vector for the incoming beam by the Mueller matrix of the "active" filter. The new Stokes vector then describes the exit beam. Using the methods of matrix algebra one can easily predict the result of any combination of "active" filters.

The Jones Calculus methodology is similar to the above except that a smaller (2 x 2) matrix is used. This smaller matrix is usually made up of complex elements and can preserve phase information.

Standardized Mueller and Jones matrices are available in many works, notibly in Schurcliff (1966).

A.3 Polarized Light and Matter

When a beam of light (polarized or not) interacts with matter, the result of the interaction depends upon both the polarization of the initial beam, and the specific nature of the matter involved.

Let us first consider (classically) the scattering of an unpolarized light wave incident upon a molecule.

The electric charges in the molecule will try to "follow" the incident electric fields. As a result, the molecule will radiate, i.e. scatter the light. The polarization of the scattered light will depend upon the location of the observer. If the incoming light is linearly polarized then the light is scattered anisotropically, and again the polarization depends upon the location of the observer. See fig. A.5.

Polarization can also be caused by reflection and refraction. Again the electric field of the incoming light will cause the charges within the material to oscillate, thus multiple scattering is observed. Consider an unpolarized beam of light (in air) incident upon a more optically dense material (glass). Applying the boundry conditions that the tangential electric and magnetic fields at the surface are continuous, one arrives at the situation shown in fig. A.6. The degree of polarization depends upon the angle of incidence θ_i. When $\theta_i + \theta_r = \frac{\pi}{2}$ the polarization of the reflected and refracted components is almost total. The incidence angle for which this occurs is named Brewster's angle θ_β, defined by $\text{Tan}\ \theta_\beta = \frac{n_2}{n_1}$. Where n_2 and n_1 are the indices of refraction for the two media.

Certain materials exhibit the phenomena of Birefringence (double refraction) when interacting with light. Some crystalline solids fall into this category, that is they are optically anisotropic. In such a crystal

SCATTERING OF LIGHT

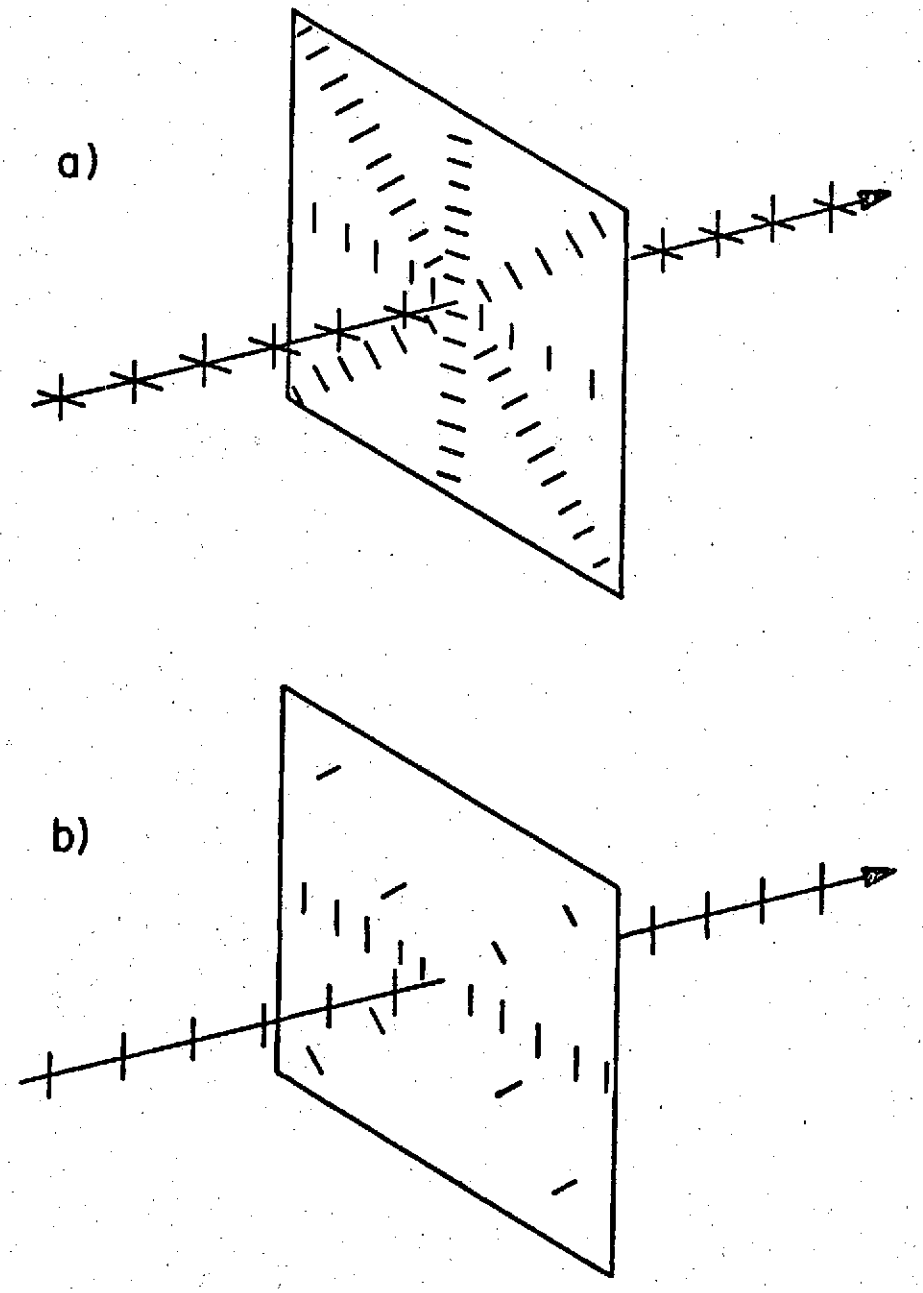

a) unpolarized incident wave
b) linearly polarized incident wave

FIGURE A5

POLARIZATION BY REFLECTION AND REFRACTION

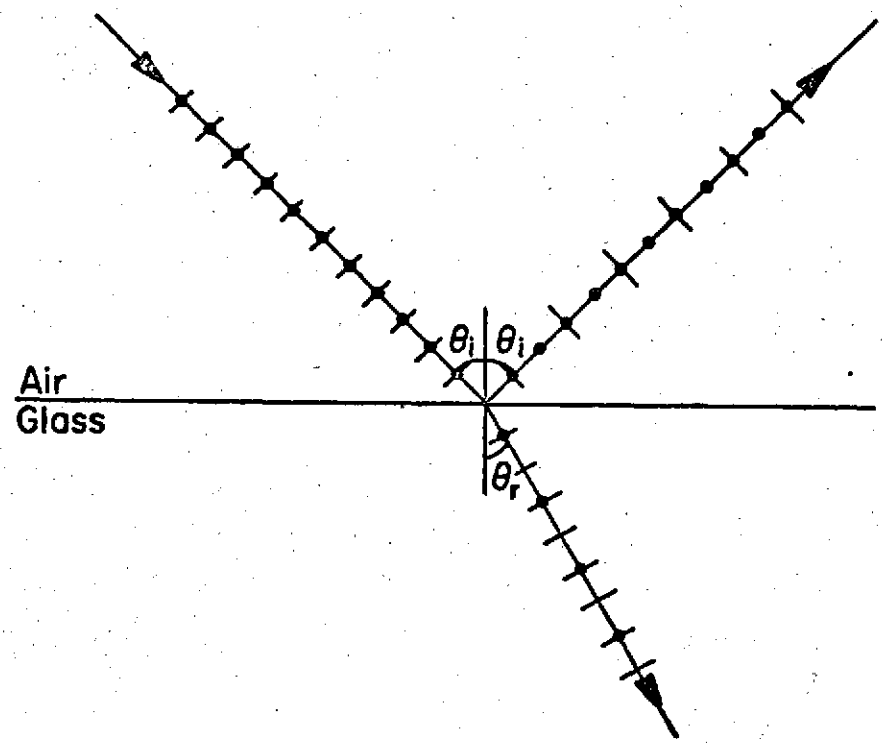

FIGURE A6

(calcite or quartz for example) an incident ray of unpolarized light will have two refracted rays (hence double refraction) as well as the usual reflected ray. One of the refracted rays will obey Snells Law...

$$n_1 \sin\theta_i = n_2 \sin\theta_r$$

This ray is then called the ordinary or 0 ray, while the refracted component which does not obey Snells Law is called the extraordinary or E ray. See fig. A.7. In 1678 Huygens discovered that the E and 0 rays were linearly polarized, and orthogonal. Birefringence is basically due to the fact that the velocity of the 0 ray is isotropic and therefore the material has the single index of refraction n_o for the 0 ray. The velocity of the E ray depends upon direction and therefore so does the index of refraction n_e for the E ray. The velocity of the rays depends upon the orientation of the electric field (the polarization) of the ray. This difference in velocity between the 0 and E rays enables the experimenter to selectively retard one of the linear polarization components. (This use of a birefringent crystal requires that the crystal be cut in a specific way... see Jenkins (1950). A crystal arranged in this manner is called a retarder and has the properties of resolving a beam into two components, transmitting the components at different velocities, and recombining them with a phase difference that depends upon, among other parameters, the thickness

BIREFRINGENCE

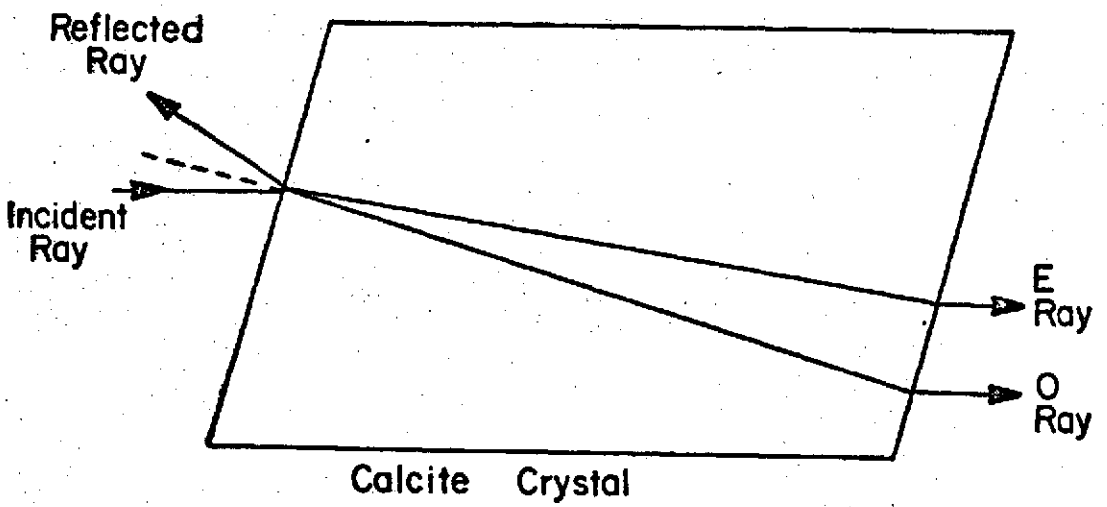

FIGURE A7

of the retarder. One can then generate elliptically polarized light by sending a beam of linearly polarized light through a retarder whose fast direction is at some angle Θ with respect to the initial plane of polarization, and whose retardance (phase angle difference) is δ. The results will be elliptically polarized unless $\Theta = \pm 45°$, $\delta = \pm 90°$ (circular); or $\Theta = \pm 90$, $\delta = \pm 90$ (linear) or if $\delta = 0°$, $180°$ (linear). A retarder then is just a polarization form converter.

The most important interactions of light with matter (for the practical use of polarized light) are dichroic interactions. Materials which exhibit dichroism will absorb one polarization form and transmit the orthogonal form. Polaroid sunglasses are a typical example of dichroic material. The lenses are oriented so as to pass linearly-vertically polarized light, therefore the horizontally polarized components are absorbed. But glare from the surface of a road, or body of water, or from many other horizontal reflecting surface is horizontally polarized, and removed by the dichroism of the sunglass lens. Although there are many materials which can be made to exhibit dichroism, the most commonly available is Polaroid Corporation's type H. This material is manufactured by alligning iodine molecules in a stretched sheet of polyvinyl alcohol. When a beam of light passes through the sheet, the component of the beam whose electric field lies along the long axis of the iodine molecules

will be absorbed. The orthogonal component is transmitted (with some attenuation due simply to the optical density of the sheet). Land (1951) has done a review of the history of dichroic polarizers (He is the inventor of the modern dichroic polarizer).

Optically active materials such as Turpentine, Quartz crystals and sugars (to be optically active a sample of the compound must contain a significant majority of one of the mirror image versions of itself; either the right or left handed version) can rotate the plane of polarization of a beam of linearly polarized light. Jenkins (1950) describes Fresnel's explanation for optical rotations. Fresnel assumed that optically active material treats the entering linearly polarized light as two equal amplitude, zero phase difference, counter-rotating circularly polarized components. He further assumed that the propagation speed was different for the Right and Left components; producing a non-zero phase difference. Then because of the non-zero phase difference, when the beam exits the material and the two counter-rotating components recombine, we once again have linearly polarized light, but the plane of polarization has been rotated by an angle $\delta/2$ (δ is the phase difference). It is apparent then that the magnitude of the rotation depends upon the amount of optically-active material the beam passes through. Although Fresnel's explanation does agree with experimental evidence it does not explain

the process on the molecular level. That explanation was first put forth by Reusch; he suggested that the molecules in an optically active substance are aligned in a helical pattern. This was later verified in other experiments.

A.4 Semiclassical and Quantum Mechanical Aspects of Polarized Light

In the previous section we have discussed the interaction of light with matter, without regard to how the light was created. We will now rectify that omission by discussing (both semi-classically and quantum mechanically) the origins of light within the most elementary radiating systems.

We begin with an electric dipole. Consider a fixed positive charge with a negative charge in linear periodic motion about it. Let us assume that our observation point is located a distance r_o from the positive charge with $r_1 \approx r_o >> r$. See fig. A.8. We can then write the retarded scalar and vector potentials (for the observer) of the moving negative charge as follows.

$$\phi = \left[\frac{-Q}{r_1 \left(1 - \frac{\dot{r} r_1}{c r_1}\right)} \right]_{t - \frac{r_1}{c}} \qquad \text{A.4.1}$$

$$A = \left[\frac{-Q\dot{r}}{c r_1 \left(1 - \frac{\dot{r} r_1}{c r_1}\right)} \right]_{t - \frac{r_1}{c}}$$

If we expand the above terms using

LINEAR ELECTRIC DIPOLE

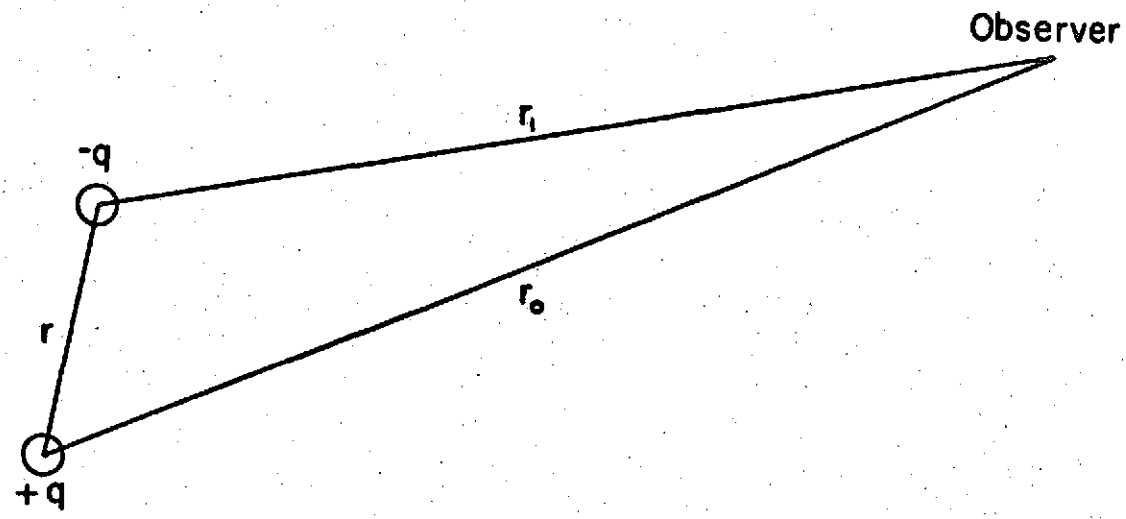

FIGURE A8

$$(1-x)^{-n} = 1 + nx + \frac{n(n+1)}{2!}x^2 + O(x^2)\ldots$$

and if we neglect terms of order $(\frac{\dot{r}}{c})^2$ and higher...

then

$$\phi \simeq -\frac{Q}{r_o} - \frac{Q}{r_o^2 c}(\dot{r}\, r_o)\Big|_{t-\frac{r_o}{c}}$$

A.4.2

$$A \simeq -\frac{Q}{r_o c}\dot{r}\Big|_{t-\frac{r_o}{c}}$$

If we now neglect the first term in the scalar potential expression (at large r_o the $\frac{-Q}{r_o}$ is cancelled out by the $\frac{+Q}{r_o}$ term from the fixed positive charge), and use the facts that

$$\bar{E} = -\nabla\phi - \frac{1}{c}\frac{\partial \bar{A}}{\partial t}$$

$$\bar{H} = \frac{1}{r_o}[\bar{r}_o \times \bar{E}] \qquad \text{A.4.3}$$

we arrive at

$$\bar{E} = \frac{Q}{r_o c^2}\ddot{r}_\perp$$

$$\bar{H} = \frac{1}{r_o}[\bar{r}_o \times \bar{E}] \qquad \text{A.4.4}$$

where $\ddot{r}_1$ is the component of the negative charges acceleration in a plane perpendicular to r_o. The observer (at sufficiently large r_o, in the wave zone) sees a plane polarized electromagnetic wave. Let us surround this oscillating and radiating di le with an imaginary sphere (radius r_o) such that the polar axis is along the dipole moment, the observed polarization direction of the wave will then depend upon where on the sphere the observer

is located. See fig. A.9. Since the dipole makes an angle θ with respect to r_o, and since $Q\bar{r} = \bar{p} = p_o \cos(\omega t)\hat{z}$ ... then

$$\bar{E} = \frac{\ddot{\bar{P}}_\perp}{r_o c^2}$$

$$\bar{H} = \frac{[\bar{r}_o \times \ddot{\bar{P}}_\perp]}{r_o^2 c^2} \qquad \text{A.4.5}$$

and

$$|E| = |H| = \frac{\omega^2}{r_o c^2} p \sin\theta \qquad \text{A.4.6}$$

where H is always parallel to the equator of our sphere and E is always perpendicular to said equator. Thus the wave is completely linearly polarized.

Let us now consider the electric rotor where the negative charge travels about the fixed positive charge in a circular path. Rather than repeat the calculations from the beginning, we can instead resolve the circular motion into two linear harmonic components with the same frequency and amplitude but with a phase difference of $\pm\pi/2$. If we again use our imaginary sphere, this time with the polar axis along the symmetry axis of the rotor, again the form of the polarization will depend upon the location of the observer. For $\theta = 0°$, 180° one observes a circularly polarized wave, at $\theta = 90°$ one observes a linearly polarized wave, and anywhere in between one observes an elliptically polarized wave.

There are of course higher order terms which we

POLARIZATION OF ELECTRIC DIPOLE RADIATION

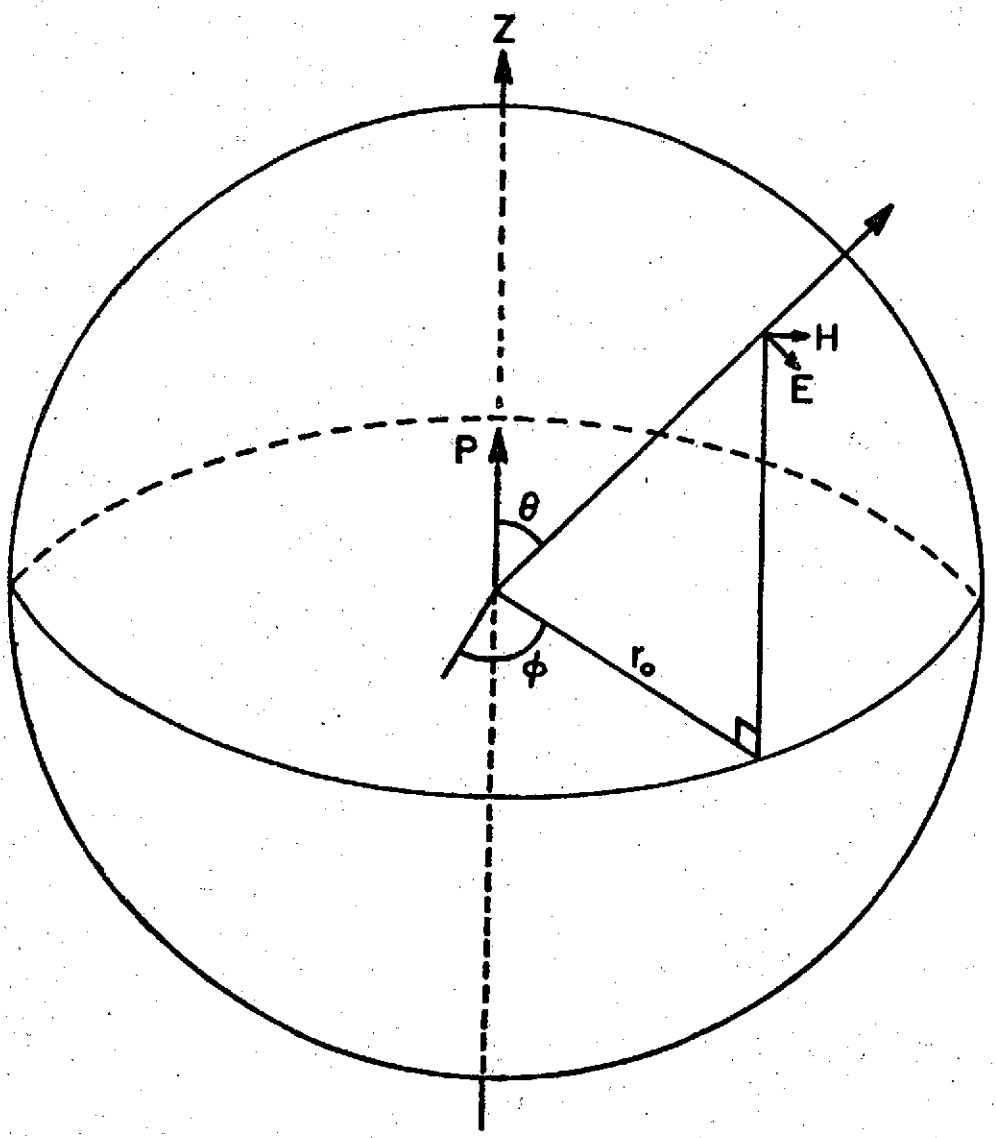

FIGURE A9

have neglected, a summary of the radiation from higher electric multipoles as well as from magnetic radiators is available in Feofilov (1961).

We can now discuss polarization in the normal Zeeman effect. Let us place our linear dipole oscillator in a magnetic field H not directed along the dipole moment. The equation of motion of the negative charge is

$$m\ddot{\bar{r}} = -m\omega_o^2 \bar{r} - \frac{Q}{c}[\dot{\bar{r}} \times \bar{H}] \qquad \text{A.4.7}$$

which can be written as the three scalar equations (choosing the z direction to be along H)

$$\begin{aligned} m\ddot{x} &= -m\omega_o^2 x - \frac{Q}{c}\dot{y}H \\ m\ddot{y} &= -m\omega_o^2 y - \frac{Q}{c}\dot{x}H \\ m\ddot{z} &= -m\omega_o^2 z \end{aligned} \qquad \text{A.4.8}$$

The z equation solves immediately the $z = z_o \cos \omega_o t$. We will try solutions of the form $x = A_x e^{i\omega t}$ and $y = A_y e^{i\omega t}$ for the x and y equations. This procedure yields

$$(\omega_o^2 - \omega^2)^2 = \left(\frac{Q\omega}{mc}\right)^2 H^2 \qquad \text{A.4.9}$$

or

$$\omega_o^2 - \omega^2 = \pm \frac{Q\omega}{mc} H \qquad \text{A.4.10}$$

therefore

$$\omega = \sqrt{\omega_o^2 + \frac{Q^2H^2}{4m^2c^2}} \pm \frac{Q}{2mc} H \qquad \text{A.4.11}$$

However for magnetic fields, H, of realizable magnitude, $\omega_o >> \frac{QH}{2mc}$ and therefore dropping terms of order $(\frac{QH}{2mc})^2$ we arrive at

$$\omega = \omega_o \pm \Delta\omega$$
$$\Delta\omega = \frac{QH}{2mc} \qquad \text{A.4.12}$$

and note $\Delta\omega << \omega_o$. We may now solve for the A_x and A_y by again using $x = A_x e^{i\omega t}$ and $y = A_y e^{i\omega t}$ in A.4.8 and then removing terms of order $(\frac{\Delta\omega}{\omega_o})^2$. We then find

$$A_x = \mp i A_y \qquad \text{A.4.13}$$

and the full x and y solutions are

$$X = A_x e^{i(\omega_o \mp \Delta\omega)t}$$
$$Y = A_y e^{i\left[(\omega_o \mp \Delta\omega)t \mp \frac{\pi}{2}\right]} \qquad \text{A.4.14}$$

Therefore when $\omega = \omega_o + \Delta\omega$, x leads y by a phase angle of $\pi/2$ and the radiation emitted by this oscillator (when viewed from the z axis) is circularly polarized; and when $\omega = \omega_o - \Delta\omega$, x lags y by a phase angle of $\pi/2$ and the radiation is again circular butopposite in direction (called σ components).

In summary, when a linear dipole oscillator is placed in a magnetic field one observes three frequencies of oscillation ω_o, $\omega_o + \Delta\omega$, and $\omega_o - \Delta\omega$. Both the intensities and polarizations of these radiations depend upon the location of the observer. If the observer is

on the z axis he will observe only circularly polarized components of frequency $\omega_o \pm \Delta\omega$. (the linearly polarized ω_o radiation has zero intensity on the z axis). However, if the observer is on a line perpendicular to the z axis, in the plane containing the dipole, he will then observe all three radiations ω_o, $\omega_o \pm \Delta\omega$. Now however the σ components ($\omega = \omega_o \pm \Delta\omega$) will appear as linearly polarized with the electric field vector perpendicular to the magnetic field direction. (Analogous to observing an electric rotor edge on) the ω_o radiation (the π component) is of course linearly polarized with its electric field vector parallel to the magnetic field direction.

This classical description of the normal Zeeman effect is limited to cases in which the source of radiation can be considered a simple system of linear dipole oscillators.

We now turn to quantum mechanics for a description of polarized light on an atomic scale. We will confine our discussion to electric dipole transitions where $\Delta\ell = \pm 1$, and $\Delta m = 0, \pm 1$. These selection rules are necessary for non zero matrix elements between the upper and lower states. The transition probability is of course proportional to the square of the matrix element. The selection rules can be demonstrated as follows. The matrix element

$$D_{kn} = \int \psi_k^* \, p \, \psi_n \, d\tau \qquad \text{A.4.15}$$

(where p is the dipole moment of the atom electron system) can be resolved into the cartesian elements

$$D^x_{kn} = -e \int \psi^*_k \, x \, \psi_n \, d\tau$$

$$D^y_{kn} = -e \int \psi^*_k \, y \, \psi_n \, d\tau \qquad \text{A.4.16}$$

$$D^z_{kn} = -e \int \psi^*_k \, z \, \psi_n \, d\tau$$

assuming that the electron moves in a central force field, we can then write

$$\psi = e^{im\phi} \, P_{lm}(\theta) \qquad \text{A.4.17}$$

where l is the orbital angular momentum quantum number, and m is the "z" component of l. There are $2l + 1$ values of m, and m ranges by integers from $-l$ to $+l$. Using A.4.17 in A.4.16 and with the z axis as the polar axis we arrive at ...

$$D^x_{kn} = \frac{e}{2} \int_0^{2\pi} \left(e^{i(m'-m+1)\phi} + e^{i(m'-m-1)\phi} \right) d\phi \int_0^{\pi} P_{lm} P_{l'm'} \sin^2\theta \, d\theta$$

$$D^y_{kn} = \frac{e}{2i} \int_0^{2\pi} \left(e^{i(m'-m+1)\phi} + e^{i(m'-m-1)\phi} \right) d\phi \int_0^{\pi} P_{lm} P_{l'm'} \sin^2\theta \, d\theta \qquad \text{A.4.18}$$

$$D^z_{kn} = e \int_0^{2\pi} e^{i(m'-m)\phi} \, d\phi \int_0^{2\pi} P_{lm} P_{l'm'} \cos\theta \sin\theta \, d\theta$$

The first two integrals will be zero unless $(m' - m) = \pm 1$ or $\Delta m = \pm 1$. The last integral will be zero unless $(m' - m) = 0$. Also note that when $\Delta m = \pm 1$ we have in effect linear dipole oscillators in the x and

y directions and circularly polarized light, (as viewed from a point on the z axis) these are again the σ components. When $\Delta m = 0$ we again have the equivalent of a linear dipole oscillator with the E vector parallel to the z direction, which is the π component. Further note that when viewed from position in the xy plane one sees the σ components as linearly polarized with E perpendicular to z and the π component as linearly polarized with E parallel to z. It can also be shown that for $\Delta m = 0, \pm 1$, $\Delta \ell$ must be ± 1. These selection rules can be generalized to the set of quantum numbers $\eta \ell j M$. Where then $\Delta j = \pm 1, 0$ but $j = 0 \rightarrow j = 0$ is forbidden and $\Delta M = 0, \pm 1$.

The above selection rules are appropriate in light of the following arguments... the angular momentum of linearly polarized light is zero, therefore when such light is emitted, the change in the angular momentum component along any axis ($m\hbar$) should not change, hence $\Delta m = 0$. Circularly polarized light carries angular momentum $\pm \hbar$ one would therefore expect $\Delta m = \pm 1$.

We are now prepared to discuss the Zeeman effect quantum mechanically. Let us choose the z axis along the external magnetic field H. This problem has been solved in many books (see Bethe (1956) pg 208) with the following result...

$$E'_{n\eta jM} = E_{n\eta j} + \frac{e\hbar}{2\mu c} g M H \qquad \text{A.4.19}$$

where

$$g = 1 - (g_s - 1)\,\frac{j(j+1) + s(s+1) - \ell(\ell+1)}{2j(j+1)} \qquad \text{A.4.20}$$

and M takes on (2j + 1) values. The energy E' therefore takes on (2j + 1) values, one of which is still the zero magnetic field value $E_{n\ell j}$. The wavelengths of the radiation are then

$$\lambda = \lambda_o \pm \frac{4\pi\mu c^2}{(M_1 g_1 - M_2 g_2) e H} \qquad \text{A.4.21}$$

The polarization rules are again, π component when $\Delta M = 0$ (and therefore $\lambda = \lambda_o$), and σ component when $\Delta M = \pm 1$ (and therefore $\lambda = \lambda_o \pm \Delta\lambda$). The apparent polarization of the π and σ components will depend upon the location of the observer. If the observer is located upon the z axis then the intensity of the π component will be zero and only the circularly polarized σ components will appear (at wavelengths $\lambda = \lambda_o \pm \Delta\lambda$). If the observer is located in the xy plane, then both the π component (linearly polarized with the E vector parallel to z, with wavelength λ_o), and the σ component (appearing a linearly polarized with the E vector perpendicular to the z axis at wavelengths $\lambda = \lambda_o \pm \Delta\lambda$) will appear. As a specific example consider Helium with s = 0, therefore J = L and g = 1. See fig. A.10. It was also shown by Feojilov (1961) that for this specific $^1p_1 \rightarrow {}^1s_o$ transition the ratio of intensities for the π and σ components (observed in the

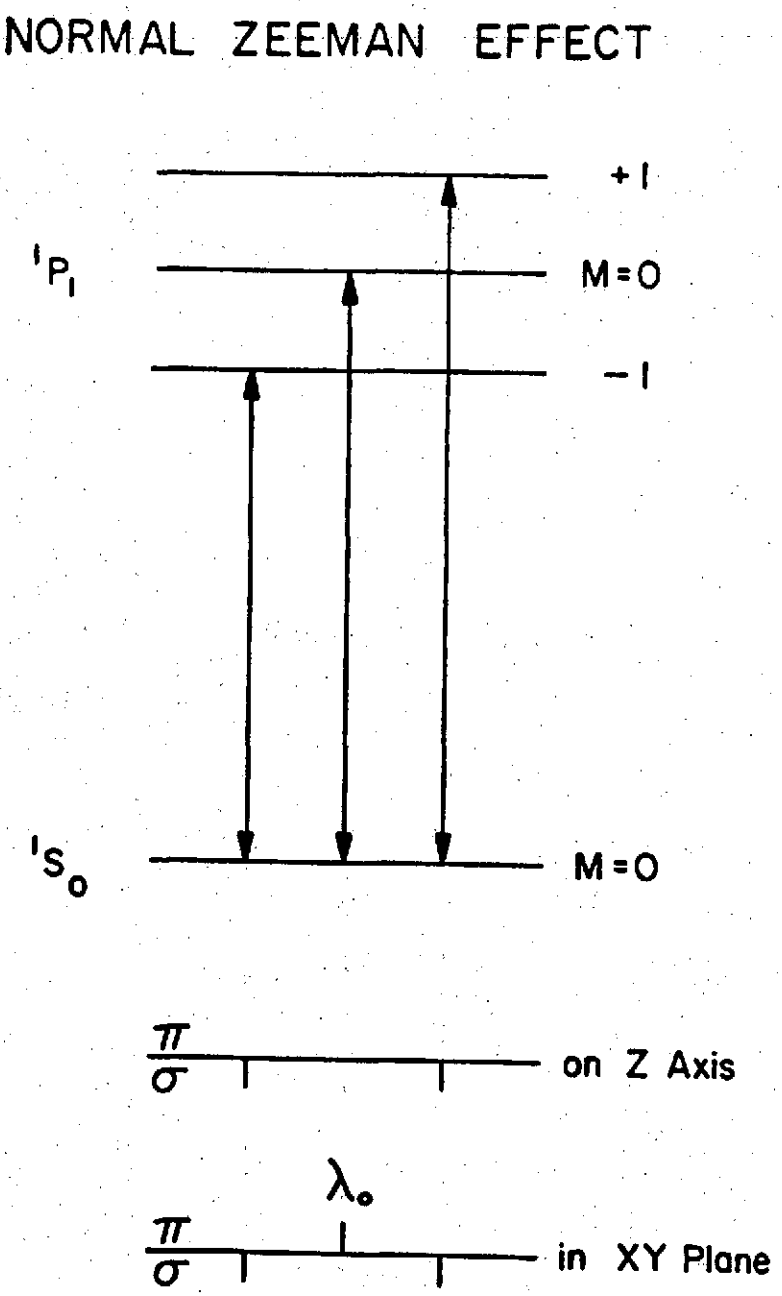

The presence or absence of π or σ radiation is indicated schematically in the lower two lines.

FIGURE A10

x, y plane) is 1:2:1 for $\sigma_{-1}:\pi:\sigma_{+1}$.

The question now arises of what happens to the π and σ components as the magnetic field H goes to zero. Certainly the wavelength splitting decreases toward zero, and in fact the magnetic sublevels become degenerate. However (experimentally) the π and σ components do continue to exist even at zero field. Heisenberg (1925) has stated the principle of spectroscopic stability... (paraphased) the state of polarization does not change when the external additional magnetic field, which is superimposed on the system in such a way that its symmetry remains unaltered, tends to zero.

The entire above discussion has concerned itself with one elementary radiator (or one atom). In general for a macroscopic system of many radiators the polarization will average to zero unless some anisotropy is introduced. In this work the anisotropy is introduced by the energetic proton beam. The beam direction is chosen as the z axis and observations are made from within the xy plane. See figure 2.

A.5 Measurement Methods for Polarized Light

The devices which are used to analyze polarized light in fact apply those phenomena which we have discussed in A.3. Some of these devices are; the linear polarizer (dichroism); the polarizing prisms, Nicol, Glan-Thompson etc. (birefringence); retarders (birefringence); and the pile of plates polarizer (reflection

and refraction).

The linear polarizers are the invention of E. H. Land and generally the product of polaroid Corporation (Cambridge, Massachusetts). The so-called H-sheet is the most common, and is covered by a number of patents. During manufacture a thin sheet of polyvinal alcohol is heated, stretched and then for support purposes laminated to a sheet of cellulose acetate butyrate. The polyvinal alcohol face is then wet with an iodine rich solution which will leave a residue of aligned iodine molecules within the polyvinal alcohol. This sheet is then laminated between plates of glass to form the completed linear polarizer. These polarizers can be made in various colors and transmittances. In this work a type HN-32 implies a peak transmittance of 32% for unpolarized incident light. The behavior of this polarizer for normal incidence is categorized in table A.2. Note that K_1 (the major principle transmittance) is defined as the ratio of transmitted to incident intensity when the linear polarizer is placed in a normally incident, linearly polarized beam of light oriented to maximize the transmittance. The minor principle transmittance, K_2, is obtained from the same ratio during minimum transmitance. The principle transmittance ratio R_t is defined as k_1/k_2. For one polarizer R_t is on the order of 1.5×10^4 (at 5000 Å). Reflection losses do occur at the surfaces of linear polarizers, however these losses (for normal incidence) are isotropic and

TABLE A.2

BEHAVIOR OF THE HN-32 POLAROID ANALYZER

Wavelength	K_1	K_2
3750	.33	.001
4000	.47	.003
4500	.68	.0005
5000	.75	.00005
5500	.70	.00002
6000	.67	.00002
6500	.70	.00002
7000	.77	.00003
7500	.84	.0002

amount to typically <4%.

There are of course many other dichroic linear polarizers which do not immediately concern us. Detailed information can be obtained from Polaroid Corporation, Cambridge, Massachusetts.

The linear polarizing prisms have been in large measure replaced by the dichroic sheet polarizers. However one great advantage the birefringent polarizer has over the dichroic type is that a polarizing prism can separate and deliver both of the orthogonal linear components, there is no significant absorbtion. Very few of these prism polarizers however can be adjusted to leave the path of the incident beam undeflected, this is the main cause of their replacement by the linear dichroic polarizers.

Polarization form conversion is done with the use of retarders. The most common retarders are quarter and half-wave plates. The quarter-wave plate will convert a beam of linearly polarized light into a beam of circularly polarized light (when properly oriented). The half-wave plate can be used to rotate the plane of polarization of linearly polarized light. There are also circular and elliptical retarders, so that in general with the proper combinations and orientations of linear polarizers and retarders one may convert from any one polarization form to another.

The pile of plates polarizer is usually used for

production and/or analysis of vacuum ultraviolet polarized light. The polarizers previously mentioned generally are unusable in the ultraviolet region of the spectrum. Therefore the pile of plates reflection/refraction polarizer arrangement, even though extremely cumbersome, is grudgingly used.

Given a beam of light of unknown polarization form, one can use the devices previously discussed in order to analyze the polarization form. Once the form has been analyzed, specific polarizing analyzers can be used to separate the orthogonal components for the purpose of intensity measurements. The results of these intensity measurements can be used to calculate the degree of polarization. The beam is then completely analyzed. In order to make the intensity measurements one needs a detector which meets two general requirements. Many different detector types can be used, the requirements being that the detector be sufficiently sensitive and also that the detector be completely polarization insensitive.

In this research the HN-32 analyzer is used to isolate the linear polarization components so that we may use a photomultiplier detector system to measure the intensities of the components. We are then able to calculate the linear polarization fraction.

APPENDIX B

THEORY

B.1 Collison Theory

We must eventually use inelastic scattering theory to describe our process...

$$H^+ + H_e \rightarrow H^+ + H_e^*$$

However, let us first review elastic scattering.

We will assume the ideal case of a fixed scattering center at the origin impacted upon by a beam of particles incident along the +z direction. We can represent the scattering center by a potential $V(\bar{r})$, and let us assume that the incoming beam is monoenergetic. If after the elastic scattering occurs, the particles are detected far from the origin by a device which subtends an angle $d\Omega$, then the differential scattering cross section is

$$\sigma(\theta,\phi) = \frac{1}{N}\,\frac{dN}{d\Omega} \qquad \text{B.1.1}$$

where N is the flux of particles in the beam, and dN is the flux counted by the detector. The total scattering cross section σ_t is then

$$\sigma_t = \int \sigma(\theta,\phi)\, d\Omega \qquad \text{B.1.2}$$

We can describe the monoenergetic beam of particles by a plane wave with wave function

$$\psi = e^{i\bar{k}\cdot\bar{z}} \qquad \text{B.1.3}$$

The wave function after the interaction will then be

$$\psi = e^{i\bar{k}\cdot\bar{z}} + V \qquad \text{B.1.4}$$

where at large r, we must have

$$V = f(\theta,\phi)\ \frac{e^{i\bar{k}\cdot\bar{r}}}{r} \qquad \text{B.1.5}$$

i.e. an outgoing spherical wave. The particle flux can be calculated from the wavefunction by using the expression for the probability current density...

$$S = -\frac{i\hbar}{2m}\left[\psi^*\nabla\psi - (\nabla\psi^*)\psi\right] \qquad \text{B.1.6}$$

When this is applied to B.1.5 and we further assume large r, then

$$S = \frac{\hbar k}{m}\ \frac{|f(\theta\phi)|^2}{r^2} = v\ \frac{|f(\theta,\phi)|^2}{r^2} \qquad \text{B.1.7}$$

where $\frac{\hbar k}{m} = \frac{p}{m} = v$ the classical velocity of the particle, and S is the scattered particle flux per unit area.

Since $d\Omega = \sin\theta\, d\theta\, d\phi$ and since an element of area in spherical coordinates is $dA = r^2 \sin\theta\, d\theta\, d\phi$ we can then write

$$d\Omega = \frac{dA}{r^2} \qquad \text{B.1.8}$$

and therefore

$$N\sigma(\theta,\phi)\,d\Omega = \frac{N\sigma(\theta,\phi)\,dA}{r^2} \qquad \text{B.1.9}$$

but $N\sigma(\theta,\phi)\,d\Omega = dN$ therefore

$$\frac{dN}{dA} = \frac{N\sigma(\theta,\phi)}{r^2} \qquad \text{B.1.10}$$

This is the scattered particle flux per unit area at angles θ, and ϕ.

We can apply B.1.6 to B.1.3 to arrive at the incident flux N

$$N = \frac{\hbar k}{m} = v \qquad \text{B.1.11}$$

using B.1.11 in B.1.10 we get

$$\frac{dN}{dA} = \frac{v\,\sigma(\theta,\phi)}{r^2} \qquad \text{B.1.12}$$

a comparison of B.1.12 and B.1.7 yields the important result that the differential scattering cross section is equal to the square of the scattering amplitude, i.e.

$$\sigma(\theta,\phi) = |f(\theta,\phi)|^2 \qquad \text{B.1.13}$$

The solution of many scattering problems is then reduced to finding the scattering amplitude $f(\theta,\phi)$.

Recall the scattering amplitude is the coefficient of the spherical outgoing wave in the asymptotic form

$$\psi^{+}(\bar{r}) \simeq \left[e^{i\bar{k}\cdot\bar{r}} + f(\theta,\phi)\ \frac{e^{i\bar{k}\cdot\bar{r}}}{r} \right] \qquad \text{B.1.14}$$

when this is used in the Schrodinger equation

$$\left(\nabla^2 + k^2\right) \psi^{+}(\bar{r}) = \frac{2\mu}{\hbar^2}\ V(\bar{r})\ \psi^{+}(\bar{r}) \qquad \text{B.1.15}$$

one arrives at (see e.g. Merzbacher (1961))

$$f(\theta,\phi) = -\frac{\mu}{2\pi\hbar^2} \int e^{-i\bar{k}'\cdot\bar{r}'}\ V(\bar{r}')\ \psi_k^{+}(\bar{r}')\ d\tau' \qquad \text{B.1.16}$$

As it stands, this result is not explicit and not useful. The first Born approximation simply replaces $\psi_k^{+}(\bar{r}')$ by a plane wave $e^{i\bar{k}\cdot\bar{r}'}$ so that

$$f(\theta,\phi) = -\frac{\mu}{2\pi\hbar^2} \int e^{-i\bar{k}'\cdot\bar{r}'}\ V(\bar{r}')\ e^{i\bar{k}\cdot\bar{r}'}\ d\tau' \qquad \text{B.1.17}$$

This approximation is generally valid for short range weak potentials, or very high energy incident particle.

The scattering amplitude is often written as

$$f(\theta,\phi) = -\frac{\mu}{2\pi\hbar^2} \int e^{+i\bar{q}\cdot\bar{r}'} V(\bar{r}')\ d\tau' \qquad \text{B.1.18}$$

where $\bar{q} = \bar{k} - \bar{k}'$, $|\bar{k}| = |\bar{k}|$, $q = 2k \sin\frac{1}{2}\theta$ and $\cos\theta = \frac{\bar{k}\cdot\bar{k}'}{|k|^2}$ (see figure B.1) and therefore we have...

$$\sigma(\theta,\phi) = \left(\frac{\mu}{2\pi\hbar^2}\right)^2 \left| \int e^{i\bar{q}\cdot\bar{r}'} V(\bar{r}')\ d\tau' \right|^2 \qquad \text{B.1.19}$$

and

MOMENTUM TRANSFER

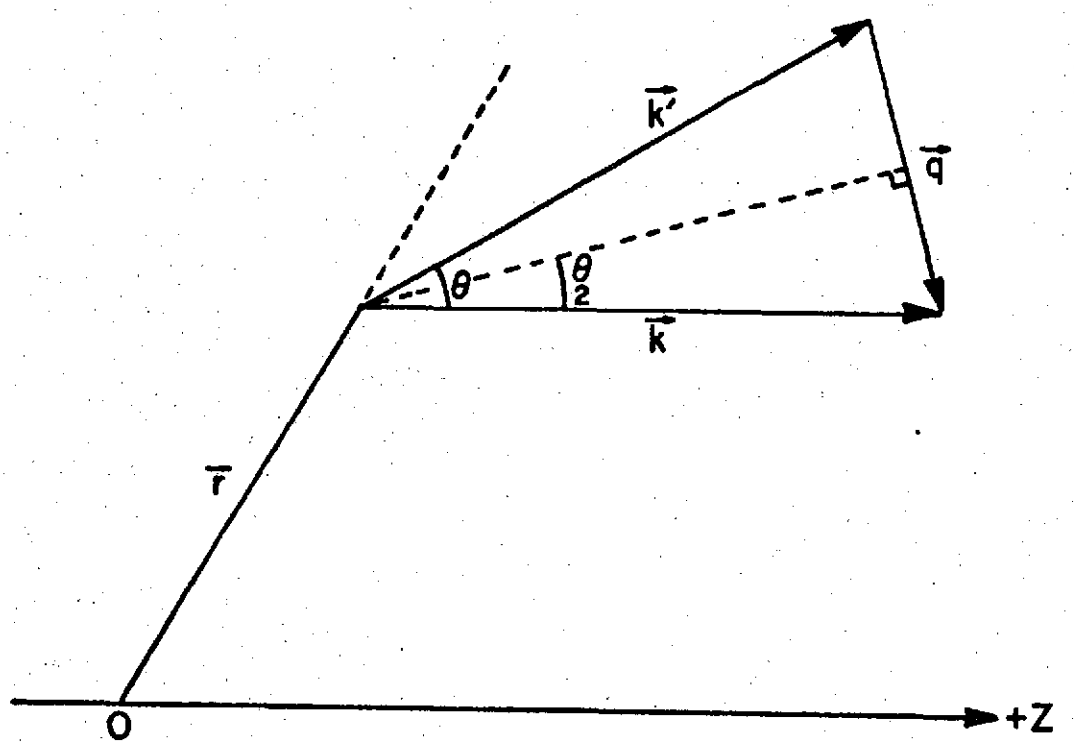

K = incident proton momentum
K' = final proton momentum
q = momentum transfer

FIGURE B1

$$\sigma_t = \int \sigma(\theta,\phi)\, \sin\theta\, d\theta\, d\phi \qquad \text{B.1.20}$$

Let us now go on to a discussion of inelastic scattering. The vectors $\bar{K}$ and $\bar{K}'$ no longer have equal magnitudes since energy is transferred to the target atom. The total system Hamiltonian is H where

$$H = H_{atom} + H_{particle} + H_{interaction} \qquad \text{B.1.21}$$

In general, the transition amplitude from a state α to a state β is given by

$$T_{\alpha\beta} = \langle \psi_\beta \mid H_I \mid \psi_\alpha \rangle \qquad \text{B.1.22}$$

For our situation, the ψ's are product wave functions

$$\psi_\alpha = \phi_o(\bar{A})\, e^{i\bar{K}_o\cdot\bar{r}} \qquad \psi_\beta = \phi_n(\bar{A})\, e^{i\bar{K}_n\cdot\bar{r}} \qquad \text{B.1.23}$$

where o and n represent the ground and excited states. Conservation of energy requires

$$\frac{\hbar^2}{2m}\left(K_o^2 - K_n^2\right) = \left(E_n - E_o\right) = \left(W_o - W\right) \qquad \text{B.1.24}$$

where E refers to the atom and W to the incident particle. The momentum transfer relations are now $\bar{q} = \bar{K}_o - \bar{K}_n$ $q^2 = (K_o - K_n)^2 + 4K_oK_n \sin^2\frac{\theta}{2}$ and $\cos\theta = \frac{\bar{K}_o\cdot\bar{K}_n}{K_oK_n}$, see again B.1. Equation B.1.22 now becomes, (in the Born approximation)...

$$T_{on} = \int e^{i\bar{q}\cdot\bar{r}} \phi_n^*(\bar{A})\, H_I(\bar{r};\bar{A})\, \phi_o(\bar{A})\, d\tau\, dA \qquad \text{B.1.25}$$

where A is representative of the atomic electron coordinates.

To obtain the differential and finally the total cross sections for the excitation, one must use B.1.25 in Fermi's golden rule...

$$\sigma_n(\theta,\phi) = \frac{2\pi}{\hbar v_o} \left| T_{on} \right|^2 \rho(\omega_n) \qquad \text{B.1.26}$$

The density of states factor, $\rho(\omega_n)$ is equal to $\frac{\omega_n^2 v_n}{(2\pi\hbar)^3 c^4}$ so

$$\sigma_n(\theta,\phi) = \left[\frac{\omega_n}{2\pi\hbar^2 c^2}\right]^2 \frac{v_n}{v_o} \left| T_{on} \right|^2 \qquad \text{B.1.27}$$

and

$$\sigma_n = \left[\frac{\omega_n}{2\pi\hbar^2 c^2}\right] \frac{v_n}{v_o} \int \left| T_{on} \right|^2 d\Omega \qquad \text{B.1.28}$$

At lower energies (or with target atom potentials of greater range), the Born approximation becomes less accurate. One then turns to the Distorted Wave Approximation. The initial and final wave functions of the particle are no longer the simple free particle wave functions.

In fact, the Distorted Wave Approximation will use the approach of Eqs. B.1.22 and B.1.27, but with wave functions which have been distorted by the interaction potential. Details are available from Bethe (1968), from Mott (1965), and also from Hasted (1964).

B.2 Cross Sections and Polarization

The polarization of light emitted (in a particular direction) by an impact excited gas will depend upon the relative cross sections for excitation of the magnetic substates of the upper level.

The methods of the preceding section can be generalized to calculate the cross sections for excitation to the various M levels. A conventional label for these cross sections is $Q_M^{(\alpha)}$ where α is the total orbital angular momentum quantum number L, and M represents the magnetic substate. Let us next define $A_M^{(\alpha,\beta)}(x)$, $A_M^{(\alpha\beta)}(Y)$, and $A_m^{\alpha\beta}(z)$ as the transition probabilities for emission of light from the Mth substate with the light's electric field vector aligned with the x,y, or z directions respectively. Also, since our system is symmetric about the z axis

$$A_M^{\alpha\beta}(x) = A_M^{\alpha\beta}(Y) = \frac{1}{2}\left[A_M^{\alpha\beta} - A_m^{\alpha\beta}(z)\right] \qquad \text{B.2.1}$$

The intensity of light emitted with its electric field vector polarized parallel (perpendicular) to the z axis

is then

$$I_{\parallel} = \sum_M A_M^{\alpha\beta}(z)\, Q_M^{\alpha}$$

$$I_{\perp} = \sum_M A_M^{\alpha\beta}(y)\, Q_M^{\alpha} \qquad \text{B.2.2}$$

We can then write the linear polarization fraction

$$\mathcal{P} = \frac{\sum_M \left[A_M^{\alpha\beta}(z) - A_m^{\alpha\beta}(y) \right] Q_M^{\alpha}}{\sum_m \left[A_m^{\alpha\beta}(z) + A_M^{\alpha\beta}(y) \right] Q_m^{\alpha}} \qquad \text{B.2.3}$$

Using the Zeeman intensity formula from Condon (1967) for a J → J-1 transition we get

$$I_{\pi} \propto (J^2 - M^2)$$

$$I_{\sigma} \propto \tfrac{1}{4}(J \pm M)(J \pm M - 1) \qquad \text{B.2.4}$$

where $A_M^{\alpha\beta}(z) \propto I_{\pi}$ and $A_M^{\alpha\beta}(y) \propto I_{\sigma}$

then Eq. B.2.3 becomes (with use of B.2.4 and $Q_m = Q_{-m}$) for a $^1P \rightarrow {}^1S$ transition

$$\mathcal{P} = \frac{Q_0 - Q_1}{Q_0 + Q_1} \qquad \text{B.2.5}$$

The theoretical problem has been reduced to finding the Q_0^{α} and Q_1^{α} for the $3\,^1P$ state of Helium.

Both the Born and Distorted Wave Approximations can be used to find the Q_0^{α} and Q_1^{α} given a proper choice of wave functions, i.e., wavefunctions in which the M dependence has not been summed over. The matrix

elements must be taken between various M states so that the transition probability will show any M dependence they might have. Mott (1965) gives an example of this type of procedure. Bell (1961) and others who have done this type calculation have used multi-parameter wave-functions whose parameters have in general been chosen to satisfy calculations of oscillator strengths. The cross sections arrived at by Bell (1961) are shown in table B1 as abstracted by this author from Bell's (1961) graphical results. Table B2 shows the values of π as calculated from the cross sections of table B1 using equation B.2.5

TABLE B1

THEORETICAL EXCITATION CROSS SECTIONS

H^+ Energy in keV	Q_o in πa_o^2		$Q_{\pm 1}$ in πa_o^2	
	Born	D.W.A.	Born	D.W.A.
100	.0238	.0198	.0271	.0150
178	.0166	.0175	.0238	.0166
316	.0107	.0122	.0192	.0158
450	.0080	.0093	.0163	.0144

Cross sections for the excitation of He to the 3^1P_o and $3^1P_{\pm 1}$ states calculated by both the Born Approximation and Distorted Wave Approximation (D.W.A.) methods. These numbers were abstracted from the graphical results of Bell (1961).

TABLE B2

THEORETICAL LINEAR POLARIZATION FRACTIONS

H^+ Energy in keV	π Theoretical from Born	π Theoretical from Distortion
100	- .065	+ .138
178	- .178	+ .026
316	- .284	- .129
450	- .342	- .215

The linear polarization fraction π calculated from Bell's (1961) theoretical cross sections.

APPENDIX C

COMPUTER PROGRAMS

C.1 LAM

This program is used to calculate the behavior of the interference filter.

```
LAM              9:19   FRIDAY  AUG 24, 1973

100 PRINT 'INTERFERENCE FILTER  LAMBDA VS ANGLE'
110 FOR N=1 TO 2 STEP .2
120 PRINT USING 130,N
130 :ANGLE      LAMBDA      N=##.###
140 FOR A=0 TO 10 STEP 2
150 LET X=RAD(A)
160 LET L=5018*SQR(1-((SIN(X))**2/(N**2)))
170 PRINT USING 180,A,L
180 :###       ######
190 NEXT A
200 PRINT
210 NEXT N
220 END
```

C.2 NEWPOL

This program is used to calculate π on a run by run basis according to equation 4.1.3.

```
NEWPOL        9:22   FRIDAY  AUG 24, 1973

100 DIM P(25)
110 PRINT 'LINEAR POLARIZATION FRACTION'
120 PRINT '# OF RUNS TO ANALYZE IS';
130 INPUT N0
140 PRINT 'LIST ALL P';
150 INPUT A$
160 FOR N1=1 TO N0
170 READ A1,A2,A3,B0,B1
180 LET C,D=0
190 FOR N2=1 TO B0
200 READ B2,B3
210 LET C=C+B2/B0
220 LET D=D+B3/B0
230 NEXT N2
240 IF A$='YES' THEN 270
250 LET Z=2
260 GO TO 310
270 LET Z=1
280 PRINT
290 PRINT
300 PRINT '   V       C       H       C          P'
310 LET F=0
320 FOR N3=1 TO B1
330 READ V,N,H,M
340 LET A=(H-C)/(M-D)
350 LET B=(V-C)/(N-D)
360 LET P(N3)=(A-B)/(A+B)
370 LET F=F+P(N3)/B1
380 GO TO 390,410 ON Z
390 PRINT USING 400,V,N,H,M,P(N3)
400 : #####  #####  #####  #####   ##.#####
410 NEXT N3
420 LET S=0
430 FOR N4=1 TO B1
440 LET S=S+(P(N4)-F)↑2
450 NEXT N4
460 IF B1=1 THEN 490
470 LET S=SQR(S/(B1-1))
480 GO TO 500
490 LET S=0
500 LET E=S/SQR(B1)
510 LET I=0
520 FOR N5=1 TO B1
530 LET G=ABS(P(N5)-F)
540 IF G<2*S THEN 560
```

```
550 LET I=I+1
560 NEXT I5
570 PRINT
580 PRINT USING 590,A1,A2,A3,B1
590 :### KEV,  #.## U HE,  ##.# U A H+,    ## TRIALS
600 PRINT USING 610,S,I,E
610 :ST DV =#.#####    ## PTS DV > 2 SIG     S.E.=#.#####
620 LET F0=F-E
630 LET F1=F+E
640 PRINT USING 650,F0,F,F1
650 :(P-SE)=#.#####     MEAN P =##.#####     (P+SE)=#.#####
660 PRINT
670 NEXT N1
680 END
```

C.3 STAT

This program is used to calculate π for a collection of runs (from results stored in a file).

```
STAT          9:25   FRIDAY  AUG 24, 1973

100 DIM P(300)
110 PRINT 'FILE TO BE ANALYZED IS';
120 INPUT A$
130 OPEN 1,A$,INPUT
140 GET M,N
150 LET F=0
160 FOR I=1 TO M
170 GET P(I)
180 LET F=F+P(I)/M
190 NEXT I
200 LET S=0
210 FOR J=1 TO M
220 LET S=S+(P(J)-F)↑2
230 NEXT J
240 LET S=SQR(S/(M-1))
250 LET K=0
260 FOR L=1 TO M
270 LET G=ABS(P(L)-F)
280 IF G<2*S THEN 300
290 LET K=K+1
300 NEXT L
310 LET E=S/SQR(M)
320 LET F0=F-E
330 LET F1=F+E
340 PRINT USING 350,M
350 :### P'S IN CALCULATION
360 PRINT USING 370,S,K,E
370 :ST DV =#.######   ### PTS DV > 2 SIG    S.E.=#.######
380 PRINT USING 390,F0,F,F1
390 :(P-SE)= ##.#####    MEAN P = ##.#####    (P+SE)= ##.#####
400 PRINT
410 PRINT
420 GO TO 110
430 END
```

C.4 TTEST

This program is used to calculate the t statistic, used as a test for the significance of the difference of means.

```
TTEST          9:26   FRIDAY  AUG 24, 1973

100 PRINT 'T TEST...INPUT MEAN,ST DV,NO.'
110 INPUT P1,S1,N1
120 INPUT P2,S2,N2
125 INPUT A$
130 S3=((N1-1)/N1)*S1↑2
140 S4=((N2-1)/N2)*S2↑2
150 F=N1+N2-2
160 Z=SQR((N1*S3+N2*S4)/F)
170 T=(P1-P2)/(Z*SQR((1/N1)+(1/N2)))
180 PRINT USING 190,F,T
190 :### DEGREES OF FREEDOM   T=###.##
200 PRINT
210 GO TO 110
220 END
```

C.5 PUTPOL

This program is used to calculate the 20 τ values for each N run and to store them in an appropriate file.

```
PUTPOL        9:29   FRIDAY  AUG 24, 1973

100 REM PUTPOL  TO ANALYZE P AND FILE IT
110 DIM O(300),P(25)
120 PRINT '# OF RUNS TO ANALYZE AND FILE IS';
130 INPUT N0
140 FOR N1=1 TO N0
150 READ I,J,K
160 LET C,D=0
170 READ B0,T
180 FOR N2=1 TO B0
190 READ B1,B2
200 C=C+B1/B0
210 D=D+B2/B0
220 NEXT N2
230 FOR N3=1 TO T
240 READ V,N,H,M
250 A=(H-C)/(M-D)
260 B=(V-C)/(N-D)
270 P(N3)=(A-B)/(A+B)
280 NEXT N3
290 IF J=.2 THEN 330
300 PRINT USING 310,J,I
310 :PRESS=##.##     ### KEV DATA NOT ADDED TO FILE
320 GO TO 710
330 A$='P100'
340 IF I=100 THEN 510
350 A$='P150'
360 IF I=150 THEN 510
370 A$='P200'
380 IF I=200 THEN 510
390 A$='P250'
400 IF I=250 THEN 510
410 A$='P300'
420 IF I=300 THEN 510
430 A$='P350'
440 IF I=350 THEN 510
450 A$='P400'
460 IF I=400 THEN 510
470 A$='P450'
480 IF I=450 THEN 510
490 PRINT 'UNACCEPTABLE ENERGY VALUE'
500 GO TO 710
510 OPEN 1,A$,INPUT
520 GET E,G
530 IF E=0 THEN 570
540 FOR L=1 TO E
```

```
550 GET O(L)
560 NEXT L
570 CLOSE 1
580 G=1
590 OPEN 1,AS,OUTPUT
600 Q=E+T
610 PUT 1:G,G
620 FOR R=1 TO E
630 PUT 1:O(R)
640 NEXT R
650 FOR N4=1 TO T
660 PUT 1:P(N4)
670 NEXT N4
680 PRINT USING 690,I
690 :#### KEV DATA ADDED TO FILE
700 CLOSE 1
710 NEXT N1
720 END
```

C.6 PUTPOLR

This program is used to calculate the 20 - values for each R run and to store them in a appropriate file.

```
PUTPOLR      9:32   FRIDAY  AUG 24, 1973

100 REM PUTPOL  TO ANALYZE P AND FILE IT
110 DIM O(300),P(25)
120 PRINT '# OF RUNS TO ANALYZE AND FILE IS';
130 INPUT N0
140 FOR N1=1 TO N0
150 READ I,J,K
160 LET C,D=0
170 READ B0,T
180 FOR N2=1 TO B0
190 READ B1,B2
200 C=C+B1/B0
210 D=D+B2/B0
220 NEXT N2
230 FOR N3=1 TO T
240 READ V,N,H,M
250 A=(H-C)/(M-D)
260 B=(V-C)/(N-D)
270 P(N3)=(A-B)/(A+B)
280 NEXT N3
290 IF J=.2 THEN 330
300 PRINT USING 310,J,I
310 :PRESS=##.##     ### KEV DATA NOT ADDED TO FILE
320 GO TO 710
330 A$='P100R'
340 IF I=100 THEN 510
350 A$='P150R'
360 IF I=150 THEN 510
370 A$='P200R'
380 IF I=200 THEN 510
390 A$='P250R'
400 IF I=250 THEN 510
410 A$='P300R'
420 IF I=300 THEN 510
430 A$='P350R'
440 IF I=350 THEN 510
450 A$='P400R'
460 IF I=400 THEN 510
470 A$='P450R'
480 IF I=450 THEN 510
490 PRINT 'UNACCEPTABLE ENERGY VALUE'
500 GO TO 710
510 OPEN 1,A$,INPUT
520 GET E,G
530 IF E=0 THEN 570
540 FOR L=1 TO E
```

```
550 GET 0(L)
560 NEXT L
570 CLOSE 1
580 G=1
590 OPEN 1,A$,OUTPUT
600 Q=E+T
610 PUT 1:Q,G
620 FOR R=1 TO E
630 PUT 1:0(R)
640 NEXT R
650 FOR N4=1 TO T
660 PUT 1:P(N4)
670 NEXT N4
680 PRINT USING 690,I
690 :#### KEV DATA ADDED TO FILE
700 CLOSE 1
710 NEXT N1
720 END
```

C.7 PUTPOLP

This program is used to calculate the 20 P values for each run and to store them according to pressure and energy.

```
PUTPOLP        9:35   FRIDAY  AUG 24, 1973

100 REM PUTPOL  TO ANALYZE P AND FILE IT
110 DIM O(300),P(25)
120 PRINT '# OF RUNS TO ANALYZE AND FILE IS';
130 INPUT N0
140 FOR N1=1 TO N0
150 READ I,J,K
160 LET C,D=0
170 READ B0,T
180 FOR N2=1 TO B0
190 READ B1,B2
200 C=C+B1/B0
210 D=D+B2/B0
220 NEXT N2
230 FOR N3=1 TO T
240 READ V,N,H,M
250 A=(H-C)/(M-D)
260 B=(V-C)/(N-D)
270 P(N3)=(A-B)/(A+B)
280 NEXT N3
290 IF J=.01 THEN 380
300 IF J=.05 THEN 470
310 IF J=.2 THEN 540
320 IF J=.6 THEN 570
330 IF J=1.0 THEN 640
340 IF J=1.5 THEN 710
350 PRINT USING 360,I,J
360 :PRESS OUT OF BOUNDS  ###, ##.##
370 GO TO 980
380 A$='T150P01'
390 IF I=150 THEN 780
400 A$='T300P01'
410 IF I=300 THEN 780
420 A$='T450P01'
430 IF I=450 THEN 780
440 PRINT USING 450,I,J
450 :ENERGY OUT OF BOUNDS  ###, ##.##
460 GO TO 980
470 A$='T150P05'
480 IF I=150 THEN 780
490 A$='T300P05'
500 IF I=300 THEN 780
510 A$='T450P05'
520 IF I=450 THEN 780
530 GO TO 440
540 PRINT USING 550,I,J
```

```
550 :USE PUTPOL  ###, ##.##
560 GO TO 980
570 A$='T150P6'
580 IF I=150 THEN 780
590 A$='T300P6'
600 IF I=300 THEN 780
610 A$='T450P6'
620 IF I=450 THEN 780
630 GO TO 440
640 A$='T150P10'
650 IF I=150 THEN 780
660 A$='T300P10'
670 IF I=300 THEN 780
680 A$='T450P10'
690 IF I=450 THEN 780
700 GO TO 440
710 A$='T150P15'
720 IF I=150 THEN 780
730 A$='T300P15'
740 IF I=300 THEN 780
750 A$='T450P15'
760 IF I=450 THEN 780
770 GO TO 440
780 OPEN 1,A$,INPUT
790 GET E,G
800 IF E=0 THEN 840
810 FOR L=1 TO E
820 GET O(L)
830 NEXT L
840 CLOSE 1
850 G=1
860 OPEN 1,A$,OUTPUT
870 Q=E+T
880 PUT 1:Q,G
890 FOR R=1 TO E
900 PUT 1:O(R)
910 NEXT R
920 FOR N4=1 TO T
930 PUT 1:P(N4)
940 NEXT N4
950 PRINT USING 960,I,J,A$
960 :#### KEV, ##.## U HE  DATA ADDED TO  ########
970 CLOSE 1
980 NEXT N1
990 END
```

C.3 PUT

This program is used to initialize storage files within the computer for later acceptance of calculated values.

```
PUT                    9:39   FRIDAY  AUG 24, 1973

100 PRINT 'FILE NAME'
110 INPUT A$
120 OPEN 1,A$,OUTPUT
130 M=0
140 N=1
150 PUT 1:M,N
160 CLOSE 1
170 GO TO 100
180 END
```

C.9 PUTPTEST

This program is used to calculate and store η as directed by the user and was used for low current runs.

```
PUTPTEST      9:40    FRIDAY  AUG 24, 1973

100 DIM O(300),P(25)
110 PRINT '# OF RUNS TO ANALYZE AND FILE IS';
120 INPUT N0
130 FOR N1=1 TO N0
140 READ I,J,K
150 LET C,D=0
160 READ B0,T
170 FOR N2=1 TO B0
180 READ B1,B2
190 C=C+B1/B0
200 D=D+B2/B0
210 NEXT N2
220 FOR N3=1 TO T
230 READ V,N,H,M
240 A=(H-C)/(M-D)
250 B=(V-C)/(N-D)
260 P(N3)=(A-B)/(A+B)
270 NEXT N3
280 PRINT USING 290;N1
290 :FILE NAME FOR RUN NO. ## IS
300 INPUT A$
310 OPEN 1,A$,INPUT
320 GET E,G
330 IF E=0 THEN 370
340 FOR L=1 TO E
350 GET O(L)
360 NEXT L
370 CLOSE 1
380 G=1
390 OPEN 1,A$,OUTPUT
400 O=E+T
410 PUT 1:O,G
420 FOR R=1 TO E
430 PUT 1:O(R)
440 NEXT R
450 FOR N4=1 TO T
460 PUT 1:P(N4)
470 NEXT N4
480 PRINT USING 490,I,J,A$
490 :#### KEV, ##.## U HE  DATA ADDED TO  ########
500 CLOSE 1
510 NEXT N1
520 END
```

APPENDIX D

QUALITATIVE CONSIDERATIONS OF THE EFFECT OF HELIUM PRESSURE ON π

In previous experimental studies of the polarization of the light from the 3^1P-2^1S transition in Helium, the researchers have either claimed that their result was independent of the pressure of Helium in the target chamber below .2 mtorr (Van Eck (1964), and Van den Bos (1969)), or they show a pressure dependence of π down to their lowest pressure of .2 mtorr (Scharmann (1969)). We have clearly shown that π is still pressure dependent below .2 mtorr. The problem which remains however is to explain that pressure dependence, and especially to explain the change in the sign of π as the He pressure is lowered. Scharmann (1969) also observed a sign change, but was not able to explain it.

In order to attempt to discover the reason for the sign change in π, we followed a suggestion made by Professor R. H. Lambert. We reanalyzed our data so as to show relative intensities of λ 5016 Å light as a function of He gas pressure. Both the parallel and perpendicular intensities were calculated by equation 4.1.2. We then normalized these results to He pressure. The results of these calculations are shown in Tables D1, D2 and D3.

We have plotted the beam current and pressure normalized results in Figures D1, D2 and D3. These intensities are proportional to the number of photons per proton per target atom received at the detector.

We had intended to look into changes in the relative intensities of parallel and perpendicularly polarized light (as a function of pressure) in order to attempt an explanation of the change in sign of π. However the relative changes in relative intensities are very small compared to the average relative intensity changes (as a function of pressure), therefore we were not able to find a probable cause for the change in sign of π.

The information gained however, has caused us to realize that significant trapping in the metastable states of He occurs within the target chamber. We have previously discussed (section 4.2) trapping at the 1^1S level and how it would tend to depolarize the λ 5016 Å light. We have also previously corrected for this effect. However capture at levels other than the ground state must now be considered. Inspection of figure 11 shows three states which do not connect (via electric dipole transitions) with the 1^1S ground state. These three states (which are long lived and called metastable) are the 2^1S, 2^3S and the 2^3P. The triplet states need not concern us since transitions between triplet states will not result in light of wavelength 5016 Å, and since the only intersystem transition of note is 2^3P-1^1S which simply leaves

TABLE D1

INTENSITY Vs He PRESSURE AT 150 keV BEAM ENERGY

He PRESSURE mtorr	AV. BEAM CURRENT μA	# OF RUNS	# OF MEASURE-MENTS	S.E. OF $I_{//}$	NORMALIZED TO BEAM CURRENT MEAN $I_{//}$	MEAN $I_{\perp}$	S.E. OF $I_{\perp}$	NORMALIZED TO BOTH BEAM CURRENT AND He PRESSURE MEAN $I_{//}$	MEAN $I_{\perp}$
.01	5.5	8	160	.0015	.082	.083	.0014	8.2 ±.15	8.3 ±.14
.05	6.6	5	100	.011	.276	.261	.01	5.52±.22	5.22±.2
.2	7.1	7	140	.012	.933	.898	.011	4.66±.06	4.48±.06
.6	7.	2	40	.051	4.133	4.082	.046	6.88±.08	6.8 ±.08
1.0	5.8	2	40	.037	8.770	8.706	.026	8.77±.04	8.71±.03
1.5	6.	2	40	.153	16.759	16.99	.161	11.03±.10	11.31±.11

TABLE D2

INTENSITY Vs He PRESSURE AT 300 keV BEAM ENERGY

He PRESSURE mtorr	AV. BEAM CURRENT μA	# OF RUNS	# OF MEASURE-MENTS	S.E. OF $I_{//}$	NORMALIZED TO BEAM CURRENT MEAN $I_{//}$	MEAN $I_{\perp}$	S.E. OF $I_{\perp}$	NORMALIZED TO BOTH BEAM CURRENT AND He PRESSURE MEAN $I_{//}$	MEAN $I_{\perp}$
.01	11.8	7	140	.001	.0629	.0615	.0009	6.29±.1	6.15±.09
.05	11.4	7	140	.002	.159	.162	.002	3.19±.04	3.24±.04
.2	10.5	10	200	.004	.594	.624	.004	2.97±.02	3.12±.02
.6	12.2	3	60	.106	1.907	2.06	.118	3.18±.18	3.44±.2
1.0	11.2	3	60	.323	4.428	4.714	.353	4.43±.32	4.71±.35
1.5	11.3	2	40	.662	11.917	12.528	.717	7.95±.44	8.38±.48

TABLE D3

INTENSITY Vs He PRESSURE AT 450 keV BEAM ENERGY

He PRESSURE mtorr	AV. BEAM CURRENT μA	# OF RUNS	# OF MEASURE-MENTS	S.E. OF $I_{//}$	NORMALIZED TO BEAM CURRENT MEAN $I_{//}$	MEAN $I_{\perp}$	S.E. OF $I_{\perp}$	NORMALIZED TO BOTH BEAM CURRENT AND He PRESSURE MEAN $I_{//}$	MEAN $I_{\perp}$
.01	11.8	4	80	.0018	.0877	.0914	.0018	8.77±.18	9.14±.18
.05	10.4	5	100	.0029	.1741	.1813	.0023	3.48±.58	3.62±.46
.2	10.3	7	140	.004	.4821	.5387	.005	2.41±.02	2.69±.03
.6	10.7	3	60	.039	1.953	2.181	.058	3.26±.07	3.64±.1
1.0	10.8	3	60	.171	3.754	4.094	.211	3.75±.17	4.09±.21
1.5	10.5	2	40	.106	5.107	5.47	.129	3.41±.07	3.65±.09

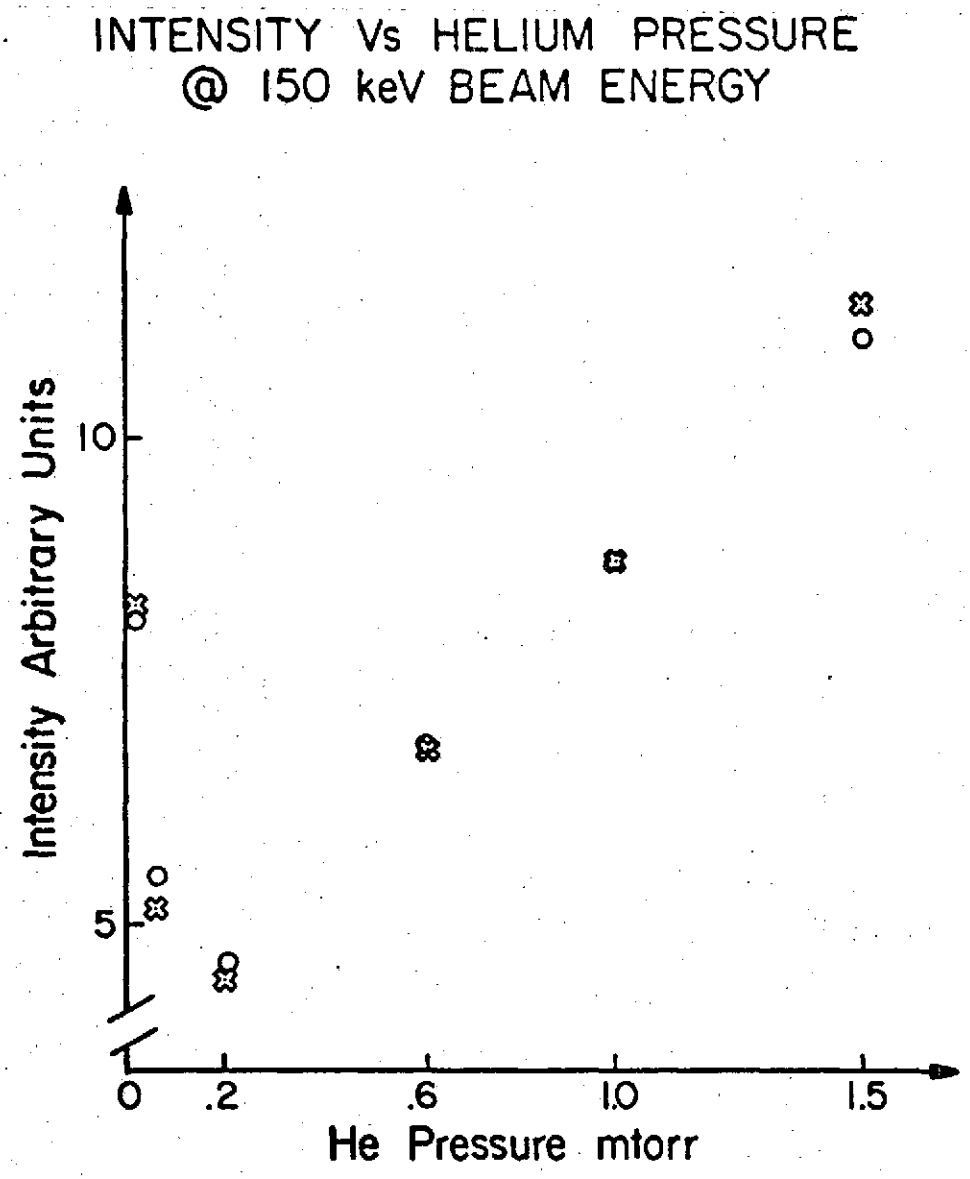
INTENSITY Vs HELIUM PRESSURE
@ 150 keV BEAM ENERGY
Intensity Arbitrary Units
10
5
0
.2
.6
1.0
1.5
He Pressure mtorr
o = I//
⊠ = I⊥

FIGURE D1

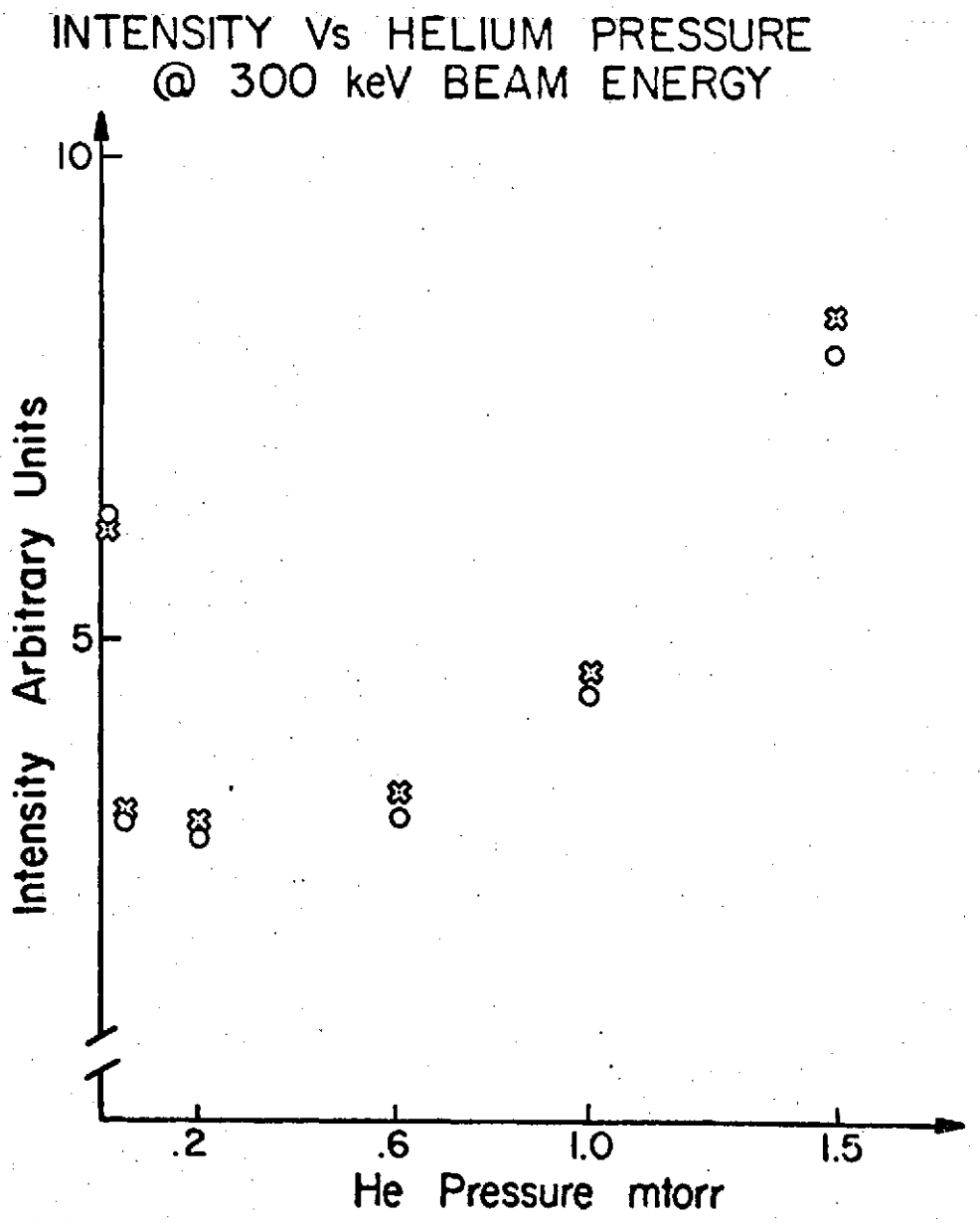
INTENSITY Vs HELIUM PRESSURE
@ 300 keV BEAM ENERGY
10
5
Intensity Arbitrary Units
.2
.6
1.0
1.5
He Pressure mtorr
o = I∥
⊠ = I⊥

FIGURE D2

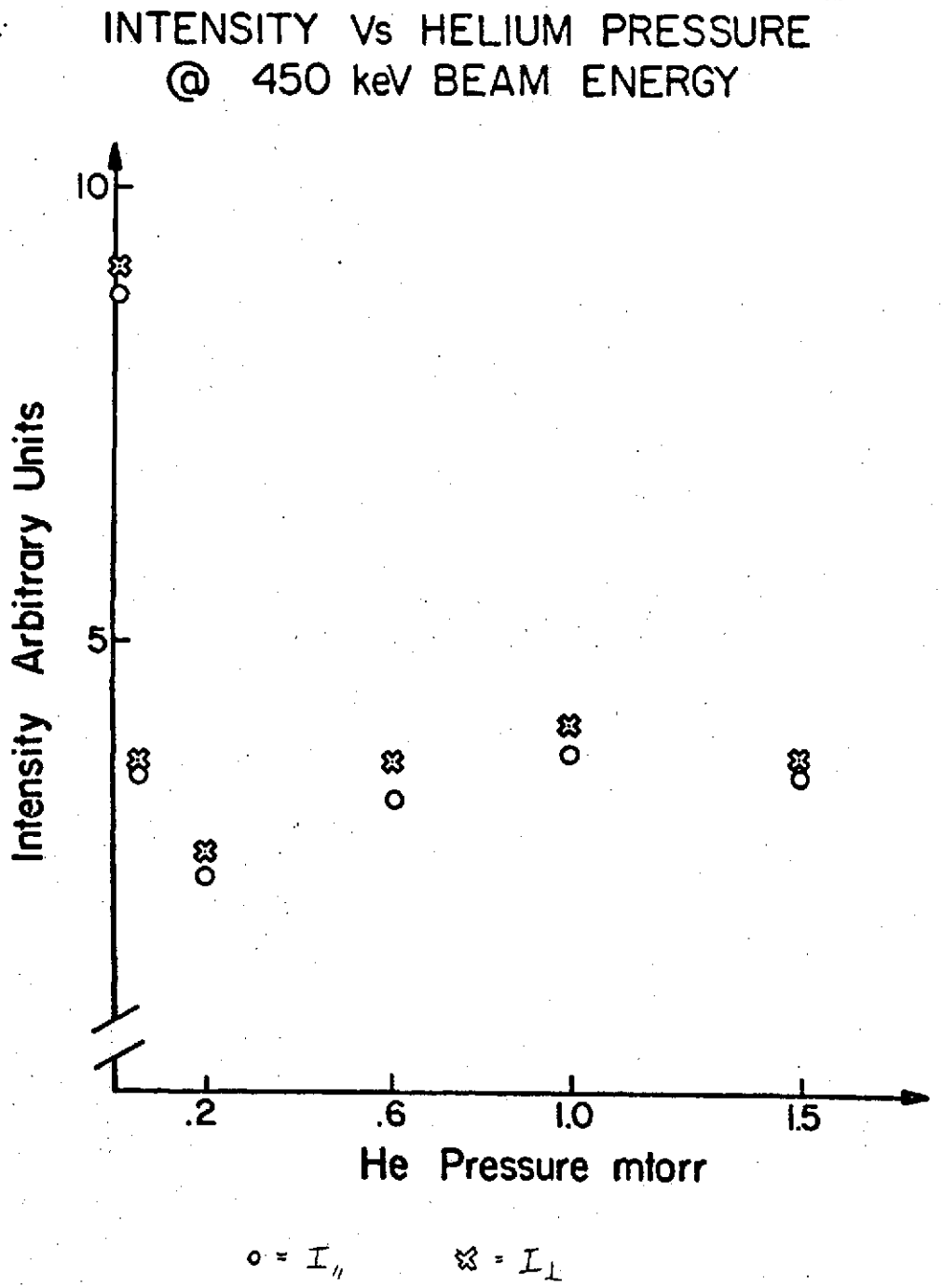
INTENSITY Vs HELIUM PRESSURE
@ 450 keV BEAM ENERGY
10
5
Intensity Arbitrary Units
.2
.6
1.0
1.5
He Pressure mtorr
o = I//
⊠ = I⊥

FIGURE D3

a ground state atom. It is then the 2^1S state with which we must concern ourselves. In order to estimate the effect on λ 5016 Å photons by 2^1S state He atoms, we must first discuss the presence of 2^1S atoms in the target chamber. Referring to calculations done in sections 4.2 and 4.3, we have at our highest working pressure (1.5 mtorr) a mean free path of 47 cm, a mean collision time of $\sim$.3 msec, and an estimated minimum wall collision time of $\sim$.02 msec. Similar calculations for our lowest working pressure (.01 mtorr) yield a mean free path of $\sim$7000 cm, a mean collision time of $\sim$50 msec, and an estimated minimum wall collision time of $\sim$.02 msec. Note that the wall collision times are minimum times and in fact the "diffusion" times would be much longer. Furthermore, we have from Hasted (1972) the fact that the natural lifetime of the metastable state He 2^1S is > 1 msec. We can then conclude that at our high pressure runs the He 2^1S level will be collisionally quenched and significant absorbtion of λ 5016 Å light will not occur. However as we go to lower pressures, the number of surviving He 2^1S atoms increases and we can expect some absorbtion of the λ 5016 Å light. Finally at very low pressures one would expect a high percentage of He 2^1S in the target chamber, but these metastables would be spread so thinly that there would be lit e photon-metastable interaction, and therefore an increase in the amount of λ 5016 Å light detected.

The results which have been normalized to both Beam Current and Gas Pressure are the relative intensities of λ 5016 Å light per proton per target atom. The minimum observed in these curves is just what one would expect (qualitatively) from our discussion of the existence of the metastable He 2^1S atoms. We thus conclude that trapping by the metastable He 2^1S atoms is responsible for the changes in relative intensity with pressure.

In conclusion then, we are still unable to explain the cause of the change in the sign of π as the He pressure changes. We have shown qualitatively that trapping is occurring at the metastable 2^1S level. This trapping provides yet another reason for the next experimenter to work at lower pressures. Only then will the photon from a beam excited 3^1P-2^1S transition be directly detected.